Chapter 5
Metal Chelate Dendrimers

Abstract In this chapter the synthetic methodologies, physico-chemical peculiarities, properties, and spatial organization of metal chelate dendrimers as a specific sub-class of polymeric metal chelates are considered. These compounds are subdivided into molecular, intracomplex, and macrocyclic types which in turn are grouped depending on the nature of the donor atoms (N,N-, N,O-, N,S-, O,O-, O,S-, S,S-, P,P-chelates, etc.). Special attention is paid to the features of the preparation of metal chelate star polymers by "arm-first", "core-first" and click-to-chelate approaches. The main data on the synthesis, spatial structure and properties of the metal chelates with hyperbranched dendrimers are summarized. The problems and future prospects of metal chelate dendrimers are outlined.

The creation of dendrimers becomes an important landmark in the development of contemporary coordination chemistry. Metallodendrimers are unique polymer compounds containing metals in different parts of dendritic architecture, which have been obtained in the first days of dendrimer chemistry and are objects of increasing interest of researchers [1–28]. Hierarchically dendrons and dendrimers are collections of 10^3–10^4 atoms with relative molar weights 10,000–100,000 and hydrodynamic sizes changing from 1 to 30 nm [29]. Due to presence of a great number of functional groups dendrimers form stoichiometric nanometer compounds of metallodendrimer type [30–33]. It is important to emphasize that following reduction of metals in these structures brings to production of nanocluster compounds covered by dendritic shell [14, 17–19, 29, 33–41]. Metallodendrimers are convenient precursors for light-harvesting molecular devices and machines: cables, switches, extenders, antennas, and nanomotors [42–44]. The use of controlled polymer architecture of dendrimers together with a suitable metal may lead to new functional materials based on well-designed redox-active sites [12], which can be used for development of molecular nanobatteries for redox probing, modified electrode surfaces, and redox catalysis [45].

In order to identify and predict the possible directions of practical use of metallodendrimers key is to incorporate the following effects: dendrimer (dendritic) effect, multivalency effect, and preorganization effect [46]. For all metallodendrimers more

G. I. Dzhardimalieva and I. E. Uflyand, *Chemistry of Polymeric Metal Chelates*, Springer Series in Materials Science 257,
https://doi.org/10.1007/978-3-319-56024-3_5

or less typical is dendrimer (or dendritic) effect, when a functional group behaves differently depending on whether it is free or bound to a dendrimer [14]. At that, properties of metallodendrimers can even change depending on dendrimer generation. Usually all possible dendritic effects are interrelated and perhaps are determined by several parameters referred to as critical nanoscale design parameters [47–49]. Size, shape, flexibility/rigidity, architecture, surface chemistry, and elemental composition of the dendrimer are related to such parameters. Dendritic effect can be observed for all classes of metallodendrimers and for any type of properties, however, it is most commonly manifested in such areas as catalysis [8, 10, 12–14, 50–55], medicine [10, 14, 16, 56–65], and materials [10, 14, 66–70]. The multivalency (cooperative) effect is due to a decrease in entropy in successive chelation reactions of one metal by the polymer ligand [46, 71–73]. The preorganization effect is associated with a decrease in the degree of freedom in the transition from monomers to polymers [46].

Metallodendrimers are classified [17, 39] depending on a place of metal location in a dendrimer architecture (Fig. 5.1): (i) metal as a core, (ii) metal as branching centers, (iii) metal in multiple locations of a dendrimer, (iv) metal as a termini group, (v) metal as a connector, (vi) metal as a transformation auxiliaries or secondary element of a construction.

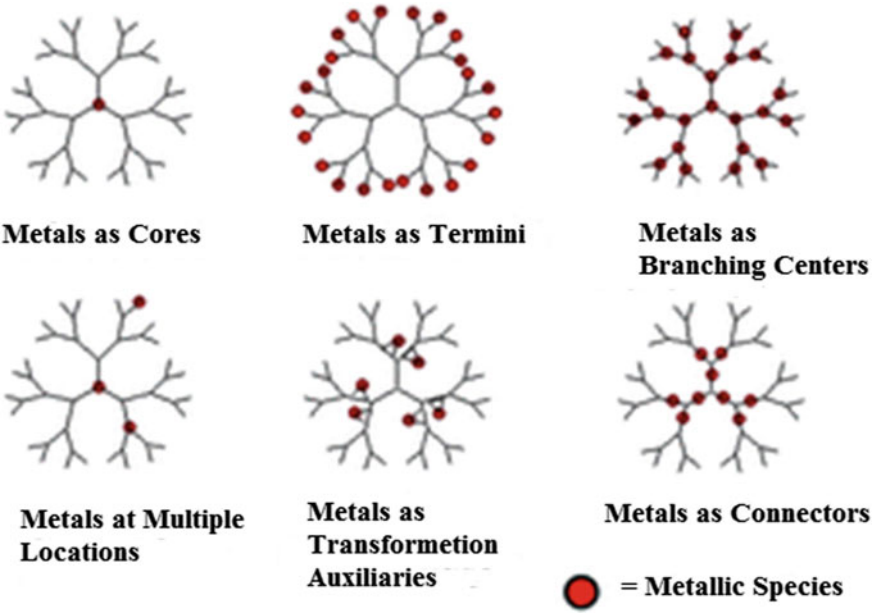

Fig. 5.1 The different roles metals can play in metallodendrimers

One of important subclasses of metallodendrimers is metal chelate dendrimers (MCDs), which contain metal chelate units in different parts of a dendritic structure. Metal chelate dendrimers are relatively young, but rapidly developed area of PMC chemistry.

Most widely used method of MCD production is direct interaction between MX_n and dendrimers containing chelating units [20]. This is substantially advanced by high solubility of dendrimers in different solvents, including water. One of efficient ways of enhancement of dendrimer solubility is fixing of different hydrophilic groups to their surface, for example, bulk oligo(oxyethylene) terminal group, which provides solubility in polar protonic solvents and prevents aggregation of dendrimers [74, 75]. Equally important is the fact the synthesis of MCD in most cases is carried out deliberately in view of their possible future applications. It should be noted that all chelating dendrimers in the synthesis process pass a number of successive chromatographic purifications, whereby the final product has a high purity. Therefore, it is possible to use the synthesis of MCD in situ without isolation of the metal chelates in a number of applications.

5.1 Molecular Metal Chelates

To date, it has accumulated considerable experimental material on the molecular MCD, and the range is wide enough chelating fragments.

5.1.1 Metal Chelates with N-Donor Ligands

The metal chelates with N-donor ligands occupy a significant place among MCD of molecular type. A typical example can be the family of pyridylimine chelates, which are located in various parts of the dendritic architecture. Thus, carbosilane dendritic mono-metallic Ni(II) chelates containing aryl-*N*,*N*′-iminopyridine ligand linked to Fréchet type dendrons are synthesized [76, 77]. It turned out that catalytic activity of these chelates with methylalumoxan (MAO) as co-catalyst is influenced more by metallic nuclearity than bulkiness of MCD. In addition, strong generation dependence concerning the topology and molecular weight of PE products is observed, at that, increasing generation leads to preferred oligomerization (chain transfer) over polymerization.

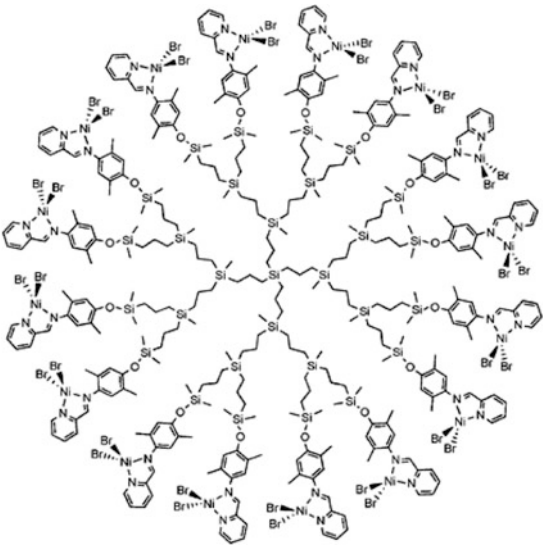

Of interest are Pd-MCDs, containing 4, 8 or 16 terminal pyridylimine chelates, which were used as catalysts for the alternating copolymerization of CO and 4-*tert*-butyl-St [78]. It should be noted that chloro methyl or cationic methyl Pd-MCDs are a *cis-trans* mixture of diastereoisomers. Besides, in this case the dendritic effect is observed: generation of the dendrimer affects the catalyst activity and the microstructure of the reaction products.

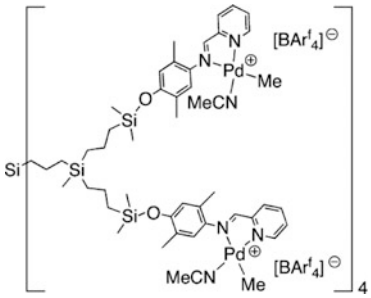

Chelation reaction of G1 PPI dendrimer modified through reaction of terminal amino groups and 2-pyridinecarboxaldehyde with $PdCl_2$(COD) in dry CH_2Cl_2 brings to production of MCD with pyridylimine Pd-containing chelates linked along perimeter [79]. The obtained MCD was isolated as a light orange, amorphous solid in 93% yield.

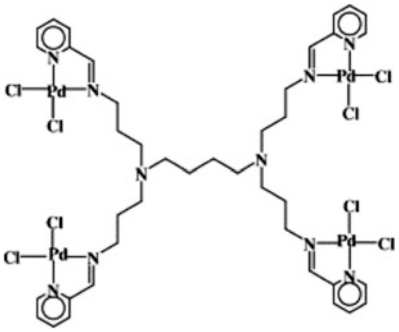

It should be noted that G1 and G2 Pd-containing pyridylimine MCD can be used as initial catalytic substance for ethylene polymerization resulted in high-molecular weight and high density PE production using MAO as co-catalyst [79] or for Heck coupling reaction [80].

Chelating dendrimer obtained by Schiff condensation reaction of tris-2-(aminoethyl) amine with 2-pyridinecarboxaldehyde reacts reaction with $[RhCl(CO)_2]_2$ and $[RhCl(COD)]_2$ with formation of respective pyridylimine Rh MCD [81]. These Rh(I) chelate dendrimers are thermally stable, have high activity, and are chemo- and regioselective in hydroformylation of 1-octen.

G1 PAMAM dendrimers were modified by pyridylimine units to afford two MCD, a tetranuclear platinum chelate and a multinuclear copper chelate (Fig. 5.2) [82]. It is important that the cytotoxicity of these MCDs were evaluated in vitro against several cancer cell lines, namely MOLT-4 (cisplatin-sensitive cancer cell line), MCF-7 (cisplatin-resistant breast cancer cell line) and Chang Liver of benign origin.

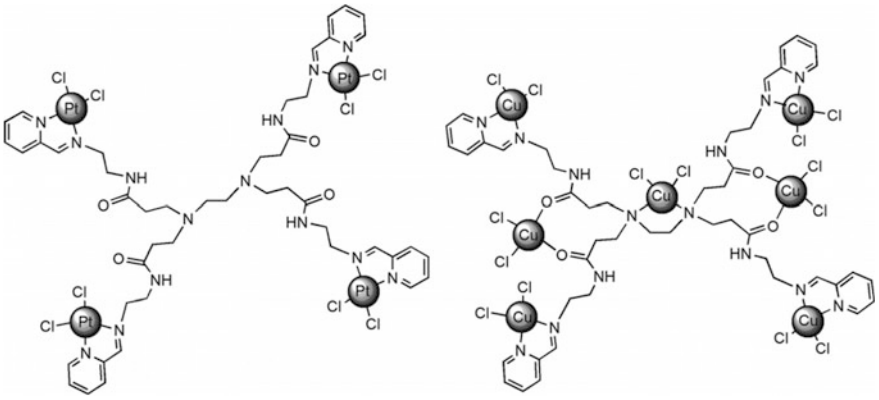

Fig. 5.2 Tetranuclear Pt-functionalized MCD (left) and a multinuclear Cu-functionalized MCD (right)

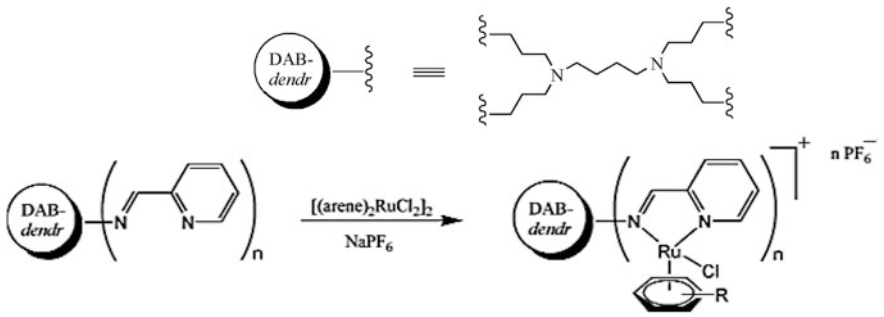

Scheme 5.1 Reaction of binuclear arene Ru precursors with pyridylimine dendritic ligands

G1–G2 Ru(II) arene MCDs based on PPI dendritic frameworks are obtained from binuclear arene Ru precursors (arene = *p*-cymene or hexamethylbenzene) as a result of reactions with pyridylimine dendritic ligands in form of hexafluorophosphate salts (Scheme 5.1) [56]. In this case structure of mononuclear Ru MCD was confirmed by X-ray diffraction analysis. These compounds are air-stable, soluble in DMSO, acetone and acetonitrile, and MALDI-TOF studies confirmed that all of the dendrimer end groups were functionalized with Ru(II) arene moieties.

Studies of cytotoxicity of MCD using A2780 and A2780cisR human ovarian carcinoma cancer cell lines in the range of concentrations 32–208 μM showed that distinct correlation is observed between MCD size and cytotoxicity, at that G2 MCD exhibited higher activity to both cell lines. The DNA binding studies confirmed high cytotoxicity observed for these chelates, because the MCD act, probably, via another mechanism than *cis*-platinum [56]. Therefore, definite positive dendritic effects are established for anti-proliferative activity and for DNA cleavage activity.

We note also the phosphorus chelating dendrimers bearing respectively 6, 12, or 24 pyridylimine end groups [83]. In situ chelation of CuI with these dendritic ligands gave catalysts, suitable for coupling of 3,5-dimethylphenol with PhI, as well as pyrazole with PhI and PhBr. In particular, the monomeric CuI complex was not efficient in the case of PhI, whereas all the MCDs were very efficient (95% yield). Besides, an increase of the efficiency was observed on going from the monomer (inefficient) to the G3 MCD (80% yield) in the case of PhBr, indicating a positive dendrimer effect.

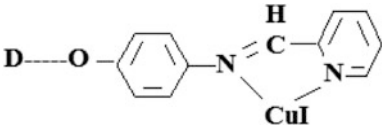

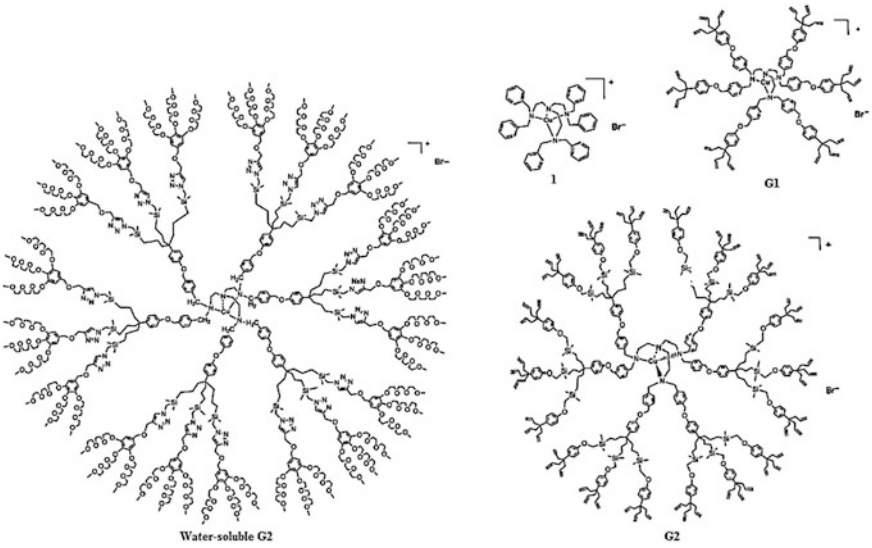

Fig. 5.3 Cu(I) (hexabenzyl)tris(en) chelate 1 and Cu(I) G1, G2, and water-soluble G2 MCD

Free pyridylimine G1–G3 dendrimer ligands and the copper MCDs have been used as anti-proliferative agents against different cancerous cells strains and it turned out that effectiveness depends on the type of end fragments. It is important that the free G1–G2 ligands and their copper chelates have nearly the same efficiency. At the same time, no cytotoxic effect was observed with metal-free G3 dendrimer, while the corresponding copper MCD has high activity [84].

It should be noted polyamine Ni MCDs active in ethylene oligomerization (with MAO as a co-catalyst) formed upon interaction of Ni salts with G1 and G2 polyamide dendrimers [85].

Of interest is a comparative study of Cu(I) (hexabenzyl)tris(en) complex and dendrimer analogues with 18 or 54 branch termini (Fig. 5.3) [86]. The Cu(I) MCDs were synthesized by heating CuBr with the chelating dendritic ligands G1, G2 and water-soluble G2 in freshly distilled dioxane at 60 °C overnight. Both parent and dendritic chelates exhibited high activities (yields and the turnover numbers) for click reactions with different substrates. MCDs also showed a positive dendrimer effect associated with steric protection against aerobic oxidation of Cu(I) to bis (μ-oxo)-bis-Cu(II) [86].

Chelation of MX_2 salts, where M = Co(II), Ni(II), Cu(II), Zn(II) and X = Cl, SCN, NO_3, to G0 and G1 multi-coordinating dendritic polyamine ligands (Fig. 5.4) derived from tris(2-aminoethyl) amine and modified on ends using di-3, 4-decyloxyphenyl groups, brings to MX_2L mononuclear MCDs [87]. All MCDs formed with mesogenic low generation ligand G0 are mesoformic apart from Ni(II) nitrate complex, and showed either smectic ambiguous or Col_h phase, depending on used salt. Temperature ranges of meso-phases also strongly depend on origin of a

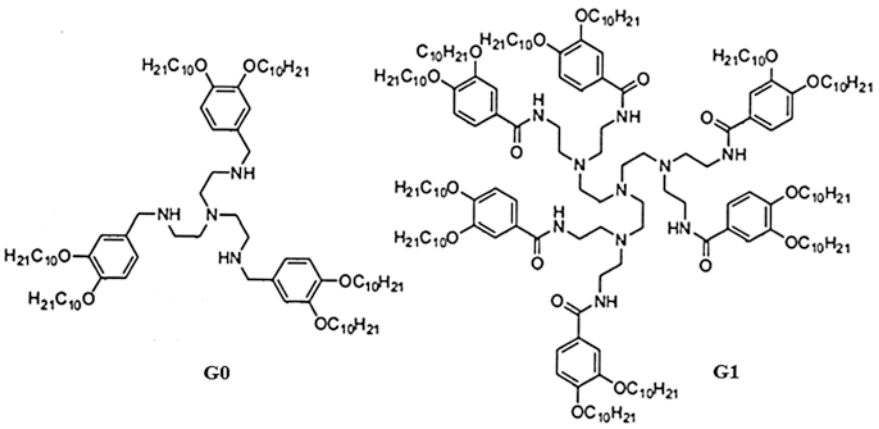

Fig. 5.4 Chemical structure of G0 and G1 dendritic ligands, forming liquid crystalline $MX_2{\cdot}L$ MCDs by binding of metal salts

metal ion, and T_i decrease in sequence Zn(II) > Co(II) > Cu(II) > Ni(II). Chelation of $CuCl_2$ by a higher generation dendrimer G1, which itself shows monotropic Col_h phase [88] and stabilizes a chelate by coordination with fourth central nitrogen atom in dendritic imino-junction, promotes increment of pure stability of Col_h meso-phase from almost room temperature to 140 °C, at which the chelate clears into isotropic liquid. MCDs can have a trigonal bipyramidal coordination geometry, which brings to $[MX{\cdot}L]^+[X]^-$ penta-coordinated ionic chelates or exist as octahedral (and neutral) $MX_2{\cdot}L$ chelates. The latter geometry was observed for Co(II) and Cu(II) chelates, Ni(II) chelates were octahedral; geometry of Zn(II) chelate was not identified. Here formation of columnar meso-phases (and smectic also) follows from nano-segregation between a strongly polar dendritic and metal fragments surrounded by aliphatic chains. With G2 dendrimer as a ligand or with Zn(II) as a central atom, columnar hexagonal phase is formed. In the opposite case lamellar meso-phases are formed.

It is important to notice that radionuclide MCDs are perfect nanoprobes for nuclear medical visualization, in particular, for Single Photon Emission Computed Tomography (SPECT) (^{99m}Tc, ^{111}In, ^{125}I), as well as for Positron Emission Tomography (^{68}Ga). Also a special attention is paid to radiolabeled (^{64}Cu, ^{18}F, ^{76}Br, ^{68}Ga, ^{111}In) MCDs targeting $\alpha_v\beta_3$ integrin, because this is a reliable strategy for estimation of angiogenesis presence, one of the best studied, and for targeted biological process.

In this view, very interesting precursors for development of chelating dendrimers are aliphatic G1–G8 polyether dendrons with a core of *p*-toluene sulfonyl ethyl ester as easily removed protective group, which can be efficiently replaced by different nucleophiles [89]. Thus, tridentate bis(pyridyl)amine chelating ligand, which forms stable complexes with Tc(I) and Re(I), was integrated into a dendrimer core using chemistry of amidation. Chelation of a ligand core with ^{99m}Tc radioactive element was achieved for G5–G7 within 10 min, and as a result, regioselective radiolabeling

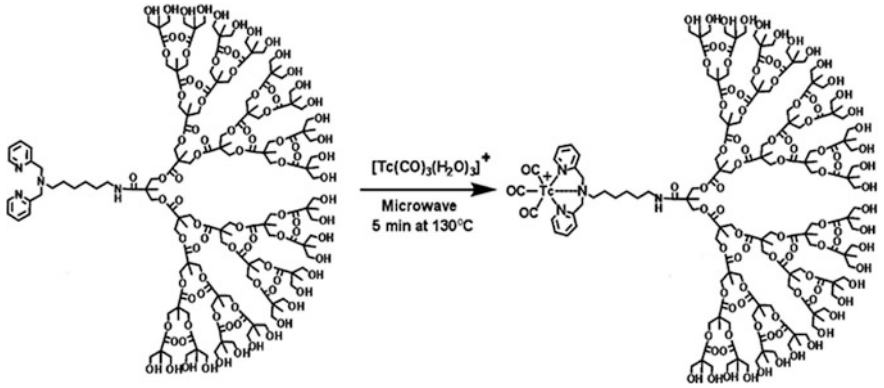

Scheme 5.2 Chelation of dendritic tridentate bis(pyridyl)amine ligand with ^{99m}Tc radioactive element

of dendrimers was reached (Scheme 5.2). It is important that biodistribution of radiolabeled dendrimers can be easily estimated using SPECT.

It should be noted using CuAAC for the terminal functionalization of G1–G3 dendrons based on poly (2,2-bis(hydroxymethyl)propanoic acid) [59]. The subsequent modification of the prepared dendrons at the core by a dipicolylamine allows to radiolabeling with ^{99m}Tc for biomedical applications.

Of interest are ^{111}In-radiolabeled dendritic nanoprobes, in vitro and in vivo tumor targeting efficiency of which was estimated in a mouse melanoma model [90]. It occurs that tumor uptake reaches such high values as 12.7 ± 1.6% ID g^{-1} at 4 h after intravenous injection in comparison with 1.5 ± 0.5% ID g^{-1} for non-functionalized nanoprobe, and correlates with a dendrimer multivalency.

The similar dendritic tridentate bis(pyridyl)amine ligands were reacted with a Cu (II) ion solution to form the targeted MCDs with 6, 12, 33, 104, and 232 Cu ions for G2–G6 dendrimers, respectively (Scheme 5.3) [91].

An important observation was made during studying chelation of Cu(I) salts with dendronized quinoline ligand containing terminal acid or ester groups [92]. It

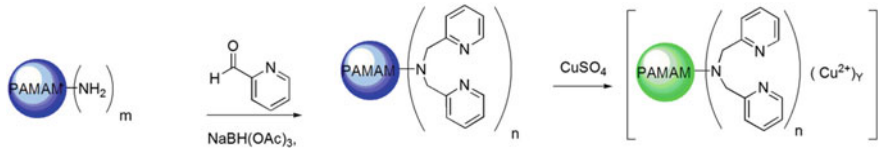

Scheme 5.3 Synthetic approach to prepare MCD based on tridentate bis(pyridyl)amine ligand

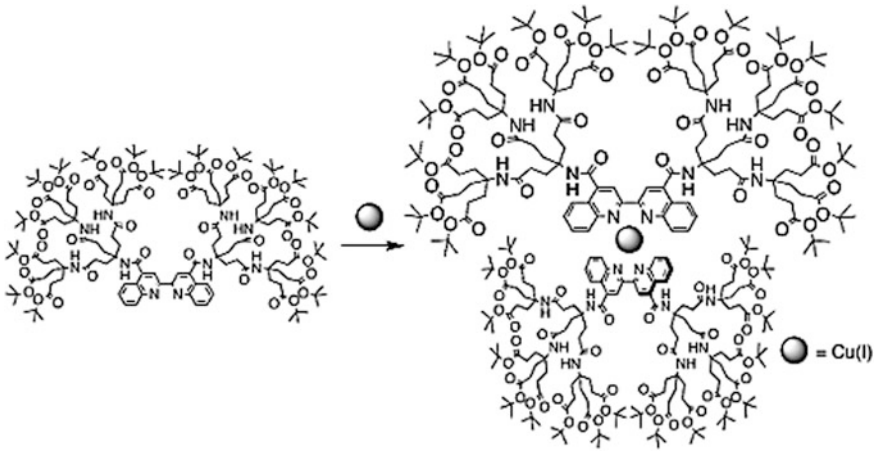

Scheme 5.4 Scheme of chelation of Cu(I) salts with dendronized quinoline ligand

is important that treatment of a ligand with Cu(I) salt brings to intermolecular cross-linking with quantitative formation of stable MCD with Cu(I) core (Scheme 5.4).

Among the numerous examples of MCD based on bpy chelating ligands, it should be noted a pH-switching metal coordination established during interaction between a chelating peptide dendrimer obtained via formation of double thioether bond between 5,5′-bis(bromomethyl)-bpy and two equivs of the peptide dendrimer $(Ac\text{-}Glu\text{-}Ser)_8(Dap\text{-}Glu\text{-}Ala)_4(Dap\text{-}Amb\text{-}Tyr)_2Dap\text{-}Cys\text{-}Asp\text{-}NH_2$ (Dap = branching 2,3-diaminopropanoic acid, Amb = 4-aminomethylbenzoic acid) on the one hand, and Fe(II) salt on the other hand (Scheme 5.5) [93]. In particular, for pH 4.0, a dendrimer links Fe(II) with formation of expected tris-coordinated dendrimer complex FeL_3 ($K_f = 2.1 \times 10^{15}$ M^{-3}), while for pH 6.5 mono-coordinated complex FeL ($K_f = 2.1 \times 10^5$ M^{-1}) is formed due to electrostatic repulsion between polyanionic dendrimer branches.

Of interest is the study a peptide dendrimer library with a 5,5′-disubstituted bpy core to determine the effect of the branched structure on the chelating ability of ligands at the core [94]. For this dendrimer, the main factor is the nature of amino acids placed at the dendrimer periphery, at that chelation is inhibited by cationic residues and promoted by anionic residues.

Studies of chelation of 6- and 18-armed dendritic polyallyl- and polyferrocenyl-containing bpy ligands produced by the coupling reaction of 4,4′-bis(bromomethyl)-bpy with AB_3- and AB_9-dendrons and $RuCl_2(bpy)_2$ showed that, contrary to bulk 18-ferrocenyl-bpy ligand, 6-allyl and 18-allyl-bpy ligands take part in the chelation giving respective Ru(II) MCDs (Fig. 5.5) [95]. In the case of ferrocenyl-bpy ligand steric volume of two nonaferrocenyl wedges in 4,4′-position of a bpy fragment prevents transformation of a transoid structure of a ligand into a cissoid structure necessary for chelation with a metal. Therefore, 18-ferrocenyl Ru(II) dendrimer was not obtained.

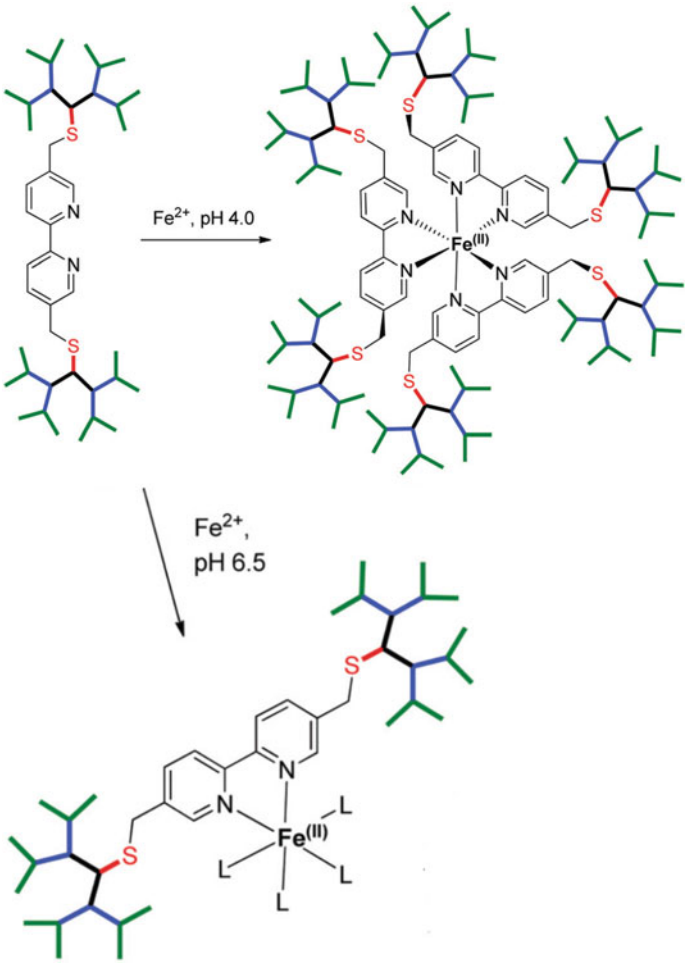

Scheme 5.5 A metallopeptide dendrimer peroxidase enzyme model. Monodentate ligand L = H_2O or amino acid side chains such as carboxylate from glutamate

MCD of molecular type with bpy ligands was obtained by reaction of MnBr $(CO)_3$ with chelating DAB-PPI dendrimers (Scheme 5.6) [96]. Dendrimers G1 contained 4 metal chelate units, and G2 contained 8 metal chelate fragments. It occurs that both dendrimer generations are stable in darkness in aqueous buffer solution during 16 h, but show photoactivated CO gas release upon excitation at 410 nm.

Luminescent Ir(III) MCDs with general formula $[\{Ir(ppy)_2\}_nL]^{n+}$, where n = 1, 3, 4, 8, L = poly(bpy)dendrimer, are obtained through placing the transition metal centers at the periphery of the dendritic core, thus increasing a fraction of metal complex per molecule and, probably, increasing photophysical response [97].

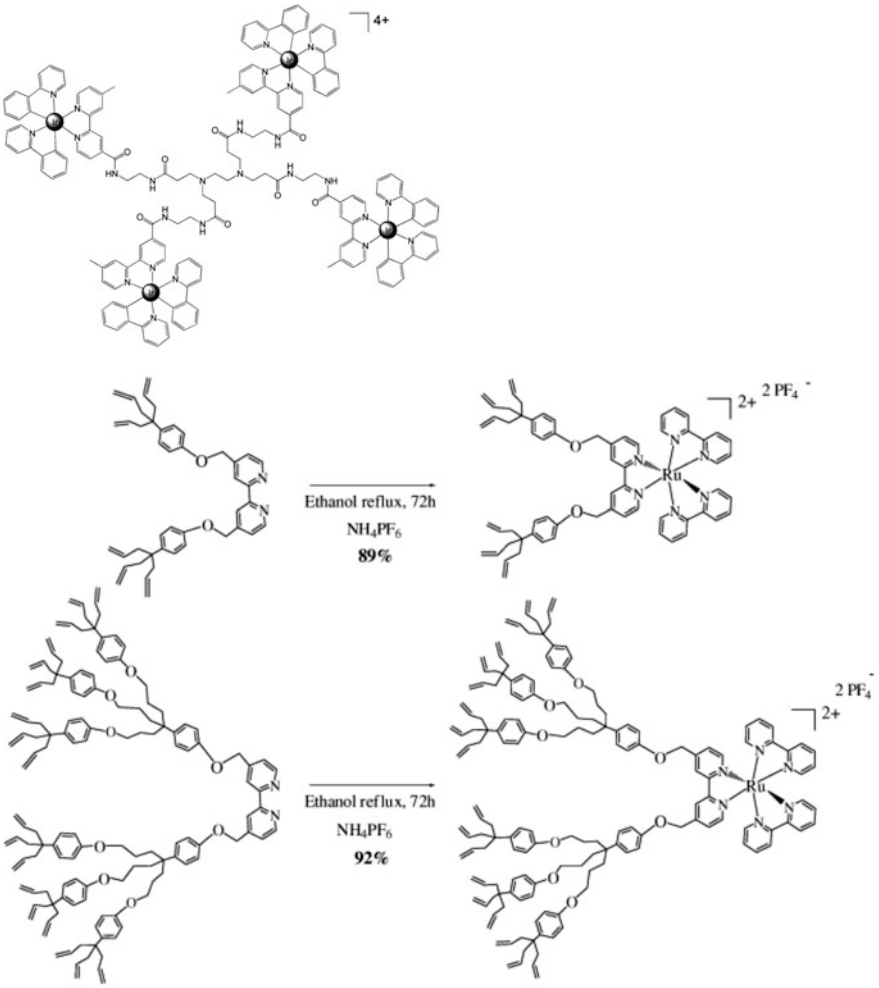

Fig. 5.5 Scheme of chelation of 6- and 18-armed dendritic polyallyl-containing bpy ligands with $RuCl_2(bpy)_2$

An assumption was pronounced that dendritic chelates are accumulated in the Golgi apparatus; therefore, they can be used as Golgi staining agents. These results confirm that integration of dendritic ligands can change biological properties of metal chelates.

Using the carbohydrate cancer marker linked to a bpy core, square planar chelates were obtained by simple addition of Cu(II) sulfate (Scheme 5.7) [98]. Cu(II)-chelated 2-acetamido-2-deoxy-D-galactopyranoside derivatives containing four and eight fragments were prepared from an aqueous solution in an efficient manner (H_2O, 48 h, 23 °C). After 48 h of stirring, the bluish solution was lyophilized to form light bluish-purple colored powder.

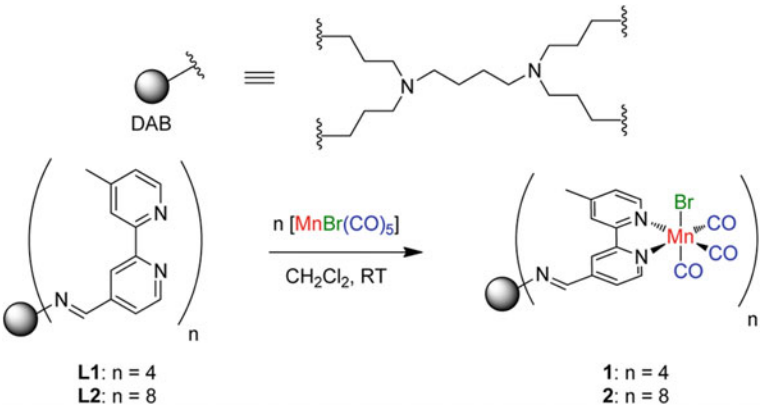

Scheme 5.6 Synthesis of tetra- and octanuclear Mn MCD **1** and **2**

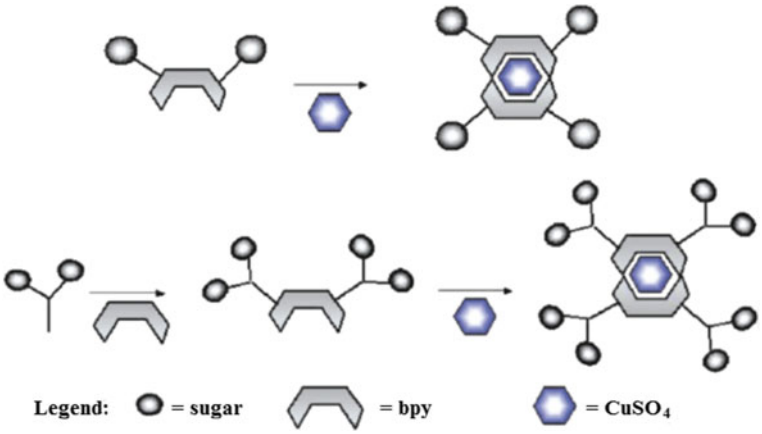

Scheme 5.7 Scheme of synthesis of Cu(II)-chelated 2-acetamido-2-deoxy-D-galactopyranoside derivatives

It should be noted using MCD based on poly (aryl ether) with a bpy core as catalysts for Diels-Alder and three-component condensation reactions [99]. The MCD was prepared in situ in dichloromethane by interaction of chelating dendrimer and $Cu(OTf)_2$.

Considerable interest is the study [100] of the coordination of Pt(II) ions by G4 PAMAM Ru-MCD containing 32 Ru bpy chelates at the periphery [101, 102]. Titration of Ru-MCD by K_2PtCl_4 solution leads to a decrease in the MLCT band and an increase in a tail below 500 nm (Fig. 5.6, left). Upon binding $\sim$20 equivs of Pt(II) by Ru-MCD, a plateau at 620 nm is observed (Fig. 5.6, right, inset) that allows to calculating the stoichiometry of the heterometallic complex.

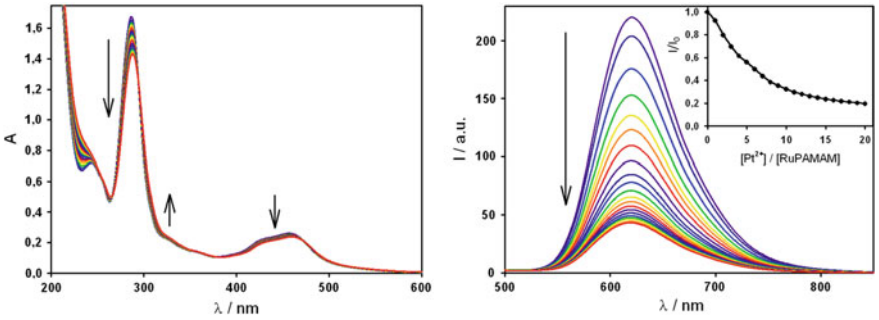

Fig. 5.6 Absorption spectra (left) and emission spectra (right) of a 1.47×10^{-6} M solution of MCD in H_2O upon titration with K_2PtCl_4. The inset shows the normalized emission intensity changes at 620 nm (λ_{ex} = 375 nm)

Table 5.1 Stability constants of the formed Cu(II) MCD

Generation	Metal	Stoichiometry	Log K	Solvent
G0	Cu(II)	3:1	16.4 ± 0.8	$CHCl_3$
G1	Cu(II)	3:1	17.5 ± 0.9	$CHCl_3$
G2	Cu(II)	3:1	15.6 ± 0.7	$CHCl_3$
G3	Cu(II)	3:1	16.6 ± 0.7	$CHCl_3$

Chelation of Cu(II) with dendritic oxybato-phen ligands (G0–G3) synthesized using 4,7-bis(4′-hydroxyphenyl)-phen treatment with respective Fréchet type dendrons carrying benzyl bromide function in a focal point was studied by liquid-liquid extraction using ^{64}Cu isotopes. Formation of 1:3 chelates (Cu:L) is shown, in which Cu(II) chromophor has an expected distorted square-planar geometry with two phen donor ligands coordinated with Cu(II) center. The third dendritic ligand, as is assumed, is bound by secondary interactions. Stability constants of 1:3 complexes are log K ≈ 16 in $CHCl_3$ (Table 5.1) [103].

The MCDs are obtained built around $[Ru(4,7\text{-diphenyl-phen})_3]^{2+}$-type core containing peripheral phenyl residuals [104]. Convergent synthesis of ligands is reached by conjugation of dendritic branches containing focal amino group with chelating phen precursor bringing to formation of sulfonamide bonds. MCD G0 to G2 and monomer analogue (Fig. 5.7) were prepared by irradiation in a microwave oven. In particular, ethylene glycol solution of Ru(III) chloride and the corresponding ligands was heated for 2 min at 200 W in the presence of a few drops of water. The appearance of bright orange color indicates the formation of the $[Ru(4,7\text{-diphenyl-phen})_3]^{2+}$-type complexes. Chelation of Ru ions gives respective MCDs containing up to 24 peripheral phenyl units in the case of the greatest dendritic structure. Dendritic effect is well seen during transition from G0 to G2, which is confirmed by increase in lifetime of excited state in aerated acetonitrile and increase in emission quantum yields as compared with low molecular weight analogues.

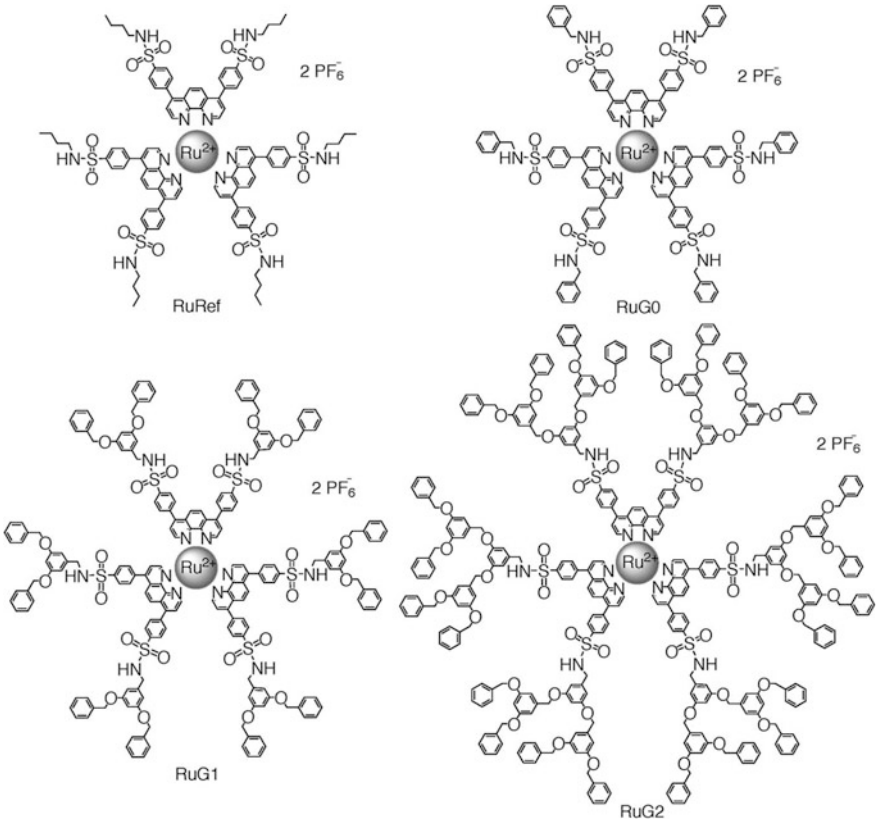

Fig. 5.7 G0–G2 MCD with phenyl end groups and reference chelate with butyl terminal groups

In contrast to chelating monomer, the Job plot for G2 of 2,9-dimethyl-phen grafted dendrimer shows two separated maxima which correspond to Cu(I) ions bound to one or two phen fragments (Fig. 5.8) [105]. This double maximum indicates that 2:1 or 1:1 chelates will predominantly exist for each Cu(I) ion depending on the molar ratio chosen.

Of substantial interest is study of tpy-containing MCD. At that, at present, it is possible to localize tpy chelating fragments in certain parts (core, cavities, focal or branching points, termini) of the dendritic architecture [5, 106].

As a typical example, we note the symmetric homoleptic and asymmetric heteroleptic benzyl ether dendrimers with $[Ru(tpy)_2]^{2+}$ core containing an electrochemically active fragment included in a polyether dendritic shell [107]. However, a purple colored side product of undefined structure was also formed together with the reddish brown bis(tpy)-Ru(II) MCD. It is important that main reaction product can be purified by column chromatography because the side product is much less polar.

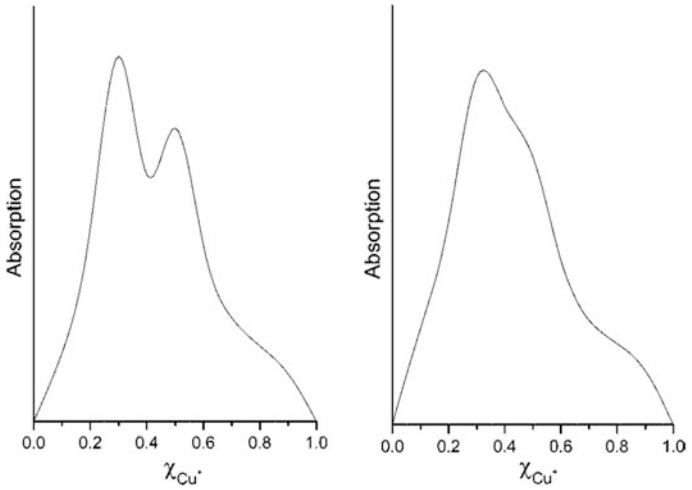

Fig. 5.8 Normalized Job plots for mixtures of the chelating phen dendrimer and $CuPF_6$ (left), and of the chelating phen monomer and $CuPF_6$ (right)

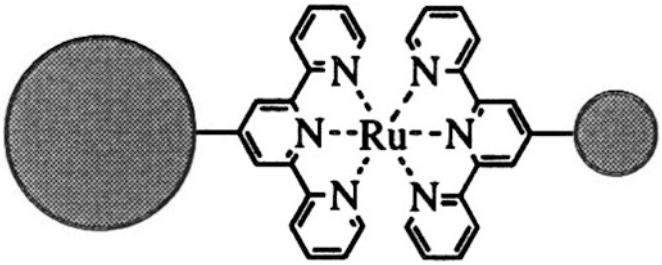

Treatment of G1–G3 dendrons with MX_n brings to formation of corresponding $[Co(tpy)_2]^{2+}$, $[Fe(tpy)_2]^{2+}$ and $[Ru(tpy)_2]^{2+}$ Fréchet type MCDs [108]. In this case the rotational freedom within the dendritic wedge leads to a rich diversity in conformational space. Studies of these structures containing a metal chelate core were carried out using X-ray diffraction analysis for G1 type.

It should be noted 1,3,5-phenylene-based MCD including a Ru-bis(tpy) complex, which was obtained by treatment of chelating dendrimer with $RuCl_3 \cdot 3H_2O$ with the following anion exchange with hexafluorophosphate ion [109]. The terminal *tert*-butyl groups allow to completely encapsulates the $Ru(tpy)_2$ cores and enhances the MCD hydrophobicity.

The homo- and heteroleptic $[Ru(tpy)_2]^{2+}$ chelates containing hydrophilic and hydrophobic dendrons were obtained [110] for development of amphiphilic vectors for potential gene delivery. Owing to staged assembly regime, dendrons can have the same or different degrees of lipophilic or hydrophilic character.

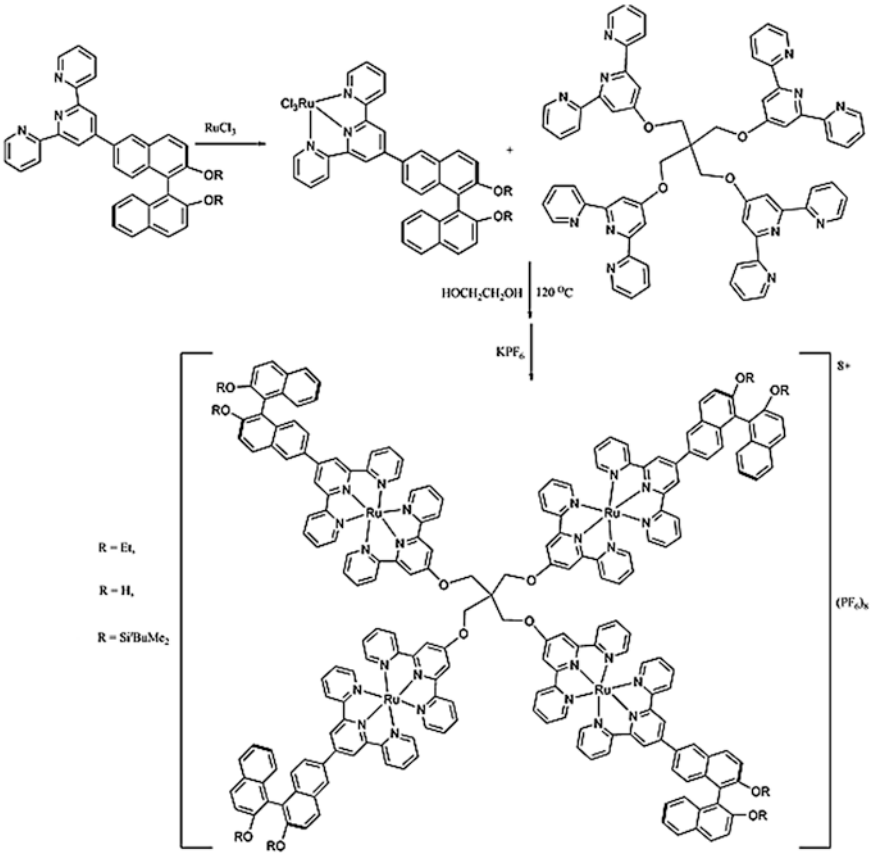

Scheme 5.8 Scheme of synthesis of Ru-tpy MCD with binaphthyl groups

Chelation of Ru(II) with π-conjugated oligothienylene-ethynylene dendrons containing tpy ligands has brought to MCDs with interesting spectroscopic properties [111]. In particular, broad absorption spectra covering from 250 to 600 nm and high molar extinction coefficients are characteristic for the prepared MCDs. The MLCT emission of the MCDs were significantly red-shifted (up to 115 nm) compared to the parent $[Ru(tpy)_2]^{2+}$ chelate.

Apart from abovementioned MCD with external counter-ions, generally neutral MCD was obtained [6, 112] containing four $[Ru(tpy)_2]^{2+}$-linked centers with internal carboxylate groups.

Undoubtedly introduction of chirality and also light-sensitive $[Ru(tpy)_2]^{2+}$ complexes into a dendritic sphere is interesting for production of new macromolecules with optical properties. For these purposes Fréchet type benzyl-bromide dendrons were functionalized with binaphthyl-tpy, which then formed a complex with tetrakis(tpy-4′-oxymethyl) methane through of Ru(III)/Ru(II) chemistry applied (Scheme 5.8) [113]. It is important that enantiopure compound is formed as a result of this reaction.

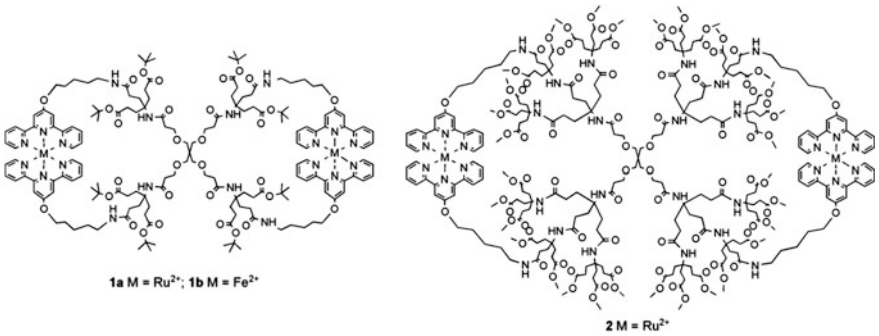

Fig. 5.9 Bis-Ru(II) spirometallodendrimers

Treatment of each generation of the chelating dendrimers with $RuCl_3 \cdot 3H_2O$ followed by addition of excess NH_4PF_6 gives after chromatography bis-Ru(II) spiro MCDs with 41 and 47% yields, respectively (Fig. 5.9) [114]. Additional evidence of easy intramolecular cyclization is obtained using the reaction of tetra-tpy dendrimer with two $FeCl_2 \cdot 4H_2O$ equivs giving (92%) respective pure Fe-spiro dendrimer. On the whole, these examples of macromolecular ring closures, are expected to provide entrance into dendrimer-based molecular devices using integration of different metals, ligands, and oxidized metal states.

PAMAM dendrimers containing en core with $[Ru(tpy)_2]^{2+}$ surface fragments are obtained by formation of peptide bond [115].

A method of production of series of MCDs based on mono-, bis-, and tris-Ru-tpy chelates with thiophene arms for photovoltaic applications is developed [116]. Energy levels of these MCD can be efficiently regulated not only by different generations of dendritic thiophene arms, but by their π-conjugated core ligands having different electron-donor (triphenylamine) and electron-acceptor (benzothiadiazole) fragments. Among different generations (G1–G3) of dendrimers, G3 has the highest efficiency of energy transformation in each series of dendrimers based on Ru chelates.

Most lanthanide ions in their stable trivalent state are luminescent and have high magnetic anisotropy [117] and are, therefore, promising basic components in projecting of multifunctional liquid crystals, for example, lanthanidomesogens [118, 119]. Therefore, using such a concept, G0 and G1 dendritic luminescent lanthanidomesogens are obtained by the reaction of $Ln(NO_3)_3$ with 2,6-bis-[(*N*-ethyl benzimidazol-2-yl)pyridine] fragments, specific central tridentate chelating ligand for Ln(III) ions [120], which has 5- and 5′-positions occupied by cyanobiphenyl-containing dendritic arms [121, 122].

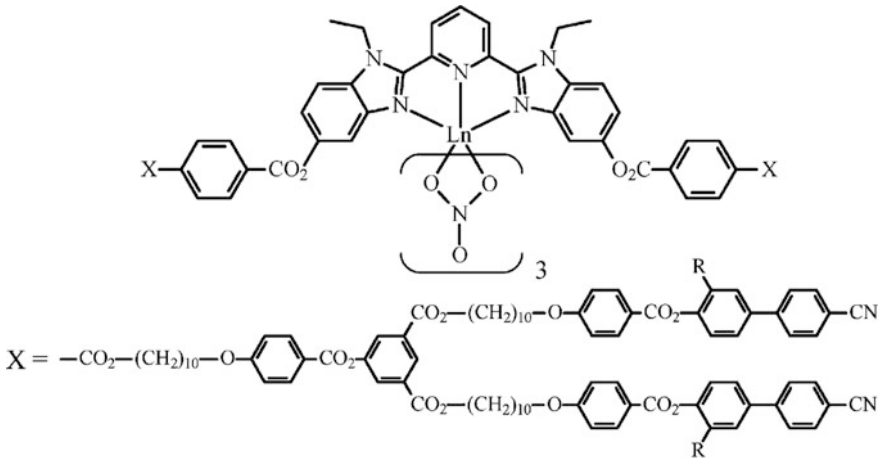

Ligands G1 show simple N single phase from 50–70 to 238 °C (R = H) and 197 °C (R = Me), and from 70–80 to 324 °C for non-methylated (R = H) and down to 205 °C for completely methylated (R = Me) G0 homologous chelates. This general thermal behavior implies some weakening of intermolecular cohesion in N phase as a result of limiting of lateral superposition between methyl-substituted cyanobiphenyl groups. In other words, peripheral cyanobiphenyl dendrimers impose microphase organization compatible with smectic mesomorphism, in which bulk nine coordinated lanthanide cores located between separated mesogenic sublayers are composed of parallel cyanobiphenyl groups.

Independently on generation, $Ln(NO_3)_3$ coordination brings exclusively to formation of monomer chelates with the lowest lanthanide ions ($[Lu(NO_3)_3{\cdot}L]$), while with intermediate (Ln = Eu–Tb) and big (Ln = Pr–La) lanthanide ions, monomer and dimer chelates exist in thermodynamic equilibrium ($2[Ln(NO_3)_3{\cdot}L] \leftrightarrow [Ln(NO_3)_3{\cdot}L]_2$). This equilibrium depends on formation of lanthanide-size-dependent construction of intermetallic nitrate-bridges and methyl substitution by dendritic ligand strands. Only G1 MCDs $[Ln(NO_3)_3{\cdot}L]$ (R = H, Me) are mesomorphous. Bilayer SmA meso-phase is observed between 80–100 and 190–200 °C (R = H, Ln = Lu, Tb, Gd, Eu, Pr), whose structure consists of central cores located between decoupled mesogenic sublayers made by parallel alignment of cyanobiphenyl groups. For methylated series (R = Me) polymorphism is observed between 80–100 and 145–160 °C: chelates with big lanthanide cations (Ln = La, Pr) give only bilayer SmA meso-phase (with periodicity d from 10 to 12 nm) over entire temperature range, while for the intermediate range and small lanthanide chelates, respectively, additional lamellar phase appears above SmA or SmA phase with comb-like interdigitated structure (Ln = Gd, Tb, d = 6 nm) was discovered, or N (Ln = Eu, Lu, Y) phase, though only in the range from 5 to 10 °C. The best segregation for different segments of molecules is reached in formation of nitrate bridges in $[Ln(NO_3)_3{\cdot}L]_2$ dimer chelates, whereas intermolecular shift of strands is

responsible for decrease in interlayer separation in the lamellar phases and/or formation of N phase, probably correlates with a tendency of chelates to existence as monomer types, but not in a form of mixture of monomer and dimer types. Presence of N phase rarely observed in lanthanidomesogens [122] is also very interesting if it advances their solubilization with N hosts and their possible application in display devices.

It should be noted that tpy groups were grafted to phosphorus G1–G4 dendrimers, giving family of chelating dendrimers [123]. The catalytic system involving Sc $(OTf)_3$ and these dendritic tpy ligands promotes the Friedel-Crafts acylation of different aromatic compounds under microwave irradiation with high yields.

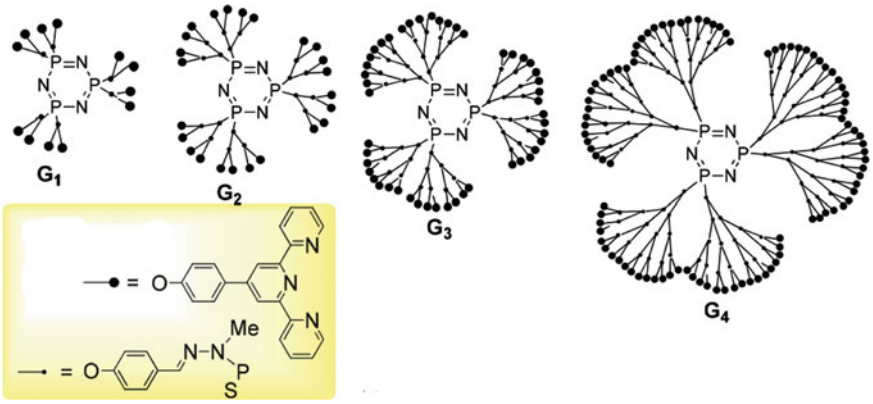

We note neutral and cationic bis(pyrazolyl)methane Pd(II) chelates with poly (aryl ether) of Fréchet type dendrons which were prepared by the interaction of $[PdCl_2(COD)]$ with corresponding bis(pyrazolyl)methane, whereas the chlorido (methyl)Pd(II) chelates were synthesized using [PdClMe(COD)] (Scheme 5.9) [124].

Scheme 5.9 Palladium MCDs

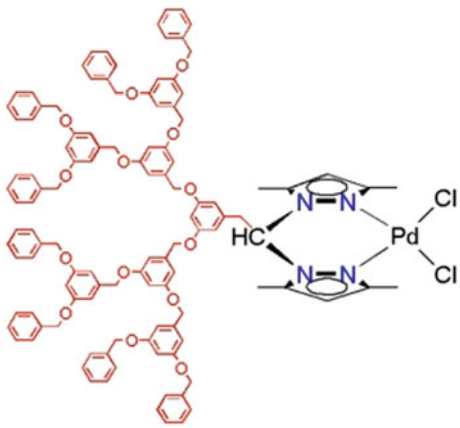

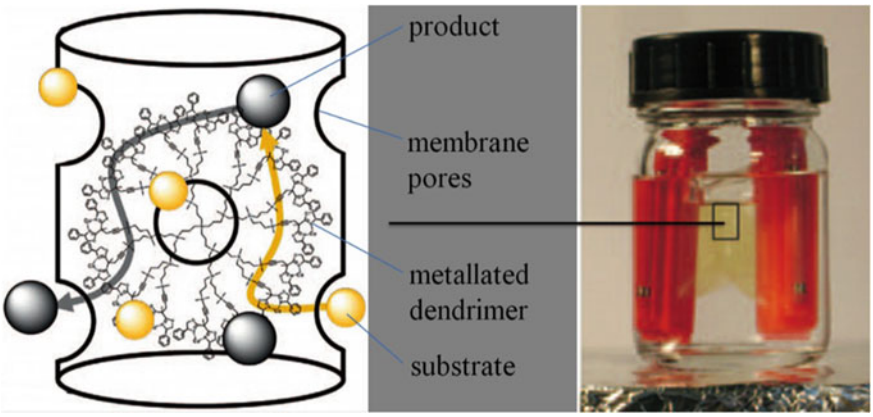

Fig. 5.10 General setup for the recycling using the «catalyst in a tea bag» principle

The Pd MCDs were used as precursors of a catalyst in Heck reaction between *p*-iodotoluene and MA.

An interesting example is the so-named «catalysis in a tea bag» (Fig. 5.10) [125]. At first, bis- and tris-oxazolines with a spacer in the ligand backbone are covalent fixed on carbosilane dendrimers, and then are used as chelating ligands for recyclable Cu(II) catalysts that were immobilized in a membrane bag.

It should be noted using dendritic azabis(oxazoline) ligands in Cu(II)-catalyzed asymmetric benzoylations [126].

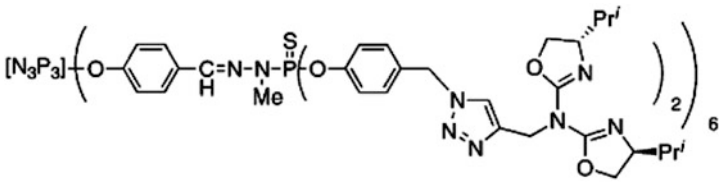

Of interest are mono- and polynuclear Pd-MCDs based on a 2-pyridyl-1,2,3-triazole chelating ligand in which solubility of the MCDs decreases with increasing metal number (Fig. 5.11) [127].

It should be noted water-soluble triazole dendrimers containing the two triazole rings at each bis-(methylol)propionic acid branching site, which are efficient chelating pockets for some transition metals. Thus, the $[PdCl_2(PhCN)_2]$ chelation with these hydrophilic dendritic ligands is completed within 5 min according to ^1H NMR analysis in situ (Fig. 5.12) [128]. The signals of several protons are shifted downfield in comparison to the starting dendrimer, suggesting a deshielding process as a result of

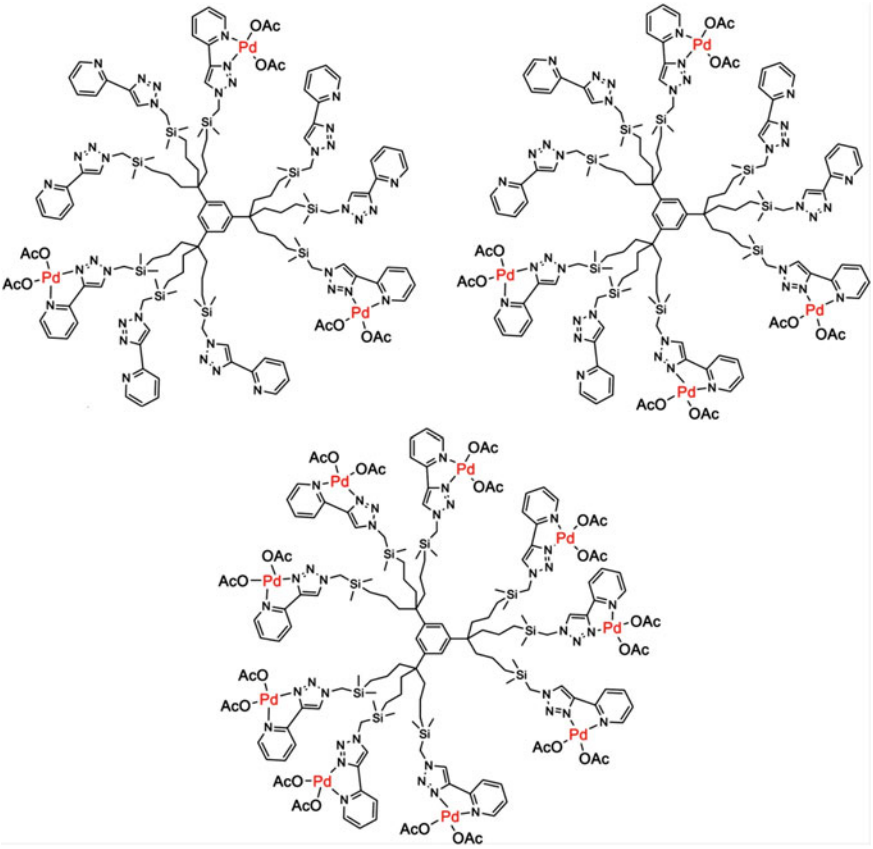

Fig. 5.11 Isolated MCD catalysts containing three, four, and nine metal centers with solubility decreasing with increasing their number

changes in dendrimer architecture and appearance of electron-withdrawing groups. Besides, the triazole protons (Fig. 5.12a, j) are facing inward in the chelating dendrimer but facing outward after the chelation with $PdCl_2$ (Fig. 5.12b). It is shown that the chelation efficiency (CE) is equal to 95 ± 5% for all dendrimers, suggesting the formation of MCDs with 3, 9, and 21 Pd-containing fragments for G1, G2, and G3, respectively.

Wide application in the synthesis of MCD has dendrimers containing chelating 2,6-bis(1,2,3-triazole-4-yl) pyridine (btp) fragment obtained through one-pot click-reaction [129].

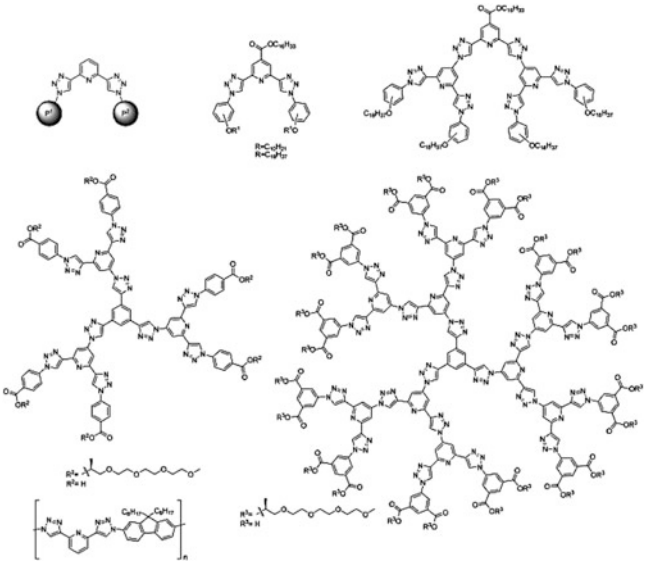

Also numerous examples of cyclometalated Ir(III) dendrimers should be noted, which are used as phosphorescent polymers for OLEDs [130]. These MCDs can be fixed on different substrates, for example, PS matrix, and additionally contain other

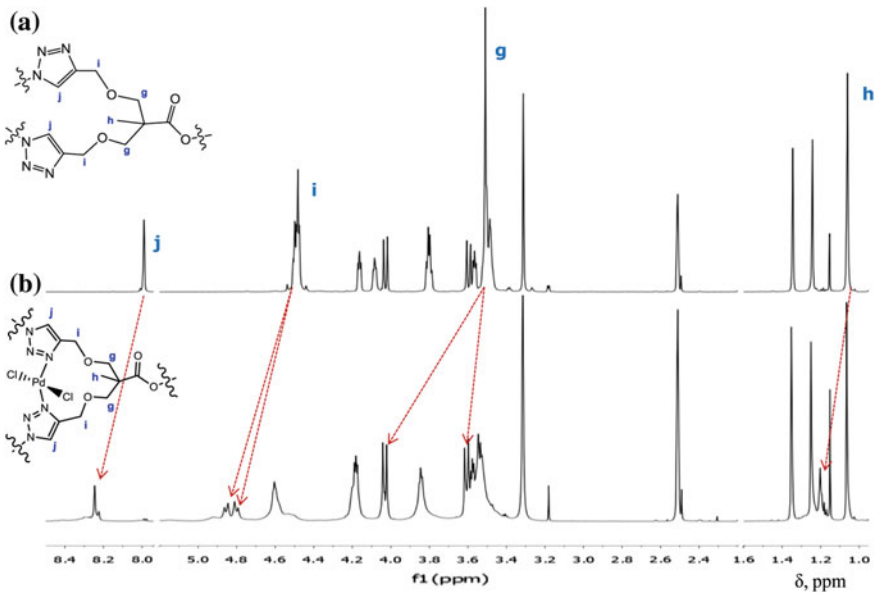

Fig. 5.12 ^{1}H NMR spectra of **a** chelating d-[G2] dendrimer and **b** Pd(II) MCD of d-[G2]. Analysis conditions: 600 MHz, DMSO-d_6, 298 K

interesting functional groups, such as, in particular, Cz charge-carrying fragments, which, besides, can prevent aggregation of chromophores [131].

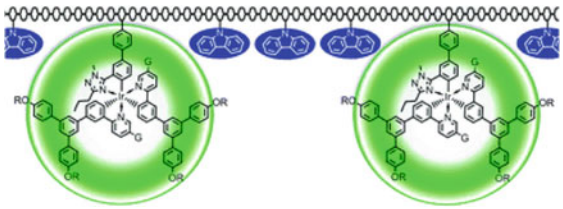

Devices produced using these MCDs, showed high EQE 11.0% (37.3 cd A^{-1}) at 100 cd m^{-2} and 8.3 V, at that, the best efficiency is achieved by mixing of twice dendronized copolymer with 50 wt% of 4,4′-bis(*N*-dicarbazolyl)biphenyl, which brings to 14,7% EQE (48.3 cd A^{-1}) at 100 cd m^{-2} and 9.3 V.

5.1.2 N,P-Ligands

Among MCD of molecular type, a substantial place has chelates with phosphorus-containing donor ligands [21, 22, 132–134]. One of the typical examples are the dendrimers incorporating γ-iminophosphine Pd chelates on the surface, which were obtained by the interaction of $PdCl_2$(COD) with N,P-donor chelating ligands (one Pd per N,P-ligand) [135]. An X-ray diffraction study corroborated the postulated structure in which the $PdCl_2$ unit is linked both to the imino nitrogen atom and to the phosphino group. The chelates were then used as catalysts for Stille couplings with various substrates.

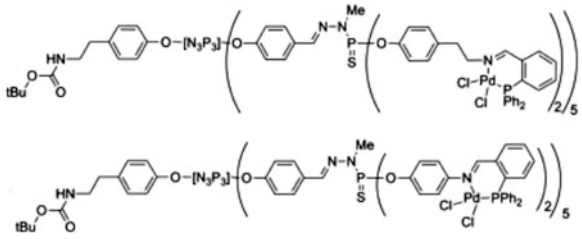

Of interest is using hexachlorocyclotriphosphazene for the preparation of bifunctional «off-center» dendrimers including one protected amine linked to the core and phosphine imines (N,P-ligands) as surface fragments [136]. The sequent interaction of the prepared dendrimers with $PdCl_2$(COD) leads to the MCD of the N,P-ligands.

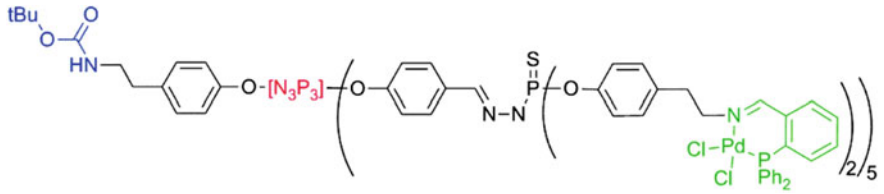

The condensation of the aldehyde terminal groups with (2S)-2-amino-1-(diphenylphosphinyl)-3-methylbutane gives the chiral G3 dendrimer, ended by 24 chelating N,P-ligands [137]. Dendrimer chelation of $[Pd(\eta^3\text{-}C_3H_5)Cl]_2$ in situ leads to a catalyst used in asymmetric allylic alkylations of *rac*-(E)-diphenyl-2-propenyl acetate and pivalate.

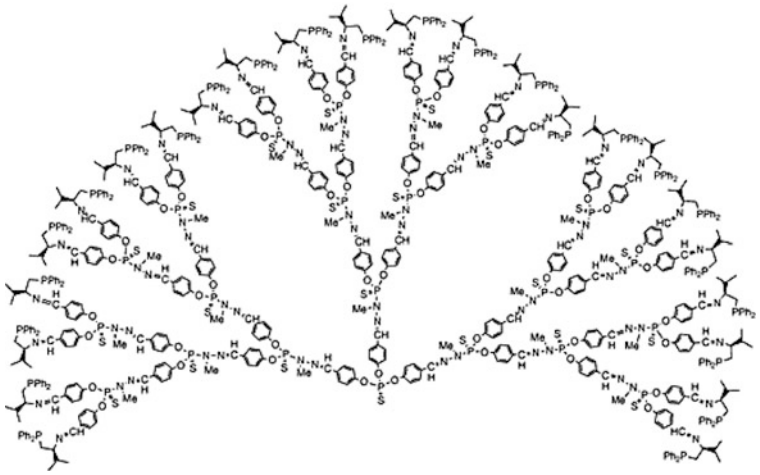

A family of N,P-chelating dendrimers up to G3 is obtained generated from a core based on 15-membered triolefinic azomacrocycle with the following fixing of γ-iminophosphane groups [138]. The dendrimers in dichloromethane solution were treated with stoichiometric amounts of $PdCl_2(COD)$ for 3 h to form the targeted MCDs with good yields. It is interesting that the MCDs were synthesized in anhydrous THF; however, after precipitation and drying, their solubility changes and they are only soluble in DMF.

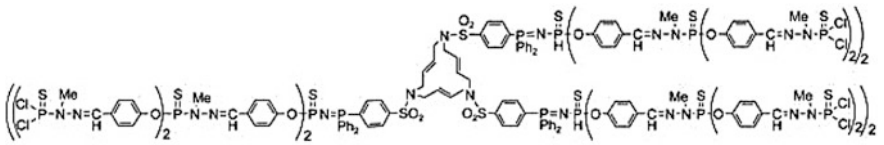

It should be noted the modular synthesis of dendritic phosphinooxazoline (PHOX) ligands and their iridium chelates with $BArF^-$ as the counter-anion [139]. The prepared MCDs were used in the Ir-catalyzed asymmetric hydrogenation of 2,4-diaryl-1,5-benzodiazepines, in which an obvious positive dendritic effect on catalytic activity was observed.

5.1.3 Metal Chelates with P,S-Ligands

A chiral ferrocenyl phosphine-thioether P,S-ligand, functionalized with a phenol group, was used for the substitution reaction on $P(S)Cl_2$ terminal groups, affording a series of chiral G1–G4 dendrimers [140]. The chelating dendrimers were used as ligands for the asymmetric allylic alkylation of *rac*-(E)-diphenyl-2-propenyl acetate. The chelation was carried out in situ by mixing the dendrimers ended by the ligands with $[Pd(\mu^3\text{-}C_3H_5)Cl]_2$, using a stoichiometry of one Pd per P,S-ligand.

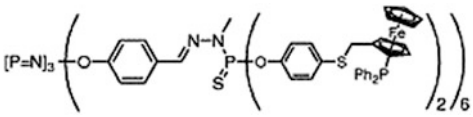

5.1.4 Metal Chelates with P,P-Ligands

The chiral diphosphine-functionalized dendrimers based on carboxyl-linked C2-chiral pyrphos ligand (pyrphos is 3,4-bis(diphenylphosphino)pyrrolidine) and G0–G4 PPI dendrimers form cationic rhododendrimers containing up to 32 metal centers (for the G4 species) [141]. The complete chelation was demonstrated by ^{31}P NMR spectroscopy and the observation of the coordination-shifted AB part of the ABX spin system (δ_A = 33.9, δ_B = 32.9; $^1J_{Rh,P}$ = 150 Hz; $^2J_{P,P}$ = 28 Hz). The similar Rh-MCDs were prepared with PPI and PAMAM dendrimers carrying from 4 to 64 chelating fragments at their periphery in dichloromethane (Scheme 5.10) [142]. It is interesting that the chelation was complete within seconds.

To explore the potential for a conformationally driven asymmetric induction of a catalytic dendrimer a pair of G1 dendrons at the 3 and 3′ positions of a 2,2′-bis

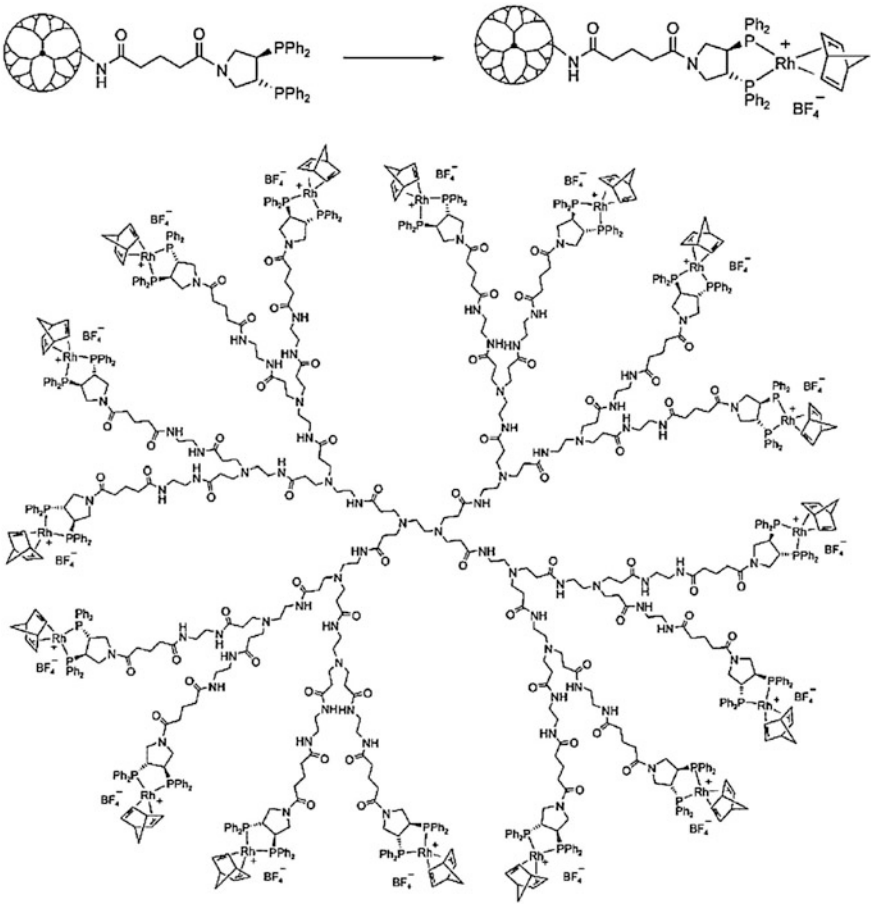

Scheme 5.10 General synthesis of the pyrphos-Rh(nbd) chelates, and {G2}-PAMAM-{glutaroyl-pyrphos-Rh(nbd)BF_4}$_{16}$

(diphenylphosphinoxy)biphenyl scaffold was prepared (Fig. 5.13) [143]. The rhodium MCDs based on these P,P-ligands interconvert among a minimum of six diastereomer conformations. Therefore, a dendritic catalyst directs the stereoselectivity of a catalytic process by dynamically transferring the conformational chirality of a dendritic architecture to the catalytic center.

PEI dendrimers up to the G3 modified by alkyldiphenyl phosphine ligand were chelated with Pd(COD)Cl_2 to give phosphine-Pd(II) MCDs (Fig. 5.14) [144]. The ^{31}P NMR spectra of Pd(II) chelates (4, 8, 12 and 16) indicated that all the phosphorus atoms were coordinated to the metal ion in an equivalent environment and MCDs have a similar bidentate mode of complexation, as in the monomer metal chelate.

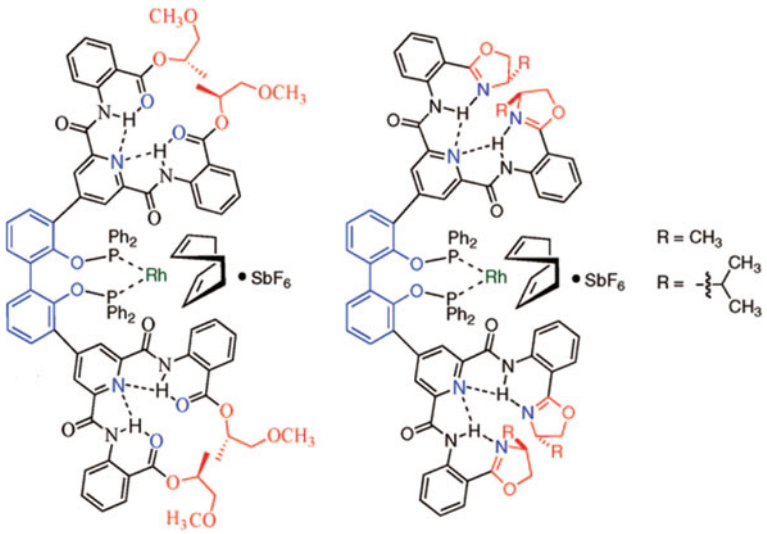

Fig. 5.13 Structure of $LRh^{+}(COD)SbF_6^{-}$ MCDs

It should be noted the chelating dendrimers with bis(diphenylphosphinomethyl) amino fragments linked to either L-tyrosine or tyramine methyl ester which form Pd-MCDs in situ [145].

Of interest is the chelation of $RuCl_2(PPh_3)_3$ by G1 dendron with diphosphine chelating fragments at the core [146]. It is important that in the MCD the metal has a square-based bi-pyramid configuration with the four phosphorus atoms of both diphosphines in a single plane and two chlorine atoms in axial positions.

Polyphosphines are used for integration of 32 or 64 $[Ru_3(CO)_{11}]$ cluster units on the ends of phosphine branches. These reactions were carried out using electron-transfer-chain catalysis with 19-electron complex $[FeCp(C_6Me_6)]$ as catalyst [147]. MCDs were obtained as a very air- and light-sensitive red powder in 50% yield after drying under vacuum for several days.

G3 MCDs with either 24 terminal palladium or ruthenium diphosphine chelates or one ruthenium diphosphine chelate located at the core were prepared by mixing the chelating dendrimers with $PdCl_2$ and $RuH_2(PPh_3)_4$, respectively [148]. The MCDs are efficient, recoverable catalysts in three general organic reactions: Stille couplings, Knoevenagel condensations, and Michael additions.

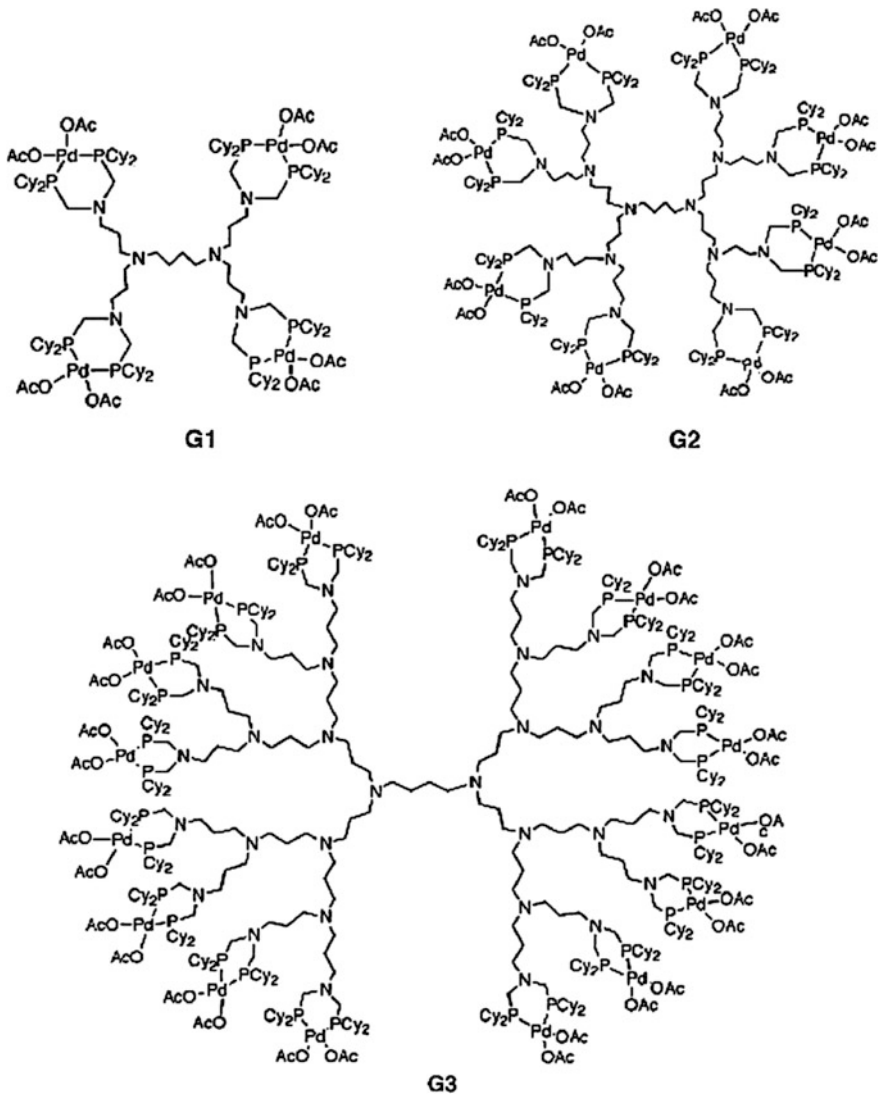

Fig. 5.14 Diphosphino Pd(II)-MCDs

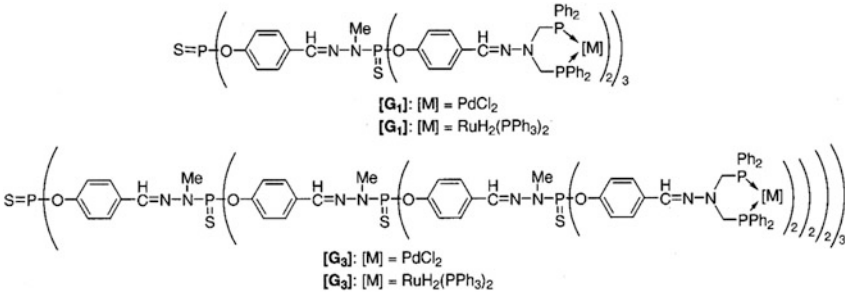

The fourteen multivalent MCDs containing diphosphine Pd(II) chelates both within and across the dendrimer generations were synthesized using G0–G3 poly (propyl ether imine) dendrimers (Fig. 5.15) [149]. The MCDs were obtained by the interaction of $Pd(COD)_2Cl_2$ with corresponding phosphines to form 6 Pd(II)-containing MCD **1**, 10 Pd(II)-containing MCD **2** and 16 Pd(II)-containing MCD **3**. The dendritic metal chelates **1–3** were amorphous solids, whereas initial chelating dendrimers were gums and foamy solids in general.

It should be noted Pd(II)-MCDs based on the commercial G1–G3 polyamino DAB-dendrimers with chelating bisphosphine ligands, in particular, bis(*tert*-butylphosphines and bis(cyclohexylphosphines) [150]. It is important that complete conversion occurs within a few hours at most.

DAB G1–G3 dendrimers terminated by Ru benzylidene chelates were synthesized from the dendritic diphosphane and $RuCl_2(=CH\text{-}o\text{-}Oi\text{-}PrC_6H_4)PPh_3$ [151]. The MCDs undergo ROMP of norbornene to formation the metallodendrimer stars, in which each branch includes, for example, 100 norbornene units. Activity of MCD catalysts was higher than that of mono-Ru model catalyst and rate of metathesis polymerization decreases with increase in a dendrimer generation [151, 152].

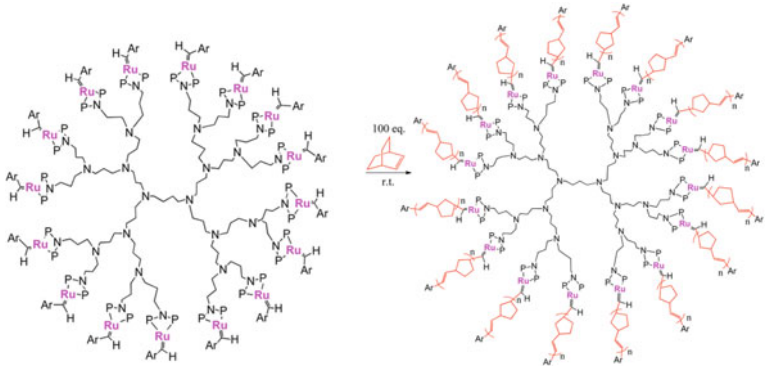

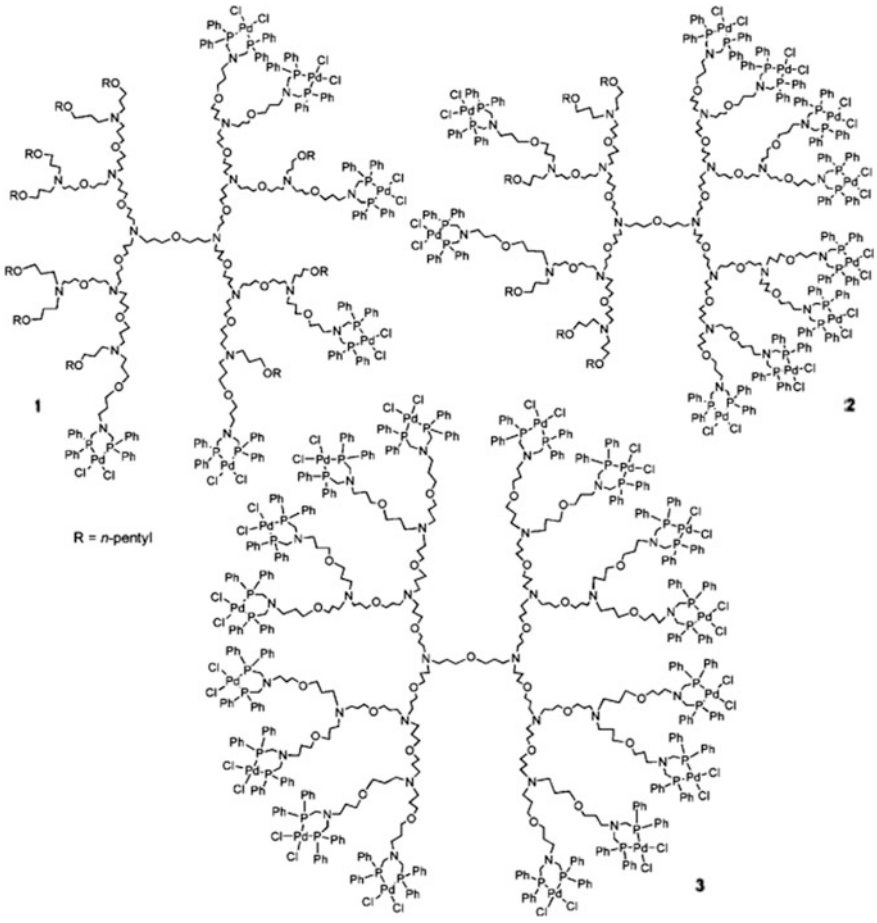

Fig. 5.15 Molecular structures of G3 partially and fully functionalized MCD

Dendrimers containing gem-bisphosphonate terminal fragments were used for the chelation of gadolinium salt Gd(triflate)$_3$ from monomer to G3 (Scheme 5.11). Magnetic susceptibility measurements indicate the presence of one gadolinium per the bisphosphonate group [153].

It should be noted Ir(BINAP)-cored dendrimers, which are used in enantioselective hydrogenation of quinolines [154]. The effects of the solvents, temperature, hydrogen pressure, and additive on the activity and enantioselectivity were investigated by using the MCD catalyst, which was generated in situ from chelating BINAP dendrimer and [Ir(COD)Cl]$_2$.

Of interest are the chiral diphosphane-containing Janus dendrimers (up to 16 BINAP units) used for in situ catalyst preparation by mixing with [Ru(*p*-cymene)Cl$_2$]$_2$ [155]. The chemical shifts of Ru-MCDs in the ^{31}P NMR spectra were very similar, indicating that the introduction of sterically demanding dendritic wedges

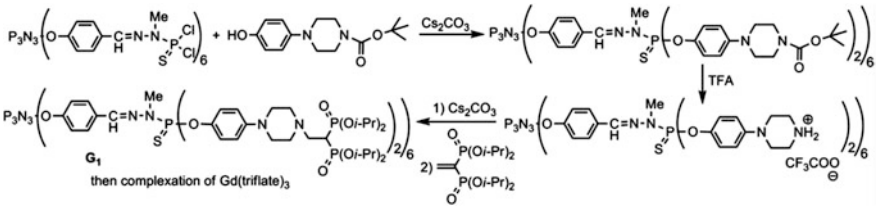

Scheme 5.11 Synthesis of dendrimers functionalized by gem-bisphosphonate end groups, used for the chelation of gadolinium salt

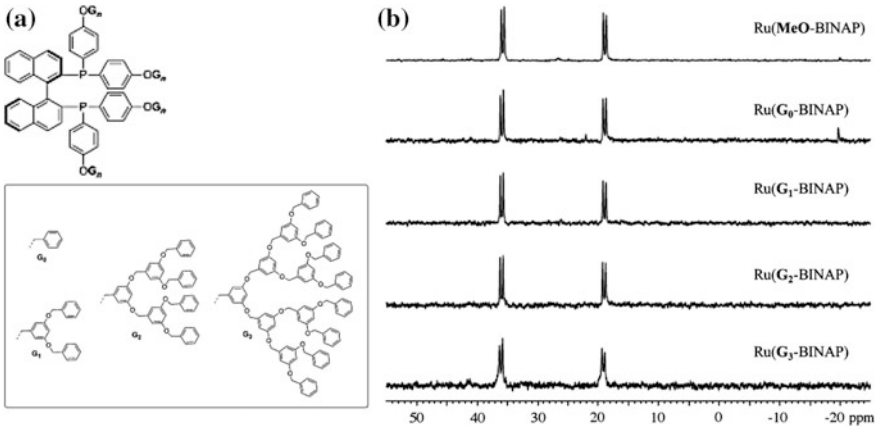

Fig. 5.16 **a** Structures of chiral Janus dendritic diphosphane ligands. **b** ^{31}P NMR spectra of dendritic [Ru(Gn-BINAP)] complexes and corresponding low molecular weight Ru complex

did not influence the chelation of ruthenium with the phosphorus atoms at the core of the dendrimer (Fig. 5.16).

Chiral copolymer with (S)-BINAP and fluorene as building blocks is used for design of chiral Ru/Ir bimetallic dendronized polymer catalysts based on Fréchet type dendritic DPEN (DPEN = 1,2-diphenylethylenediamine) ligands using M–L coordination strategy (Fig. 5.17) [156]. The prepared MCDs are applied to Ir-catalyzed asymmetric hydrogenation of quinaldine and showed perfect activity at moderate enantioselectivity. At that, the reaction rate is higher than that of a monomer catalyst and can be associated with efficient protection of catalytically active Ir center by bulk dendritic pendants, which decrease formation of inactive Ir dimer.

A kind of chiral dendritic [$RuCl_2$(BINAP)(DPEN)] catalysts with a «sandwich» multi-layer structure has been synthesized via metal chelation reactions of [$RuCl_2$

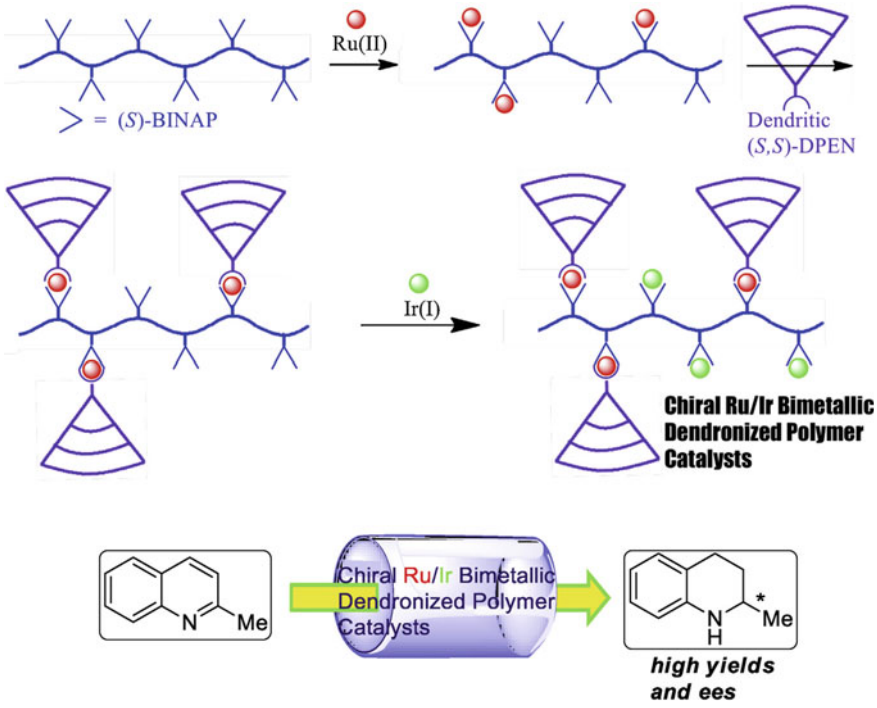

Fig. 5.17 Working hypothesis for catalyst design: synthesis of chiral Ru/Ir bimetallic dendronized polymer catalysts and their application in asymmetric hydrogenation of quinaldine

$(C_6H_6)]_2$ with dendritic chiral diamine and dendritic chiral diphosphine ligands [157]. In the MCDs the metal chelate layer is «cramped» between layers of poly (aryl ether) dendrons.

It should be noted some remarkable examples involving rhodium MCD with diphenylphosphino ligands on a solid support such as silica gel (Fig. 5.18) [158, 159]. The phosphonated dendrimers were chelated by simply stirring with chloro (dicarbonyl)rhodium(I) dimer in degassed dichloromethane at room temperature for 3 h under argon and the rhodium contents of G1 and G2 are 0.74 and 0.83 mmol g^{-1}, respectively.

Of interest are Pd-MCDs prepared by the interaction of the phosphonated G0–G3 dendrimers with dichlorobis(benzonitrile)palladium(II) [160, 161]. It is

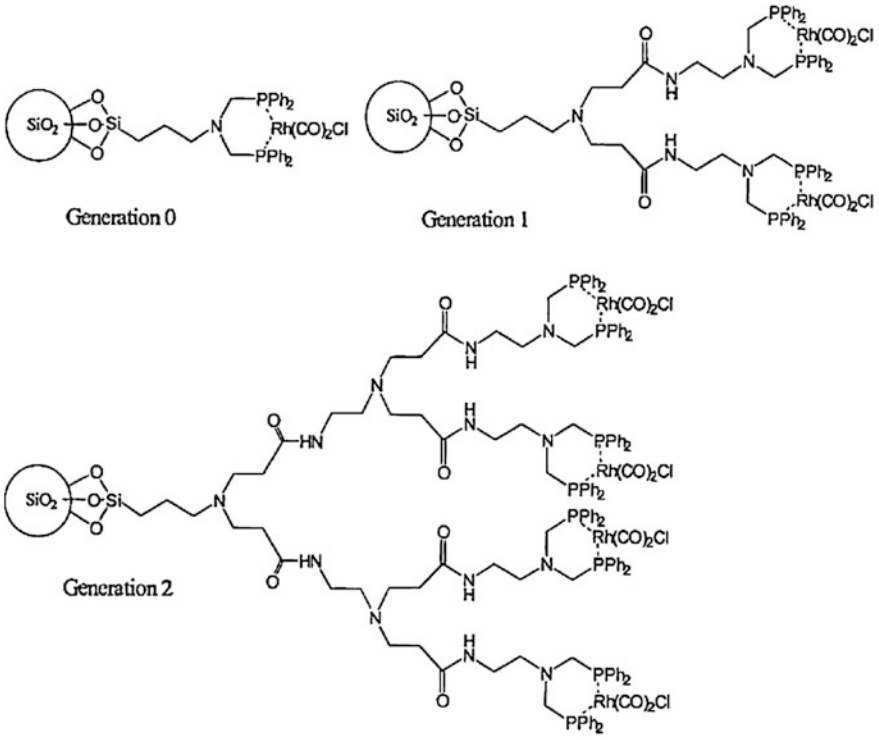

Fig. 5.18 Rhodium MCDs with diphenylphosphino ligands on a silica gel

important that extending the length of the PAMAM arms (Fig. 5.19) [160, 162] or using large pore PE-MCM-41 instead of amorphous silica [163] leads to an increasing metal content.

The Pd chelate based on 4-amino(*N*-methylendiphenylphosphino) pyridine has been reacted with the ruthenocarbosilane dendrimer to afford Ru–Pd concentric metal layered dendrimer [164].

5.1.5 Pincer Complexes

Dendritic SCS-pincer palladium chelates were prepared in good yields (60–89%) and high purity (palladium loading >97%) [165]. Palladation of dendrimer was achieved via direct C–H-activation with $[Pd(MeCN)_4](BF_4)_2$. The treatment of the formed cationic acetonitrile pincer complex by a saturated aqueous sodium chloride solution leads to replace the acetonitrile ligand by the stronger chloride ligand.

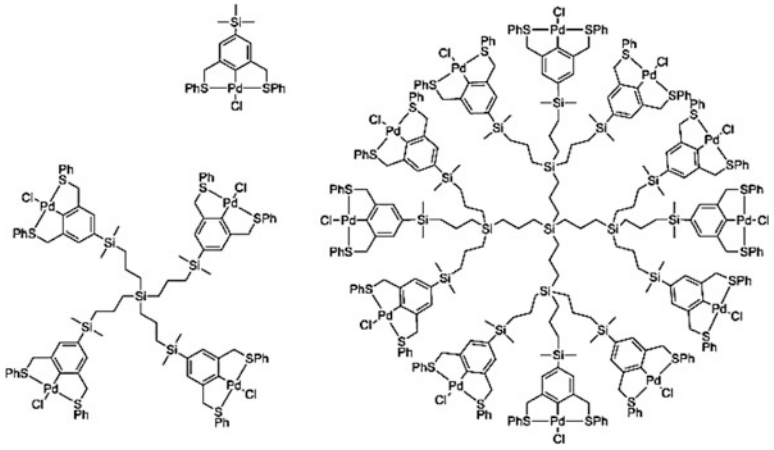

The dendritic SCS-pincer Pd-complexes were prepared by an amide coupling of an activated ester pincer derivative with a primary amine (commercially available amino-terminated PAMAM dendrimers) in order to investigate the effects of the dendrimer backbone on catalysis [166].

It should be noted the pincer-PCP Pd(II) complexes based on a tridentate diphosphinoaryl ligand immobilized on silica supported dendrimers [167].

A solid-phase synthetic approach to obtain dendritic PAMAM ligands anchored onto PS beads and their rhodium pincer complexes was developed [168]. The dendronized polymeric chelates were applied for the hydroformylation of several olefins. In another example the dendronized polymers up to the G3 containing NCN-pincer palladium complexes at the periphery were used as catalysts for the aldol condensation of benzaldehyde with methyl isocyanoacetate [169].

5.1.6 Chelating Dendrimers as Metal Sensors

Appropriately developed luminescent dendrimers can play a role of ligands and sensors for luminescent and non-luminescent metal ions [170]. Dendritic effects of dendrimers are useful for sensor development of specific metal ions using chelation with a selective ligand present on a dendrimer surface. Thus, PAMAM dendrimers functionalized by (4-dimethylaminoethyl) amine-1,8-naphtalimide on the surface were built for detection of divalent metal ions. Due to the fact that (4-dimethylaminoethyl) amine groups quenched PET of 1,8-naphtalamide, a dendrimer does not provide fluorescence in the steady regime. After bonding with metal ions, (4-dimethylaminoethyl) amine does not function any more as quencher, and fluorescence can be observed generated by 1,8-naphtalimide. Increase in fluorescence depends on nature of coordinated metal ion because of difference in bonding force, at that, each size of PAMAM dendrimer provides selectivity of a certain type of a metal ion [171, 172].

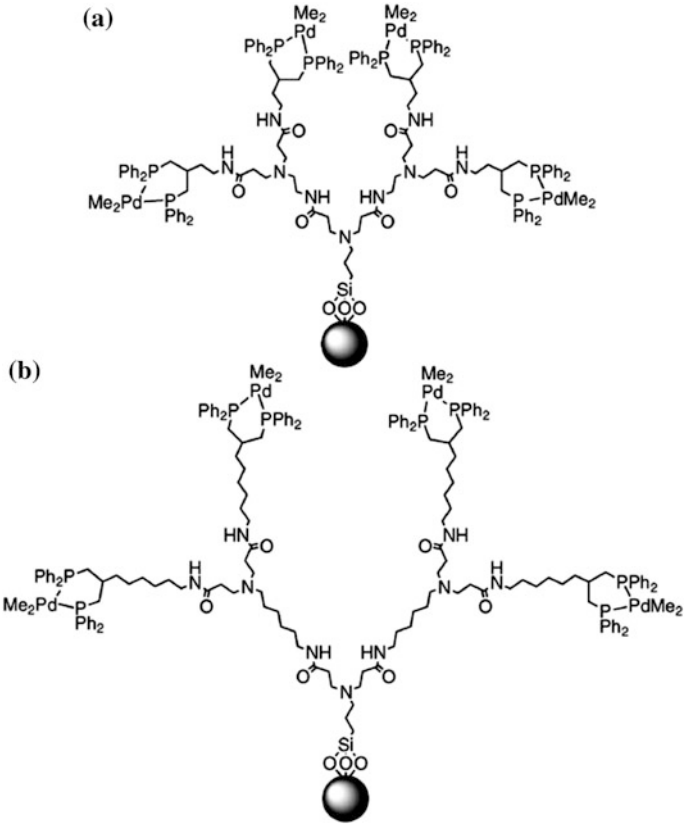

Fig. 5.19 **a** A G2 PAMAM Pd dendrimer supported on silica. **b** The PAMAM-C6 analogue, which differs in the number of carbon atoms separating the intermediate amido and the branching amine functionalities

Thus, G1 dendrimers with Fe(II) ions give the strongest increase in a signal, and G2 dendrimers are optimal as sensors of Cu(II) or Fe(II) [173, 174]. Other G0 and G2 PAMAM dendrimers with surface 4-allylamino-1,8-naphtalimide units showed the best results as sensors of Zn(II) ions [175].

High selectivity for detection of Cu cations found with green-yellow fluorescent PAMAM dendrimers peripherally modified by 1,8-naphtalimides (Fig. 5.20) [176].

The green fluorescence intensity of G1 PPI dendrimers with 1,8-naphthalimide fragments increases in the presence of different transition metal ions [177]. The quenching the fluorescence emission was observed during the interaction of the fluorophore (1,8-naphthalimide) and the receptor (*N*,*N*-dimethylamino group) initiating PET (Fig. 5.21a). The introduction of the metal ions in the dendrimer solution leads to a change of its properties (Fig. 5.21b). It is important that the *N*,*N*-dimethylaminoethylamine fragment at C-4 position of the 1,8-naphthalimide structure can coordinate with metal ions.

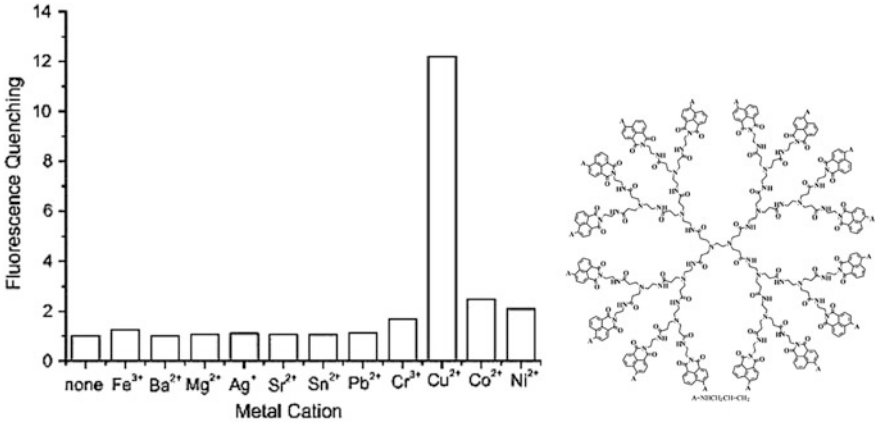

Fig. 5.20 Fluorescence quenching factor of PAMAM dendrimers with terminal 1,8-naphtalimides in presence of different metal cations (5×10^{-5} mol L^{-1}) in DMF solutions. The dendrimer concentration is $c = 1 \times 10^{-5}$ mol L^{-1}

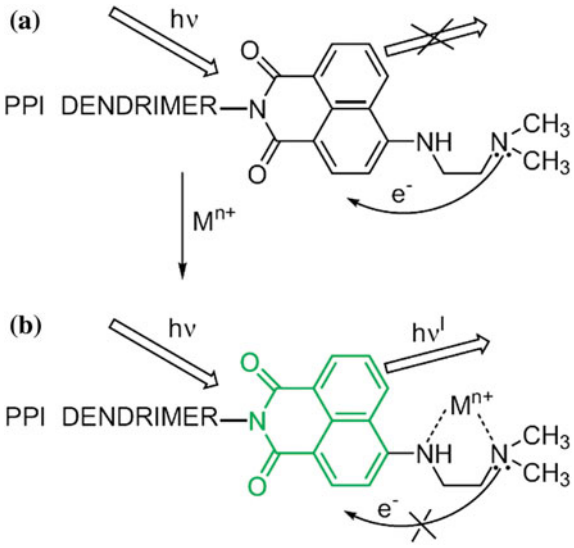

Fig. 5.21 Proposed mechanism of fluorescence enhancement of 4-*N*,*N*-dimethylaminoethylamino-1,8-naphthalimide-labeled PPI dendrimer

We shall also notice G3 PAMAM dendrimers functionalized with 2,3-naphthalimide chromophore groups on terminal branches, which with Eu(III) form luminescent complexes corresponding to the dendrimer:lanthanide ratio 1:8 [178]. For these MCDs an overall average CN of 7.5 was postulated. Luminescence lifetimes show that a metal cation is perfectly shielded from non-emitting deactivation by a dendritic structure.

Another often used label for studying chelation processes with participation of dendrimer ligands is a dansyl-group fixed on a dendrimer surface. It is important that the dansyl groups are independent from each other. If Co(II) salt is added, fluorescence quenching is due to Co(II) ion chelation in dendrimer interior, and this quenching is more distinguished with increase in a number of generations. Chelation showed that it is completely reversible. Fluorescence of all peripheral dansyl groups is quenched, when one Co(II) ion is incorporated in a dendrimer [179, 180], while in polyamide-core dendrimers a less number of dansyl units are quenched [181]. Lanthanide ions Nd(III), Eu(III), Gd(III), Tb(III), Er(III), and Yb(III) quenched dansyl fluorescence of dendrimers having PLL cores instead of PPI cores, and with Nd(III), Er(III), Yb(III) sensibilized NIR emission of a lanthanide ion was observed [182].

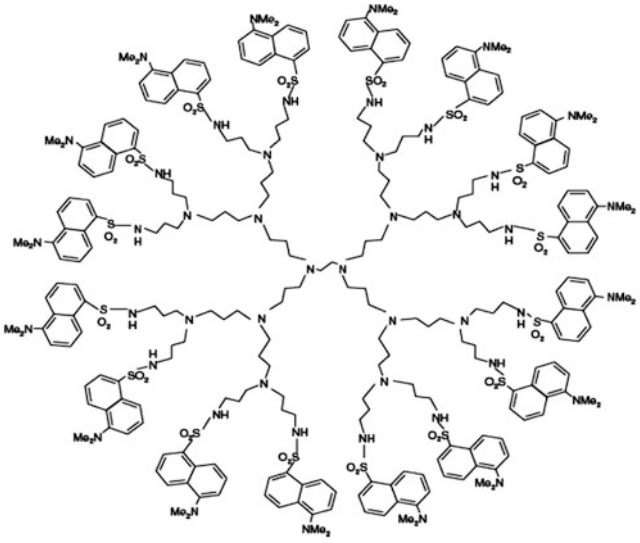

A family of POPAM dendrimers with terminal 4, 16, and 32 dansyl fragments and molecular clip consisting of two anthracene side walls and bridging block of benzene disulfate are good ligands for Zn(II) ions [183]. The interaction between dansyl dendrimer and anthracene-functionalized clips is mediated by Zn(II) ions and a number of metal ions and molecular clips linked to each dendrimer increases with a number of generations. It is important that energy transfer goes from anthracene, giving the fluorescent excited state with almost unitary efficiency.

5.2 Intracomplex Compounds

By now, a wide variety of MCD intracomplex type, including various metal chelate units, obtained.

5.2.1 Salen-Type Chelates

A large body of research concerning MCDs of intracomplex type with salicylaldimine ligands has been carried out. As a typical example, we note Ni dendrimer chelates obtained by chelation of a metal compound to periphery of salicylaldimine-containing G1–G3 DAB-PPI-dendrimers [184–186]. All three MCDs were isolated as green solids, with yields ranging from 75 to 85%. Using a catalytic system based on these MCDs with $EtAlCl_2$ co-catalyst, a tandem process has place, in which ethylene is oligomerized with following Friedel-Crafts alkylation of the reactive solvent, toluene, which brings to a range of alkylbenzenes.

G1–G2 salicylaldimine-containing PPI dendrimers was used to obtain some Cu and Co chelate dendrimers [187], which are efficient catalysts in aerobic hydroxylation of phenol using H_2O_2 and molecular oxygen as oxidants. It is important that the nature of the MCD as well as by the pH of the reaction medium have a substantial effect on the selectivity to the products.

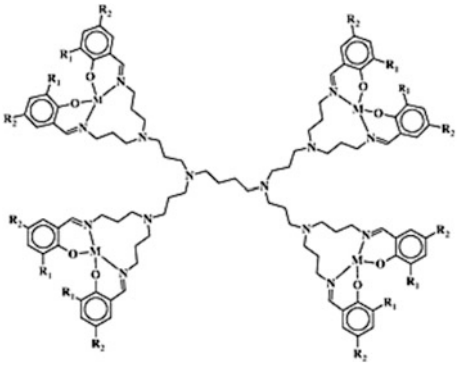

Ni-chelate dendrimer is synthesized with PAMAM, 3,5-di-*tert*-butyl-2-hydroxybenzaldehyde and Ni chloride through Schiff base-forming reaction and chelation [188]. Studying catalytic activity of Ni MCD in ethylene oligomerization using MAO as a co-catalyst, showed that activity and selectivity is determined by dendritic structure, in particular, G2 metal chelates have higher activity. The dendritic salicylaldimine Cu and Zn chelates were similarly prepared by template method with 88.2 and 65.2% yield, respectively [189]. Studying salicylaldimine dendritic Cu complex as catalyst in oxidation reaction of ascorbic acid showed that this complex has good mimic enzyme catalytic kinetics. In particular, the catalytic reaction had the same features of the pseudo-first order reaction as the enzyme reaction, and the reaction rate increased under high concentration conditions of mimic enzyme complex and pH 7–7.5 [190].

Co(II)-salicylaldimine dendrimer and a 21-bases oligonucleotides (NH_2-5′-GAG GAGTTGGGGGAGCACATT-3′ and 5′-AATGTGCTCCCCCAACTCC TC-3′) were assembled LbL on a gold electrode in order to generate electrochemical DNA-biosensor based on MCD [191]. In presence of complimentary oligonucleotide, formation of double-chained DNA increases impedimetric resistance of charge transfer from 6.52 to 12.85 kΩ. On the other hand, mismatched DNA fragments did not cause any changes in resistance, which resulted in stable and simple assembling of DNA biosensors.

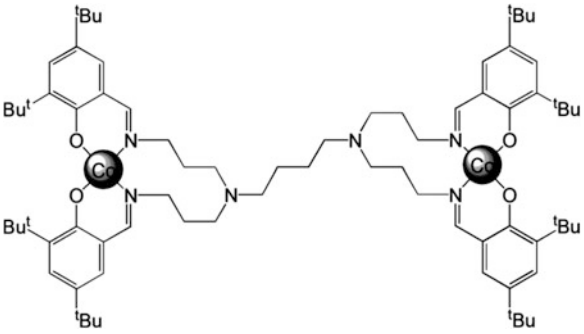

We shall notice dendritic salicylaldimine Ru chelates interesting for their biomedical applications [64]. Thus, MCD containing tetranuclear and octanuclear chelate G1–G2 Ru(II) arene dendrimers based on PPI frameworks is synthesized from binuclear arene precursors, $[Ru(arene)_2Cl_2]_2$ (arene = *p*-cumene, hexamethylbenzene) using the reaction with salicylaldimine dendritic ligands in ethanol at room temperature [48]. These compounds are stable in air, and MCDs are soluble in most polar organic solvents, and all terminal groups of a dendrimer are functionalized with Ru(II) arene fragments. In this case at chelation with participation of a polymer dendritic ligand dimeric Ru complexes are monomerized.

Cationic heterometallic ferrocenyl-derivatives MCDs of intracomplex N,O-type are obtained by the interaction of Ru(II)-arene-1,3,5-triaza-7-phosphatricyclo [3.3.1.1]decane with salicylaldimine ligand (Scheme 5.12) [192]. G1–G4 MCDs

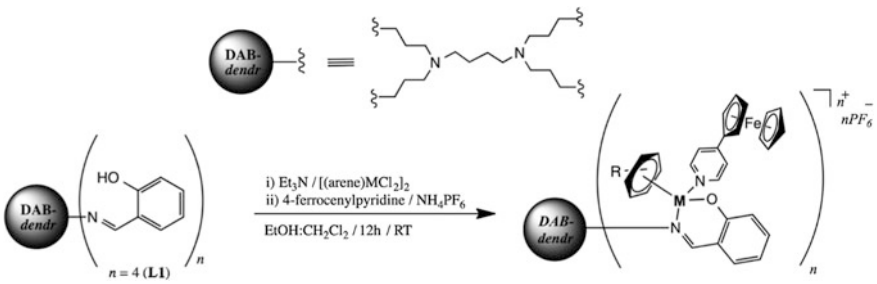

Scheme 5.12 Preparation of cationic heterometallic ferrocenyl-derivatives MCDs of intracomplex N,O-type

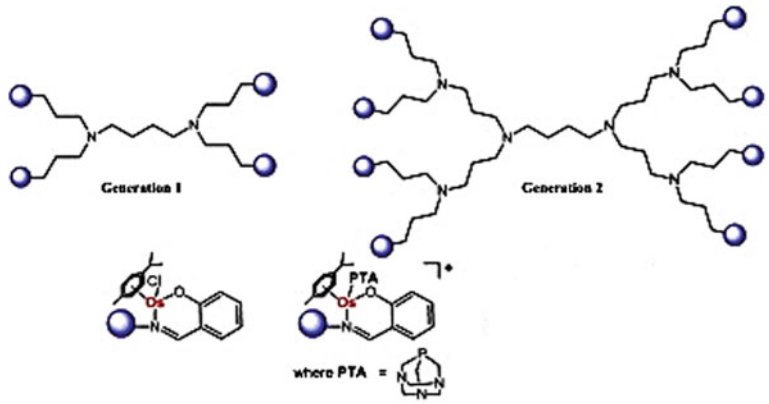

Fig. 5.22 Structure of Os(II) salicylaldimine dendritic chelates

contain up to 32 peripheral metal chelate units and show higher antiproliferative activity in vitro as compared to a monomer analogue.

Also similar salicylaldimine PPI dendrimers including Os-arene peripheral fragments have been synthesized, which showed high anticancer activity (Fig. 5.22) [193]. All MCDs were prepared as yellow solids, in moderate to high yields (48–88%). It is important that there is a loss of two-fold symmetry about the *p*-cymene fragment upon chelation of the bidentate *N*,*O*-salicylaldimine ligand.

Considerable attention is attracted to liquid crystalline salicylaldimine MCDs [194, 195]. Thus, VO(II) chelates formed with salen-ligands containing terminal G0–G1 lipophilic fragments show wide temperature ranges of hexagonal (Col_h) and rectangular (Col_r) columnar meso-phases [196]. As generation increases from G0 to G1, melting and clearing temperatures decrease more substantially for the latter, therefore, meso-phases exist in wider temperature ranges for G1. It also occurs that presence of two times more divergent aliphatic chains with increase in generation contributes to domination of rectangular symmetry over hexagonal. The main

structural parameter, which has an effect on thermal stability of meso-phases is, however, origin of a cross-linking spacer between two imine chelating fragments, because it has an effect on strength of molecular interactions through a dative bond between dipolar vanadyl groups, and therefore, determines reliability of the formed linear pseudo-polymer structure and helps to meso-phase stabilization. Optimum is reached when propylene spacer is considered, because chelates reflect stronger polymer linear chains with respect to higher clearing temperature and thermal stability of meso-phases (about 150–170 °C). In contrast to this, rigid ethylene spacer brings to monomer types, while a bulk spacer brings yet to polymer linear chains, but with weaker dipolar interactions, both show lower clearing temperatures (about 156 and 108–115 °C, respectively) than intermediate systems. It seems that additional steric factors related to protruding geminal methylene groups also contribute to considerable decrease in stability of a meso-phase, despite formation of a polymer chain, though less interconnected. Presence of this polymer chain in combination with a great number of divergent aliphatic chains also can be associated with unusual inversion of the meso-phase here observed, i.e. lower symmetry (rectangular against hexagonal) is discovered at higher temperatures. This, most probably, can be caused by limitation of core side diffusion, which impedes mesogens in tighter registry with limited conformation variants. As regards supramolecular organization in columnar meso-phases, G0 chelates should be coupled in correlated structures, which are then self-assembled into columns, while chelates with G1 dendritic ligands are packed directly in columns, as purely discotic compounds do. In both cases polar fragments are separated in the interior of columnar cores and surrounded with aliphatic medium.

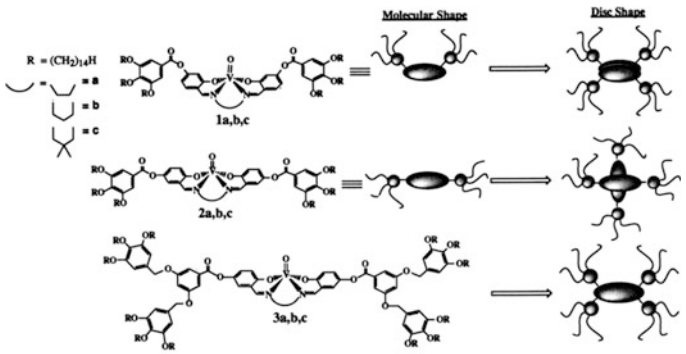

Similarly, binuclear Cu MCD are obtained through self-assembling two bidentate phenyl-iminopropyl ketone ligands containing divergent G1 dendron fragments in 3- and 5-positions of phenyl ring ($R_1 = R_2 = H/OC_nH_{2n+1}$, n = 5–8, 10, 12, 14, 16) [197].

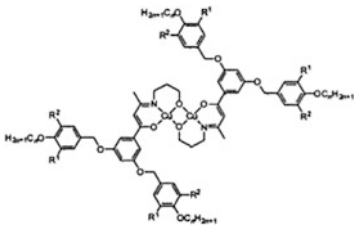

It is important that the ligands were not isomorphic themselves. Highly lipophilic bimetallic chelates ($R_1 = R_2 = OC_nH_{2n+1}$) with chain lengths between hexyl and dodecyl show Col_h phase between 83–99 and 97–117 °C. A decrease in a number of aliphatic chains ($R_1 = H$ and $R_2 = OC_nH_{2n+1}$ or $R_1 = R_2 = H$) or using other chain length has a negative effect on mesomorphism onset. Here also columnar formation follows from monomer chelate packaging.

PPI-based dendrimers functionalized at the end by four or eight coordinated 4-(alkoxybenzoyloxy)-salicylaldimines, respectively, were used as chelating ligands for the formation of bi- (G0) and tetranuclear (G1) Cu(II) MCDs, respectively [198]. Although all organic ligands show SmC and SmA phases [199], chelation of Cu(II) ions will stronger affect mesomorphic properties of respective multi-metallic MCDs. Suppression of mesomorphism (G0: n = 10, T_m = 179 °C; G1: n = 10, T_m = 110 °C; n = 14, T_m = 80 °C) or a decrease in temperature range of the meso-phase (G0: n = 14, Cr 163 SmC 197 I; n = 18, Cr 167 SmC 187 I; G1 n = 18, Cr 35 SmC 108 I) is observed more systematically for corresponding metal-free chelating dendrimers. Transition temperatures during chelation are slightly increased for dimetallic MCD, whereas for tetrametallic MCD temperature range is similar to that for ligands, at that only SmC phases are formed. Structure of smectic phases of dendritic chelating ligands is explained by parallel alignment of peripheral mesogenic blocks diverging up and down from a molecular center, while chelation brings to partial decomposition of this parallel disposition and opening of dendritic strands, thus decreasing micro-segregation with molecules located in neighboring layers. This model is confirmed by deterioration of periodicity of a layer, and widening of molecular range of chelates, as compared with ligands. Chelation of different amounts of Cu(II) ions with respective derivatives of liquid crystalline PPI G0–G1 dendrimers containing peripheral di-3,4-decyloxyphenyl amide groups, showed Col_h meso-phases (as well as metal-free chelating dendrimers [200]).

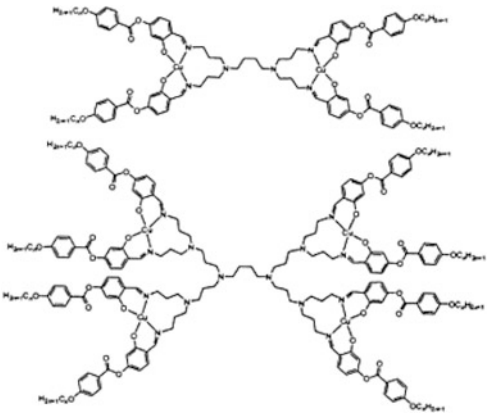

At low content of Cu(II) ions in dendritic ligand metal ions form monomer chelates having a columnar meso-phase with plane N_2O_2 coordination geometry with participation of carbonyl oxygen and amide nitrogen atom. At the same time at intermediate and high content of metal ions two metal chelate units were identified, in particular, pseudo-tetrahedral N_2O_2 mode with participation of the same donor atoms, and square-pyramidal N_2O_3 mode with additional bridge with tertiary amine nitrogen atom from internal core of a dendrimer with possible intermolecular interactions [201, 202].

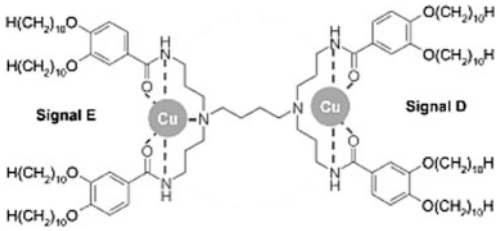

In blue salicylaldimine G1 Cu-MCD, having dimer structure, temperature activated effect of valence tautomerization accompanied by electron transport, with activation energy 0.35 meV is discovered [203].

In a spin-alternating Fe(III) chelate with G2 dendrimer branching of the salen-type a new phenomenon is found, «magneto-ferroelectric crossover», which is simultaneous synchronic change in spin state and electric polarization of Fe(III) centers during spin transition at $T_{1/2}$ = 312 K. The chelate consists of three types of magnetic iron centers: one S = ½ low-spin (LS) and two S = 5/2 high spin (HS) centers with strongly and weakly distorted octahedral crystal fields. Another prominent feature of this MCD is co-existence in one material of magnetic ordering

(4.2–50 K), magneto-electric effect (50–200 K), and spin-crossover of the transition (200–330 K) (Fig. 5.23) [204, 205].

It is interesting that Fe ions existing in HS state are chelated by decyloxybenzoate substituted G1–G5 PPI dendrimers in two types of iron-chelating centers with octahedral and tetrahedral symmetry (Fig. 5.24). Octahedral (high symmetry) centers are placed on a dendritic core boundary, while tetrahedral centers with strong rhomboid distortion of Fe environment are distributed over all branching of the dendritic core. It is found that all iron-containing dendromesogens display light-harvesting and fluorescent properties [206].

Co-existence of spin-crossover and magnetic ordering is found in dendritic Fe (III) chelate $[Fe(L)_2]^+PF_6^-$, where L = 3,5-di[3,4,5-tris(tetradecyloxy)benzoyloxy]

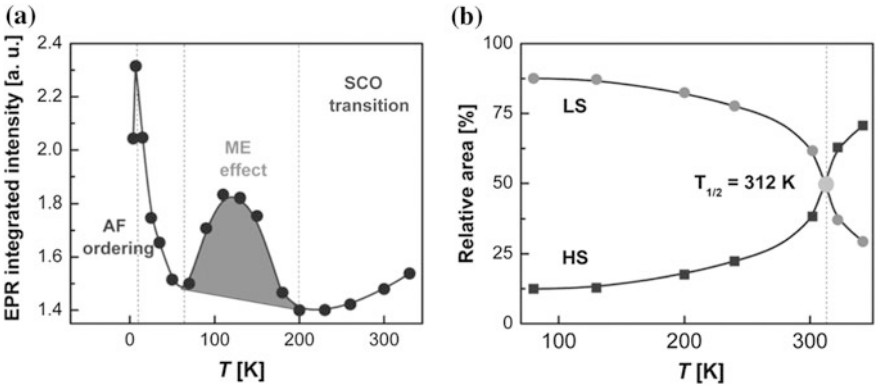

Fig. 5.23 **a** The temperature dependence of the EPR lines integrated intensity of the whole EPR spectrum. **b** The temperature dependence of the relative areas of HS and LS fractions

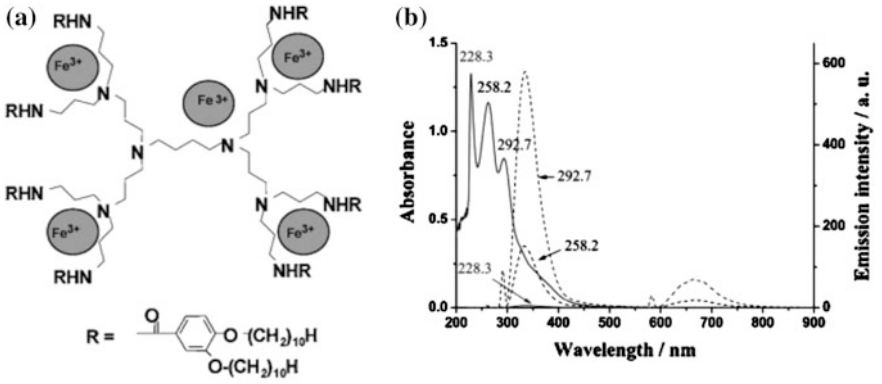

Fig. 5.24 **a** Structure of MCD with two types of iron-chelating centers. **b** Absorption (solid line) and fluorescence (dashed lines) spectra of MCD. The sample was excited at 292.7 (dashed line), 258.2 (dotted line) and 228.3 (short dotted line) nm

benzoyl-4-salicylidene-*N*-ethyl-*N*-ethylenediamine [207]. It should be noted that for this MCD antiferromagnetic exchange interactions predominate in the first temperature interval (4.2–70 K), while spin transitions between LS and HS centers predominate in the second temperature interval (70–300 K). Besides this MCD has antiferromagnetic ordering below 10 K.

5.2.2 8-Hydroxyquinoline Chelates

A dendritic HQ ligand, based on a PAMAM-type dendron, was chelated with Zn(II) by treating dendron by $Zn(OAc)_2$ [208]. The luminescence intensity of the G2 dendron was higher than that of G1, and upon chelation with Zn(II), a bathochromic shift was observed; the intensity of the Zn(II) MCD was higher than that of the analogous dendritic ligands. The emission spectra in visible region for monomeric chelate ZnQ_2, dendritic G1 and G2 chelates are quite similar, indicating that the shape and chemical properties of the dendrimer branches do not substantially affect the ZnQ_2-based chromophoric core.

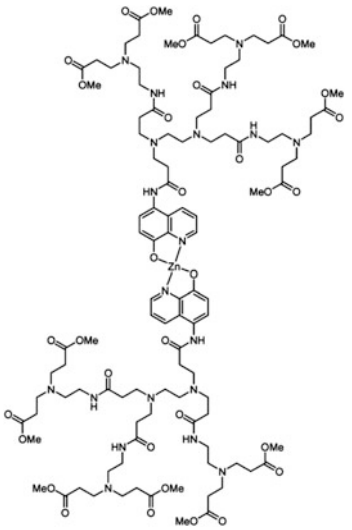

5.2.3 Pyrrolide-Imine Chelates

Bimetallic dendritic (pyrrolide-imine) Cu(II) and Ni(II) [DAB-{(N-$CHC_4H_3N)_4$}Cu_2], [DAB-{(N-$CHC_4H_3N)_4$}Ni_2] chelates have been obtained with good yield

[209]. Both the copper and nickel MCDs are fairly stable at room temperature in the solid state but show signs of decomposition in solution. The obtained MCDs are active catalysts of phenol hydroxylation using H_2O_2 and molecular oxygen as oxidants, at that Cu chelates showed generally higher activity as compared with their Ni analogues, however, Ni catalysts have far higher selectivity with respect to catechol than the Cu analogues.

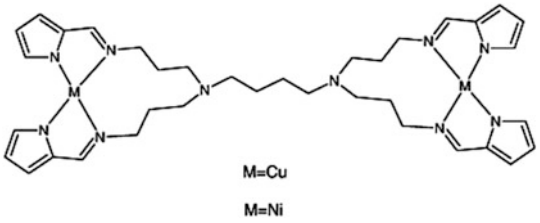

5.2.4 O,O-Chelates

Salicylate, catecholate, and hydroxypyridinonate bidentate chelators have been coupled to the surface of both PPI and PAMAM dendrimers up to the G4 (64 end groups) [210]. The metal-chelating properties of these dendrimers have been investigated by using batch spectrophotometric titrations. It is important that tris-bidentate and lower denticity modes of metal binding were identified. Metal chelation is specifically localized to the chelating end groups, with complexation halting at the formation of tris-bidentate complexes in the HOPO-based systems.

Studying chelation of Eu(III) with dendritic β-diketone ligands containing dbm core and poly (aryl ether) dendron obtained using the convergent method, showed that the linking point of a dendron to dbm plays important role in production of Eu MCD (Scheme 5.13) [211]. In particular, only dendritic β-diketonate ligands containing dendrons substituted in dbm phenyl group with $EuCl_3 \cdot 6H_2O$ form Eu (III) dendritic chelates from G1 to G3 with good yields. At the same time the β-diketonate ligands, which have dendrons linked to 2-position of dbm, can't form Eu(III) MCD, because the sterically demanding dendritic structure substituted in the 2-position might influence the formation of Eu(III) chelates. Integration of phen as a second ligand into these dendritic β-diketonate Eu(III) chelates gives mixed-ligand Eu(III) dendritic complexes with enhanced luminescence intensity.

The phonon-absorbing lanthanide chelates are synthesized by chelation of dendritic β-diketone ligands to Eu(III) [212]. Ligands are benzoyltrifluoroacetone units with poly (aryl ether) dendron branches. MCDs show Eu emission at the absence of residual emission with ligands with increase in generation from G0 to G3, which is associated with simultaneous manifestation of two effects: antenna and

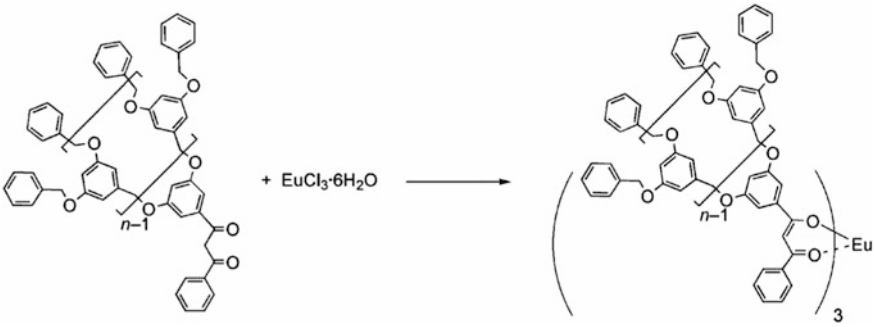

Scheme 5.13 Scheme of chelation of Eu(III) with dendritic β-diketone ligands

isolation of a metal center. The data on lifetimes show that G3 MCD is the longest lived type.

Phosphorus-based dendrimers with surface β-diketones is predominantly in the enol form obtained through intramolecular hydrogen transfer [213]. The chelating dendrimers were used for the in situ chelation of CuI, using either 2 or 4 diketone ligands per Cu. These MCDs catalyzed O-arylations of 3,5-dimethylphenol by aryl bromides. The absence of the dendrimer effect is explained by the decomposition of the dendrimer under the reaction conditions, which led to the release of the peripheral diketone moieties.

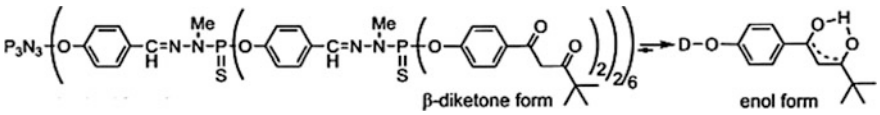

5.2.5 *S,O-Chelates*

Surface modifying PAMAM dendrimers with *N*-benzoylthiocarbamide brings to chelating ligands having high selectivity to ions of such metals as Co(II), Cu(II), Hg (II), Pb(II), and Zn(II) [214]. All metal ions can link quantitatively to chelating dendrimers at pH 9, however, most stable MCDs are formed with Cu and Hg ions, which can be selectively separated from other metal ions, and dendrimers can be regenerated and repeatedly used.

5.2.6 P,O-Chelates

Using dendritic or monomer P,O-ligand with an equimolar amount of $Ni(COD)_2$, mono-ligated chelates were formed [215]. When a second equivalent of monomer P,O-ligand was added to the solution of mono-ligated chelate an orange precipitate of bis (P,O)-nickel chelate immediately is formed. In contrast to the experiments with parent monomer ligand, addition of a second equivalent of dendritic P, O-ligand to the solution of mono-ligated chelates did not result in the formation of precipitate, and only a small amount (17%) of the bis(P,O)-nickel MCD is present in solution. These results demonstrate the ability of dendritic P,O-ligand to suppress the formation of inactive bis(P,O)-nickel MCD in toluene. Thus, dendritic P, O-ligand was anticipated to form a more productive catalyst than parent monomer ligand in the oligomerization of ethylene.

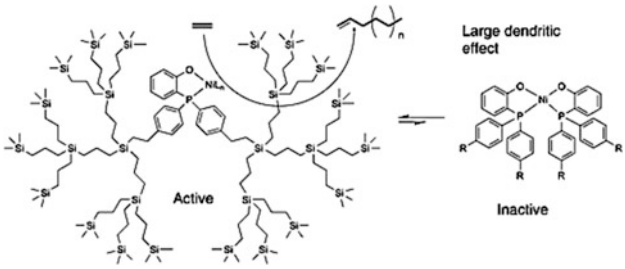

5.2.7 Metal Chelates with Polydentate Ligands

Recently much attention is given to chiral conformation order in dendritic structures [216]. In order to have a possibility to create and control chiral secondary structure in MCD, deep understanding the effect of chiral subunits on macroscopic structure is needed. Thus, chiral intramolecular H-bound dendrons, which are packed in dynamically biased helical conformation, can be «locked» in kinetically controlled conformation via chelation to Cu(II) ions [217]. Coordination of each chelating polydentate pyridine-2,6-dicarboxamide repeating dendron unit to Cu ion makes this subunit to exist only in syn-syn conformation and sharply rigidifies the dendron structure (Fig. 5.25).

The chelating polydentate dendritic structures was grafted to epoxy-activated mesoporous PMMA beads (Sepabeads EBEP-400) followed by metal coordination by terminal chelating groups for formation of MCD grafted catalysts (Fig. 5.26) [218]. The obtained catalyst was used for production of β-amino alcohols using regioselective method through nucleophilic opening of oxirane ring with different aromatic amines without solvents under soft conditions of reaction. It is found that

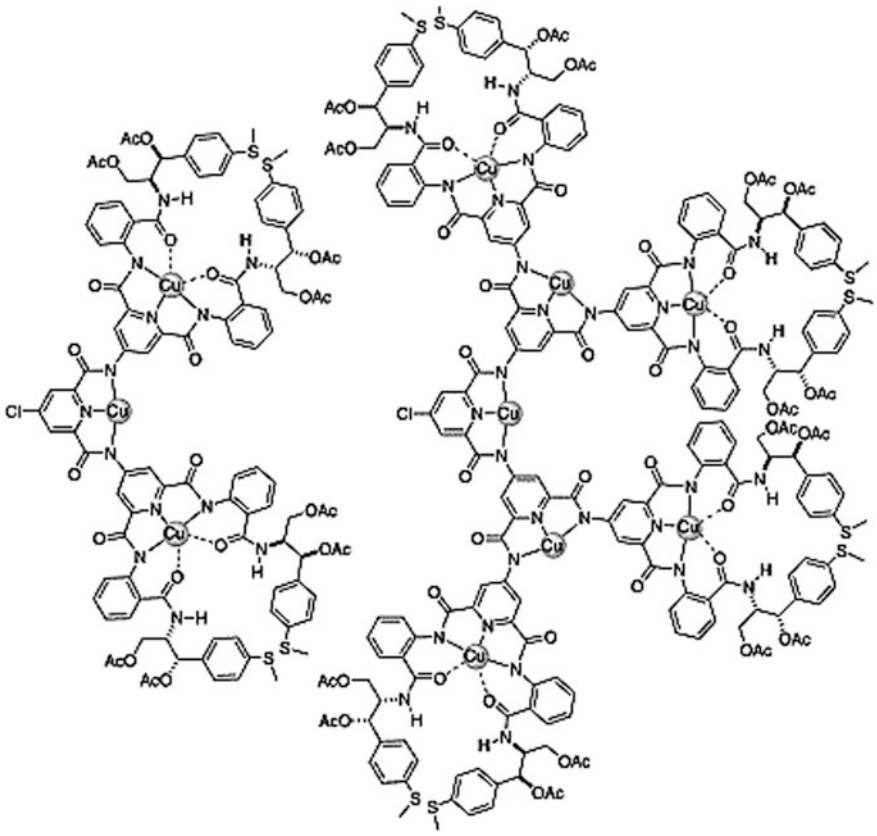

Fig. 5.25 G2 and G3 dendrons coordinated to three and seven copper(II) centers, respectively

MCD-based catalyst is efficient and is repeatedly used without loss of activity, selectivity, and efficiency.

It should be noted using of the dendrimers containing polydendate ligands for the preparation of contrast agents [219–223], in particular, through PSM (Scheme 5.14) [220, 221, 224, 225]. As a typical example, we note PSM of the commercially available PAMAM and PPI by DTPA with consequent chelation by $GdCl_3$ [226]. It is important that increasing generation of Gd-DTPA MCD leads to substantial increase of the r_1 and r_2 values.

The mixed gadolinium and yttrium chelates of the G5 DTPA-based dendrimer were obtained by changing the ratio between Gd-DTPA and Y-DTPA chelates along the periphery. It should be noted that yttrium was used as a diamagnetic probe

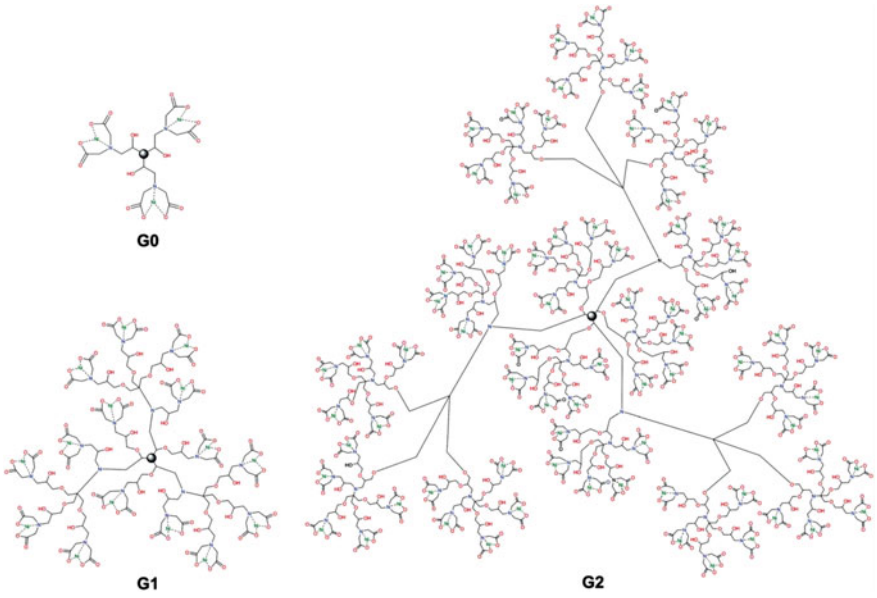

Fig. 5.26 Representation of Ni(II) loaded G0, G1, and G2 series of metallodendritic structures on surface of PMA-based Sepabeads EBEP-400

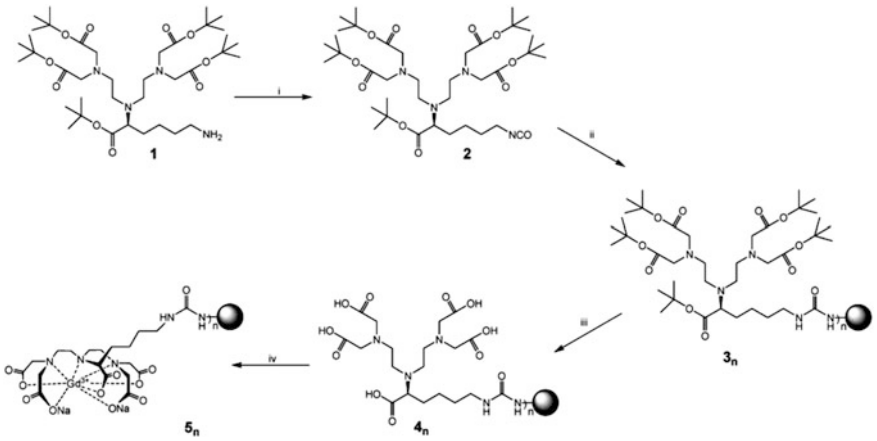

Scheme 5.14 Gd-DTPA-terminated PPI dendrimer

because it has a size similar to that of gadolinium, thus keeping the local mobility and molecular weight comparable. It is important that gadolinium was preferentially incorporated. Additionally, the heterometallic MCD exhibited a substantial increasing the ionic longitudinal relaxivity on going to higher fractions of gadolinium, indicating a real dendrimer effect.

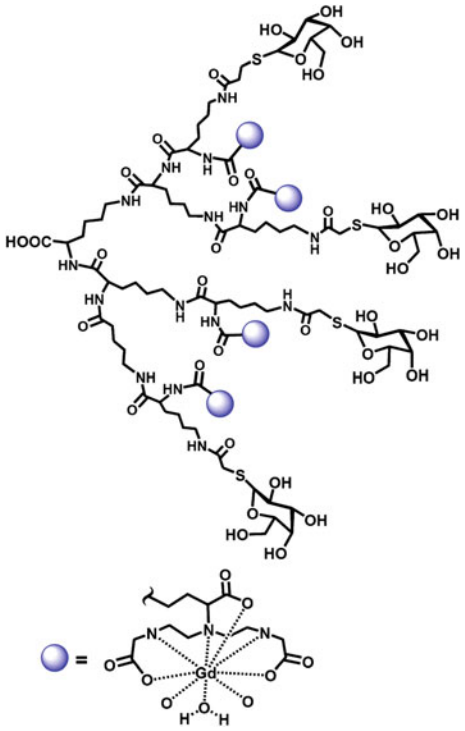

Fig. 5.27 PLL dendron bearing galactose and Gd chelates for cancer diagnosis

The *tert*-butyl ester-protected DTPA-terminated PPI dendrimers were chelated with $GdCl_3$, to create Gd-DTPA-terminated dendrimers [G1 (n = 4 Gd(III) ions per molecule), G3 (n = 16) and G5 (n = 64)] [227].

PLL dendron bearing galactosyl moieties and Gd-DTPA chelates was prepared by the mixing the chelating dendrimer with more than 1.5 equivs of $GdCl_3 \cdot 6H_2O$ at pH = 5.0–5.5 (Fig. 5.27) [228]. The MCDs having highly controlled structures and a single molecular weight show a two-fold increase in r_1 relaxivity to 9.1×10^3 $(Gd\ M)^{-1}\ s^{-1}$ compared to Gd-DTPA. It is important that no obvious cytotoxicity of this multifunctional dendritic agent is discovered in vitro.

The $EPTPA^{5-}$ chelate (H_5EPTPA is ethylenepropylenetriamine-*N*,*N*,*N*′,*N*″,*N*″-pentaacetic acid) was linked to PAMAM dendrimers of three different generations (5, 7, and 9) through benzylthiourea linkages [229]. The proton relaxivities measured at pH 7.4 for the MCDs G5-$(Gd\text{-}EPTPA)_{111}$, G7-$(Gd\text{-}EPTPA)_{253}$ and G9-$(Gd\text{-}EPTPA)_{1157}$ decrease with an increase of temperature, indicating that slow

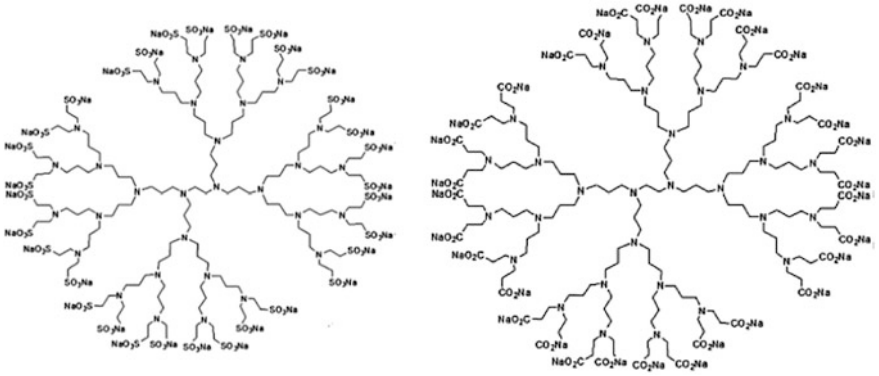

Fig. 5.28 Proposed structures for polysulfonate and polycarboxylate dendrimers

water exchange does not limit relaxivity. The Gd(III)-MCDs were prepared by mixing equimolar amounts of $Gd(ClO_4)_3$ and chelating dendritic ligand in water using a slight ligand excess (5%).

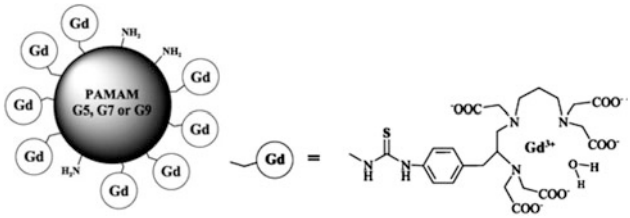

Among other polydentate dendritic ligands, we note G1–G3 sulfonated and carboxylated PPI-dendrimers with en core which showed specific picture in chelation of metal ions (Fig. 5.28) [230]. In particular, at low copper concentration up to 1:1 molar ratio between Cu(II) and dendrimer there is CuN_2O_2-mode on the dendrimer core. At higher concentrations of Cu(II) there is peripheral ion disposition coordinating one nitrogen atom and 3 oxygen atoms in square-planar geometry under limited mobility conditions. Finally, at high concentrations copper ions are timed to external dendrimer surface with CuO_4-mode. For sulfonate dendritic systems, weaker interaction of Cu(II) with nitrogen centers and stronger interaction with oxygen from SO_3^- groups is typical.

In another example, G3 triazine polydentate dendrimer (Fig. 5.29), containing multiple, iron-sequestering desferrioxamine B fragments is obtained in seven steps in 35% overall yield [231]. It is important that dendrimer chelates iron(III) ions with neither cooperativity nor significant interaction from the dendrimer backbone.

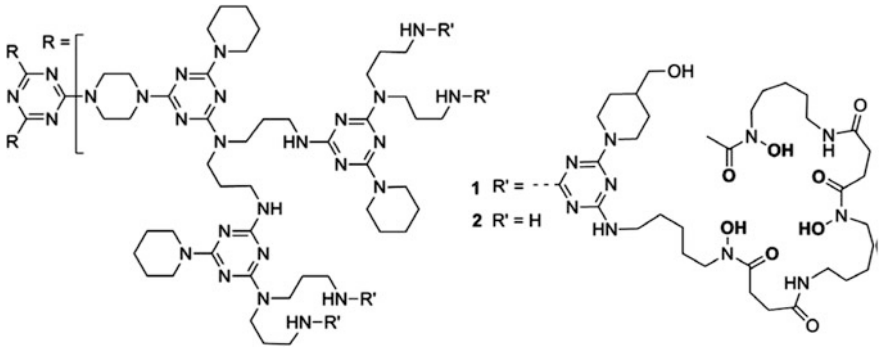

Fig. 5.29 Dendrimer displays 12 desferrioxamine B groups that form hexadentate chelates with Fe(III) using the groups shown in bold

The absorbance of Fe(III)-MCD is linear up to 11 mol equivs of Fe(III):L and this linear relationship suggests that iron chelation by this polydentate dendrimer is not cooperative.

5.3 Macrocyclic Complexes

The dendrimers and dendronized polymers containing macrocyclic complexes are the object of increased attention of researchers.

5.3.1 Metal Complexes with Pseudo-crown Ethers and Crown Ethers

The worm-like dendronized polymers having dendrons based on oxathiaethers showed high metal coordination properties [232]. Extensive characteristics of chelating properties with respect to a wide range of metal cations exhibited high and selective affinity of chelating dendrimers to Ag(I) and Hg(II) cations (Fig. 5.30). Its origin is explained by presence of specific M···S and M···O interactions (M = Ag or Hg) in a cage structure formed by dendritic fragments. Stoichiometry of complexation is determined by degree of steric hindrances in dendronized polymers. A result of complexation is Coulomb stabilization of charged dendronized polymers, which has a strong effect on their thermosensitive properties showing possible chemosensor applications.

Complexation of the dendronized PMAs with dibenzo-24-crown-8 branching blocks with K(I) ions brings to a significant expansion of a chain (Fig. 5.31) [233]. However, electrostatic repulsion does not contribute considerably into a chain expansion due to excessive bonding of counter-ions even far below Manning limit.

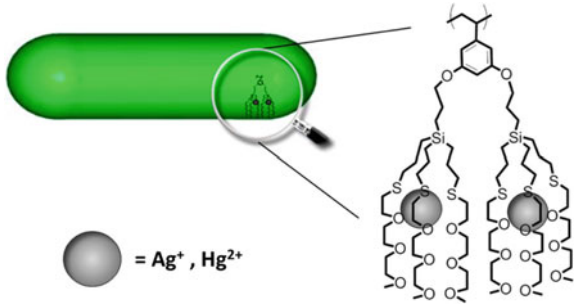

Fig. 5.30 Ag and Hg complexes with worm-like dendronized polymers bearing oxathiaether-based dendrons

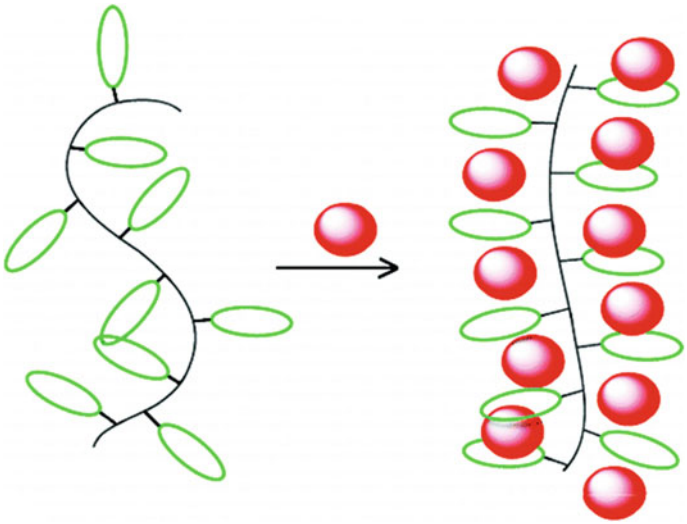

Fig. 5.31 Schematic representation of a potassium complexation with the dendronized PMAs with dibenzo-24-crown-8 branching blocks

Most probably, conformation change in fragments of the crown ether during coordination of K(I) ion in parallel to short-range interactions between ion pairs formed along a chain, causes the observed considerable increase in rigidity of the chain in terms of a Kuhn statistical segment length, l_k, with l_k = 8 to 19 nm and from l_k = 19 to 45 nm for G1 and G2 dendronized polymers, respectively. In other words, steric repulsion induced by guest-host interactions fits well for control over polymer conformation with densely grafted side chains.

We note also the dendrimer functionalized semi-crown ether incorporating up to 96 redox-active tetrathia-fulvalene moieties on the periphery, which was deposited onto a Pt electrode upon cycling. The macrocycle is suitable for the complexation of Ba(II) and the first dendrimer modified electrode able to reproduce the

electrochemical sensing of a metal cation thanks to the grafting crown ether/tetr athia-fulvalene units on the periphery of the dendrimer. It should be emphasized that this dendrimer constitutes one of the examples of sensing with organic redox active dendrimers [234].

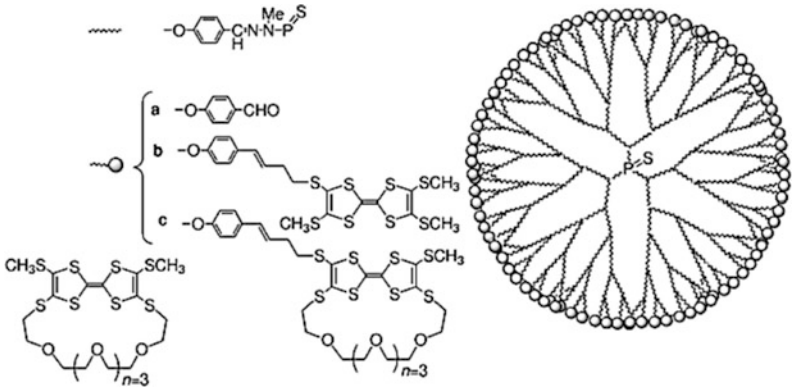

Of interest is using crown ether-functionalized dendrimers for extraction of alkali metal picrates [235]. It is important that depending on the generation of the dendrimer the positive and negative dendritic effects are observed.

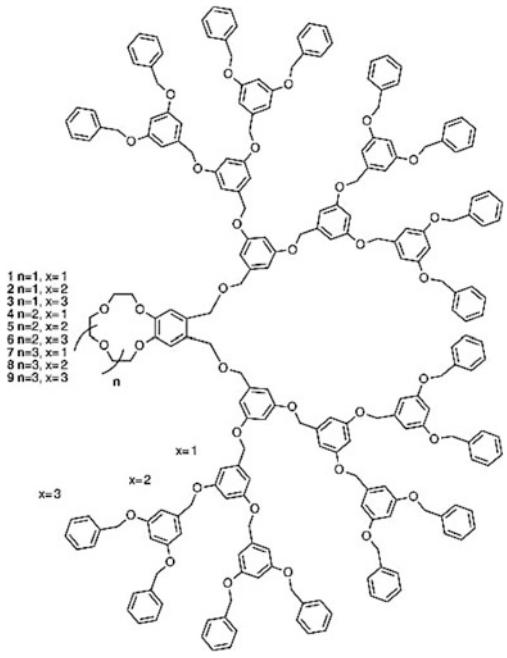

It should be noted the preparation of Na(I)-selective electrodes based on PVC membranes with silacrown modified carbosilane dendrimer, which works well over a wide concentration range with high selectivity [236].

Of interest is complexation of alkali ions with light-harvesting phenylacetylene monodendrons containing crown ether fragments [237].

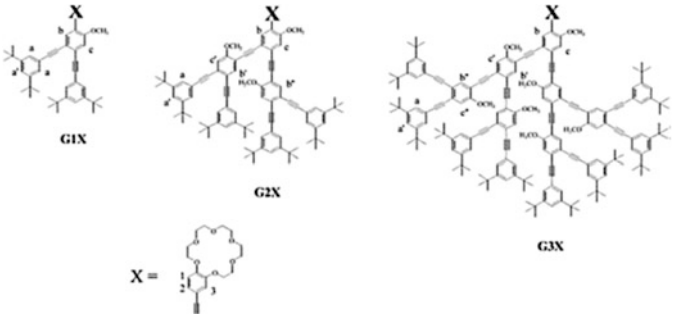

The crown ether-functionalized tetraphenylethene dendrimer was synthesized via the thiol-ene click reaction of thiol-derivatized tetraphenylethene with maleimide-functionalized benzo-15-crown-5 (Fig. 5.32) [238]. In the prepared com-pound the tetraphenylethene core and four outer benzo-15-crown-5 moieties serve as the AIE-active motif (AIE is aggregation-induced emission) and K(I)-binding function-alities, respectively. In particular, upon K(I) addition, dendrimer can be effectively induced to aggregate due to K(I)-mediated cross-linking via the formation of macro-cyclic complex in a sandwiched manner. This process is accompanied with the turn-on

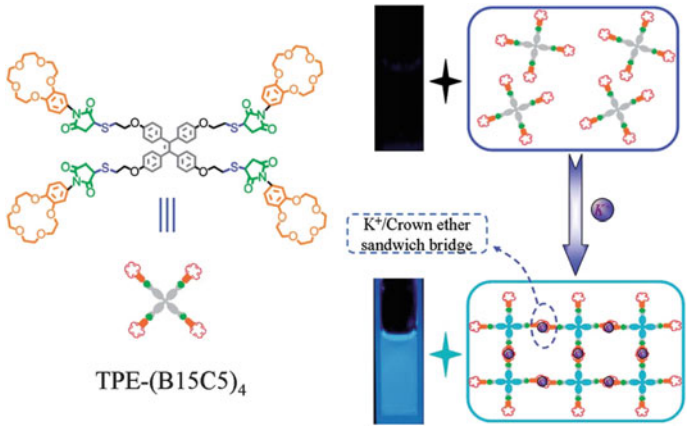

Fig. 5.32 Complexation of K(I) with crown ether-functionalized tetraphenylethene dendrimer

of fluorescence emission via the AIE mechanism. Thus, the prepared dendrimer can serve as highly sensitive and selective fluorometric off-on K(I) probes.

5.3.2 *Metal Complexes with Cyclam-Containing Dendrimers*

A large body of studies deals with MCD containing cyclam core [239–248]. Thus, a dendrimer with a cyclam core, dimethoxybenzene branches and naphthyl ends with Zn(II) gives bis-cyclam complexes $[ZnL_2]^{2+}$, which prevent formation of exiplexes as a result of naphthyl fluorescence [249, 250]. Similar photophysical results were obtained with lanthanide Nd(III), Eu(III), Gd(III), Tb(III), Dy(III) ion complexes, but data on emission correspond better with 1:3 and 1:2 dendritic complexes [251]. Upon titration of dendrimers containing two covalently bound cyclams as a core with $[Zn(CF_3SO_3)_2]$ or $[Cu(CF_3SO_3)_2]$, spectral emission changes, thus providing evidence of the 1:1 complexation, then substituted by 2:1 complex, though the results were different in absorption and emission spectra of these two metal ions [252]. Studying complexation between $[Ru(bpy)(CN)_6]^{2-}$ and dendrimer metal-cyclam core showed that the complex is formed with a dendrimer containing 12 dimethoxybenzene units and 16 naphthyl ends. In this complex a dendrimer plays a role of light-harvesting second coordination sphere and transfers collected energy to $[Ru(bpy)(CN)_6]^{2-}$. Moreover, the complex can be disrupted by addition of either acid or base exhibiting two distinct optical outputs according to an XOR and an XNOR logic, respectively [253, 254].

Cyclam-core G1 MCD with peripheral and in-core Ni centers is synthesized by interaction between tetrakis(salicylaldimine)cyclam ligand with Ni acetate [255]. MCD is cationic with two acetate groups as counter-ions and was isolated as a lime green solid in a yield of 63%. The trinuclear dendritic complex is used as a precursor of a catalyst in vinyl polymerization of norbornene using MAO as a co-catalyst with formation of macromolecular polynorbornene.

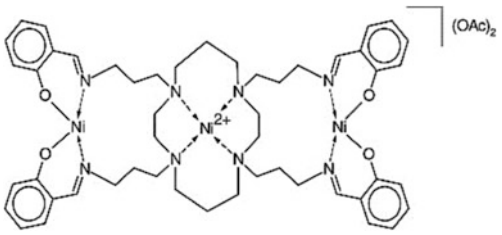

A dendrimer, which carries two cyclam units bound to azobenzene fragment and luminescent naphthalene peripheral blocks, was obtained (Fig. 5.33) [256]. It occurs that this dendrimer performs three different functions (light-harvesting,

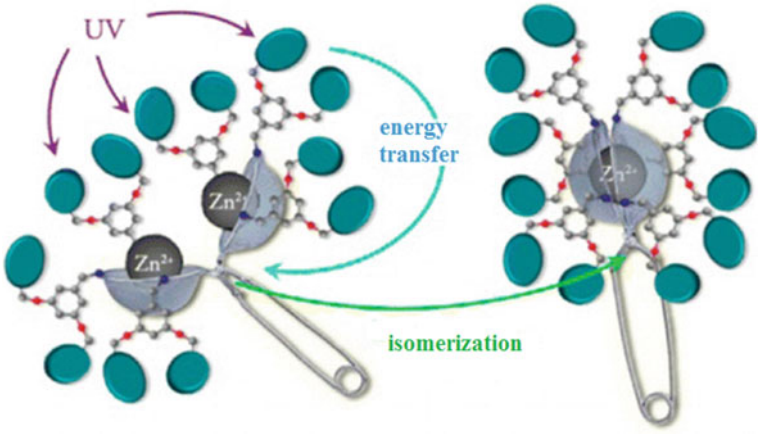

Fig. 5.33 Schematic representation of the functions performed by G1 dendrimer. Different coordination ability by the cyclam moieties (blue circles) of G1*(trans-azo)* (left) and G1*(cis-azo)* (right), light-harvesting by naphthalene units (grey ovals) and sensitized photoisomerization of the core azobenzene

photoisomerization, and metal ion coordination), which can interact or change depending on a metal ion nature. In other words, this is an example of easily controlled molecular tweezers, in which Zn(II) coordination provides 100% efficient photosensibilization of azobenzene switches, while Cu(II) switches off azobenzene isomerization.

Of substantial interest is the study of complexability of the dendrimers based on cyclam cores and linked PAMAM dendrons decorated along their perimeter with four or eight dansyl-chromophores [244]. It turned out that energy transfer to a central ion is a function of dendrimer generation. In addition, the energy transfer efficiency is determined by the geometry of the coordination node.

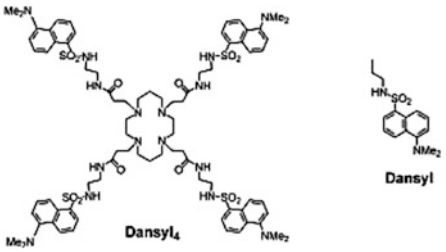

Nanolatexes of diameter 15 nm, having the cyclam fragment on the surface, were modified by a phosphorus dendritic compound containing an activated vinyl group at the core, and carrying Girard-T reagents as terminal fragments, for inducing

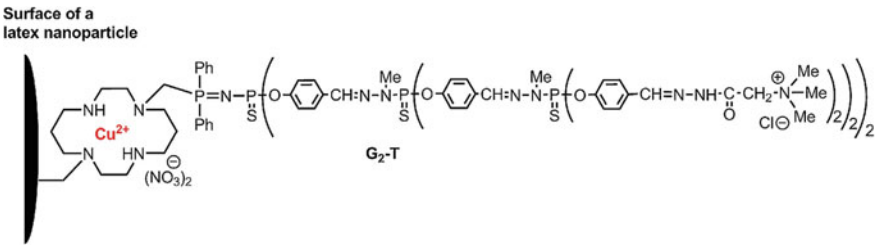

Fig. 5.34 A water-soluble dendritic structure linked to nanolatex through a tetraazamacrocycle suitable for the complexation of Cu(II)

solubility in water (Fig. 5.34) [257]. The dendronized nanoparticles retain the Cu(II) chelation ability, thus indicating the permeability of the dendritic shell.

5.3.3 *Metal Complexes with Cyclen-Containing Dendrimers*

In Eu-cyclen core dendrimers formed by click-reaction between dendrons carrying an azide group at the focal point and tetravalent cyclen core containing four alkyne groups, triazole not only acts as a stable spacer but also as a sensitizer, transferring their singlet-singlet excitation to UV range (270–290 nm) to partially occupied luminescent lanthanide 4f-shell (Fig. 5.35a) [240]. It should be noted that luminescence decay time from the lanthanide $^5D_0 \rightarrow {}^7F_2$ emission increases with increasing dendrimer generation, indicating that the shielding effect of the dendron wedges has a significant impact on the photo-excitation relaxation and energy transfer (Fig. 5.35b). Thus, the obtained triazoles intra-locked in close proximity to the macrocycle core promoted interesting photophysical properties.

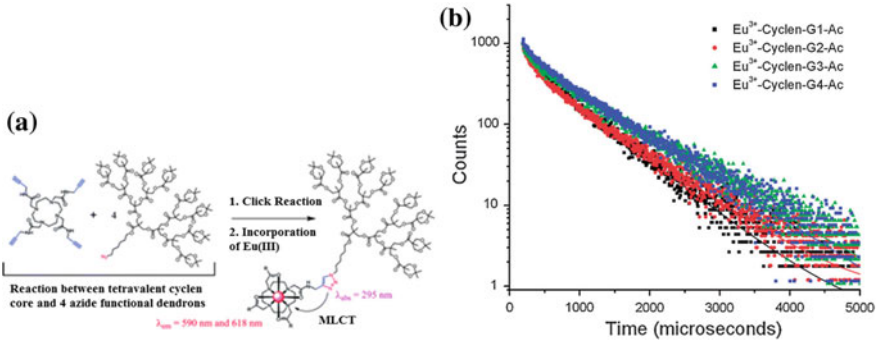

Fig. 5.35 **a** Scheme of synthesis of triazole sensitized Eu-dendrimer chelates. **b** Time-resolved luminescence recorded at 618 nm of various Eu(III)-cyclen dendrimers in THF solutions excited at 270 nm: G1 (black squares); G2 (red dots), G3 (green triangles), and G4 (blue diamonds)

5.3.4 Metal Chelates Based on Dendrimers with Triazacyclononane Fragments

Another example of macrocyclic MCD are PPI dendrimers with peripheral triazacyclononane fragments coordinated with Zn(II) ions [258]. Using control over molar ratio of triazacyclononane during production, 6 dendrimers were synthesized with 0, 20.5, 32.5, 53, 75, and 100% triazacyclononane groups on a surface. As occurs, a dendrimer with completely functionalized triazacyclononane groups is the most active catalyst of RNA model substrate cleavage, and its activity is by 270 times higher than that of the low molecular weight analogue and by five orders of magnitude more efficient than non-catalyzed reaction. Moreover, studies of cooperative effects showed that each active center contains two Zn(II) chelates, pointing to the fact that two ions act cooperatively in the RNA cleavage reaction.

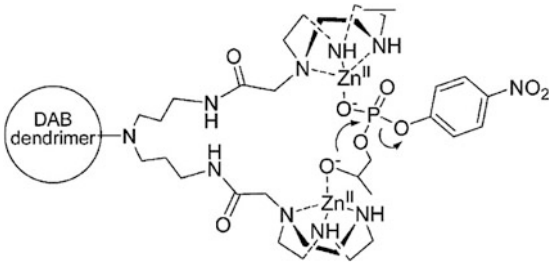

Lyzine-dendrons functionalized by triazacyclononane were fixed on Tentagel resin, and their Zn(II) MCDs were obtained (Fig. 5.36). It occurs that the cleavage reaction rate of RNA model substrate increases as a dendron size increases, at that increase in catalytic efficiency was determined by improved affinity of substrate conjugation. The obtained Michaelis-Menten parameters were in good agreement with the data obtained for homogeneous analogues, which points to the same type mechanism of catalytic reaction [259].

We should also notice peptide dendrons and dendrimers of increasing generation, functionalized at periphery by triazacyclononane forming a strong complex with Zn(II) ions [260]. These MCD show higher increase in cleavage rate of RNA model displaying, for example, in the case of D_{32} dendrimer increase about 80,000 (k_{cat}/k_{uncat}) at the concentration 600 nM.

5.3.5 Tetrapyrazinoporphyrazine Complexes

Derivatives of tetrapyrazinoporphyrazine containing rigid dendritic fragments are used to produce macrocyclic MCDs [261]. Absorption spectra of Mg-porphyrazines

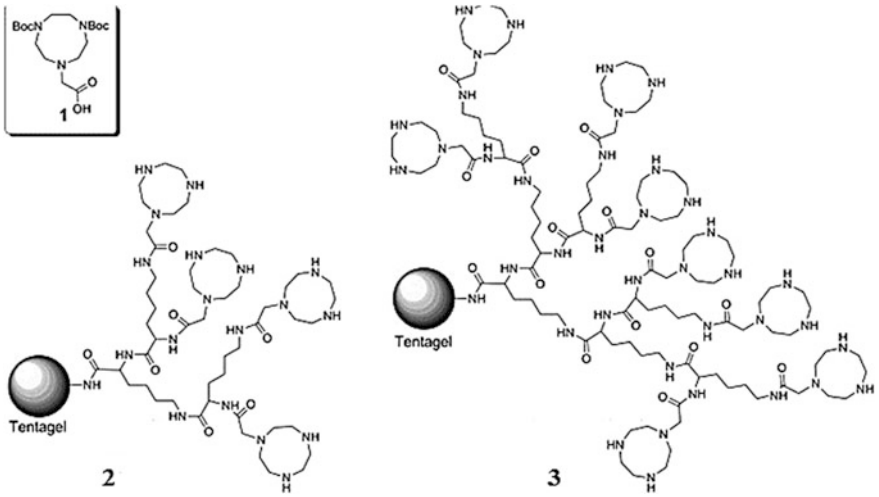

Fig. 5.36 Tentagel triazacyclononane resins **2** and **3** obtained in a single step by reacting Tentagel with triazacyclononane-derivative 1

show that splitting of Q band for 653 and 737 nm is caused by a combination of a transition moment between a pair (or more) chromophores.

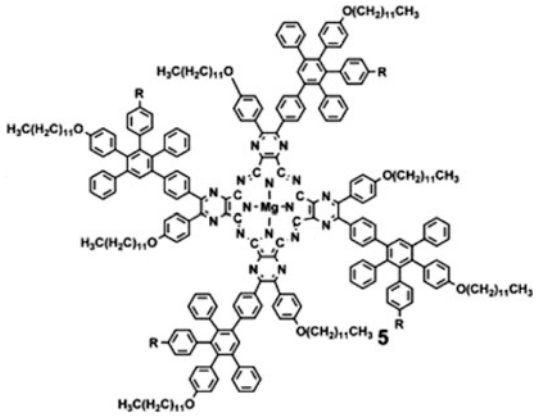

5.3.6 *Porphyrin Complexes*

Numerous studies are devoted to M-Pp dendrimers obtained by direct metallation of free-base Pp containing dendrimers [16, 21, 262]. The majority of M-Pp MCDs

possess a M-Pp unit as the interior core fragment only, although usually Pp units are mostly introduced at the surfaces of readily (commercially) available dendritic structures, such as PAMAM dendrimers.

As a typical example, we note the synthesis of photosensitizers by metallation of Pp core dendrimers with Al, Ag and Zn [263]. Experiments show effective two-photon excited FRET for Pp excited triplet state, which subsequently generates singlet oxygen by Al and Zn MCDs. In particular, efficiency of singlet oxygen photosensitization is most effective using Al, then using Zn, and the least effective then using Ag. In fact, Ag-metallated dendritic photosensitizers were non-fluorescing and unable to generate a measurable amount of singlet oxygen. With proper selection of the inserted metal, it was possible to tune efficiency two-photon induced singlet oxygen.

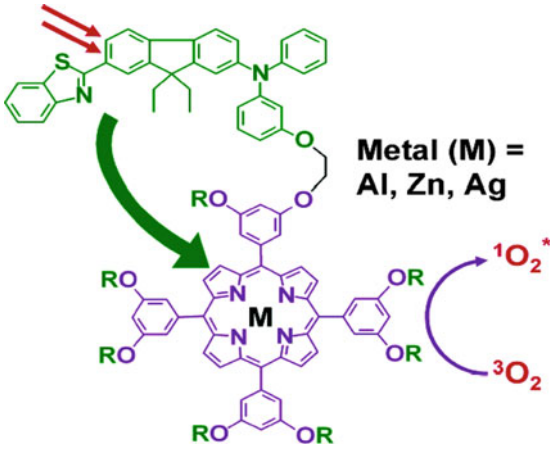

The corresponding free-base Pp dendrimer was metallated with $FeCl_2$ in dry THF to form the MCDs possessing a Fe-Pp catalytic core and polyether dendritic arms [264]. Lower generations of MCD show a normal hyperbolic kinetic behavior, whereas G3 and G4 MCDs exhibit a sigmoidal kinetic profile associated with cooperative effects due to aggregation phenomena. This behavior resembles that observed for Fe-Pp containing biomolecules such as cytochromes and hemoglobin.

It should be noted metal-chelating Pp-PAMAM dendrimers which were synthesized via the microwave method [265]. The metal-binding properties of the Pp-PAMAM dendrimers were studied by means of the polymer-supported nanofiltration technique. The nylon membranes modified with Pp-PAMAM dendrimers retained Pb(II), Cr(II) and Fe(II) with a retention rate of 99%, and Co(II) and Cd(II) with a retention rate above 50%.

Interesting examples are the complexes for optical amplification based on Er (III)-cored M-Pp dendrimers [70]. Initially, the 5,10,15-$(G2)_3$-20-(4-methoxycarbonylphenyl)-Pp was metallated with $PtCl_2$ in anhydrous benzonitrile and then

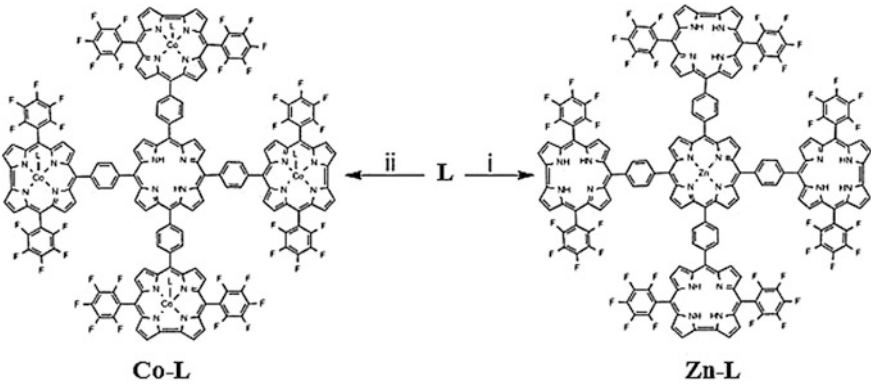

Fig. 5.37 The complexation of Co(II) or Zn(II) with dendritic Pp with four corroles

reacted with $ErCl_3$. The Er(III)-cored complex with Pt(II)-Pp bearing G2 Fréchet-type dendrons displayed intensity seven times greater than that of its parent Pt(II)-Pp. The emission lifetime of the Er(III)-cored dendritic complex was found to be 40 ms in deoxygenated THF solution. This result showed that energy transfer from the M-Pp to the Er(III) core proceeded through a triplet state.

It should be noted MCDs containing Fe-Pp core and boron ether end fragments [266]. It turned out that the end modification leads to changes in the conformation and catalytic behavior of the resulting MCDs, therefore these MCDs were called catalytic chameleon dendrimers.

An interesting observation was made in the study of complexation of dendritic Pp with four corroles [267]. It was found that different chelating properties of such macrocycles allow selective introduction of Zn(II) to the central Pp and Co(III) in the peripheral corroles (Fig. 5.37). The selective metallation is very important for the design of MCDs, in which one type of macrocycle is used as photosensitizer and the other for performing catalysis.

Selective metallation of the surrounding corroles under reaction conditions where the central Pp remained free indicates the known high affinity of corroles to cobalt(II). The ^1H NMR spectrum (Fig. 5.38) confirms the presence of four Co-PPh_3 moieties by the relative integrations of their *para*-H, *meta*-H, and *ortho*-H resonances (δ = 7.1, 6.7 and 4.7 ppm, respectively) with the Pp's β-pyrrole CH resonance (δ = 9.4 ppm). Finally, the two inner NH protons that appear at −2.3 ppm clearly testify that the central Pp was not metallated.

5.3.7 Phthalocyanine Complexes

The metal complexes with dendritic Pc obtained by direct metallation of free-base Pc have been little studied [16, 268]. For example, it should be noted the synthesis

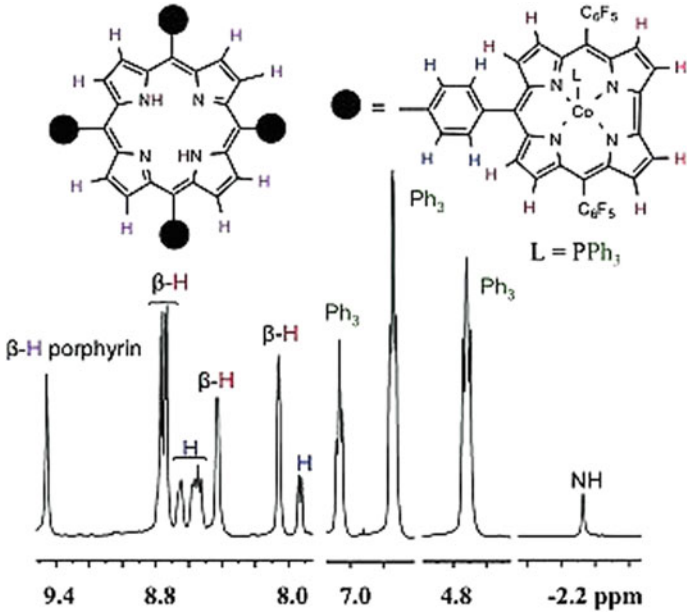

Fig. 5.38 ^{1}H NMR spectrum of Co-L in [D_6]benzene

of the G2 cobalt-metallated Pc dendrimer possessing Newkome-type dendrons (Fig. 5.39) to catalyze the oxidation of mercaptoethanol by dioxygen [269]. The dendritic structure around the Co-Pc prevented the molecular aggregation among Pc moieties in polar solvents and thin films. The electron-transfer process was hindered in the Co-Pc MCD that is the result of a shielding effect by the dendrimer branch on the Co-Pc core. The influence of Pc aggregation, resulting from strong intermolecular stacking, led to increased catalytic activity, as well as enhanced catalytic stability.

Of interest is the study of the complexation of copper and cobalt chlorides with a G1 dendrimer containing an octa-substituted Pc core (Fig. 5.40a) [270]. The Pc core has D_{2h} symmetry and corresponding Q-band splits into two main absorptions (ca. 670 and 700 nm). At the same time, Co-Pc dendrimer has D_{4h} symmetry, for which a single Q-band at 674 nm and a vibrational band at 610 nm are characteristic (Fig. 5.40b). It should be noted that a broad band is observed between both bands due to a dendrimer aggregation. However, in the spectrum of G7 Co-Pc MCD (the insert in Fig. 5.40), the intermediate band has totally disappeared indicating an absence of any aggregation for a G7 dendrimer.

It should be noted that triplet quantum yields are substantially increased during transition from tetra-glycosylated Zn-Pc MCD to octa-galactosylated Zn-Pc MCD [271].

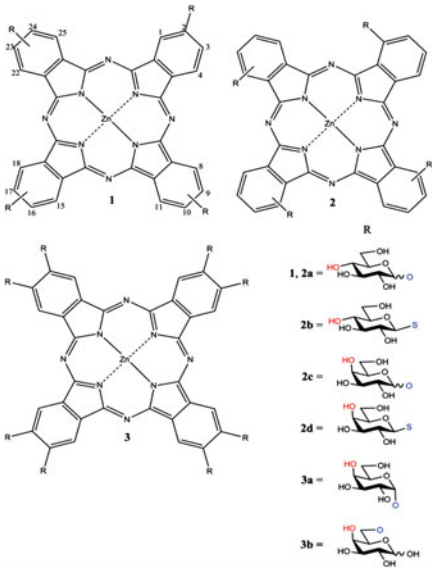

5.3.8 *Metal Chelates with DOTA and Related Ligands*

The DOTA ligand and its DO3A analogue are important chelators commonly used for biomedical applications as therapeutic radiopharmaceutical and/or MRI contrast agent [272]. MRI applications of dendrimers containing DOTA and DOTA-like ligands are particularly appealing, because the dendrimer can be labeled with multiple Gd chelates, creating a strongly paramagnetic macromolecule with higher relaxivities on a molar basis than conventional LMC, due to slower molecular tumbling rates of large macromolecules [10, 273]. The branched structure of the chelating dendrimers imparts rigidity and a high density of functional groups for the multivalent display of Gd for therapy and diagnosis [24, 219–225, 274, 275]. The dendrimers with DOTA or DO3A ligands have been mainly used as an alternative scaffold capable of carrying multiple chelating ligands (among them DOTA or DO3A) to incorporate radiopharmaceuticals at well-defined positions [219, 276]. It should be emphasized that the behavior of contrast agents based on Gd(III)-MCD in vivo depends on the modification of the properties of the dendrimer, such as the size of the core and the chemistry of the outer shell.

A more versatile topology within the dendritic structure is the dendrons, where the surface can be decorated with the same ionic groups as spherical dendrimers, but the focal point can be functionalized with different groups by orthogonal chemistry [6]. Very few examples have been reported conjugating a DOTA or

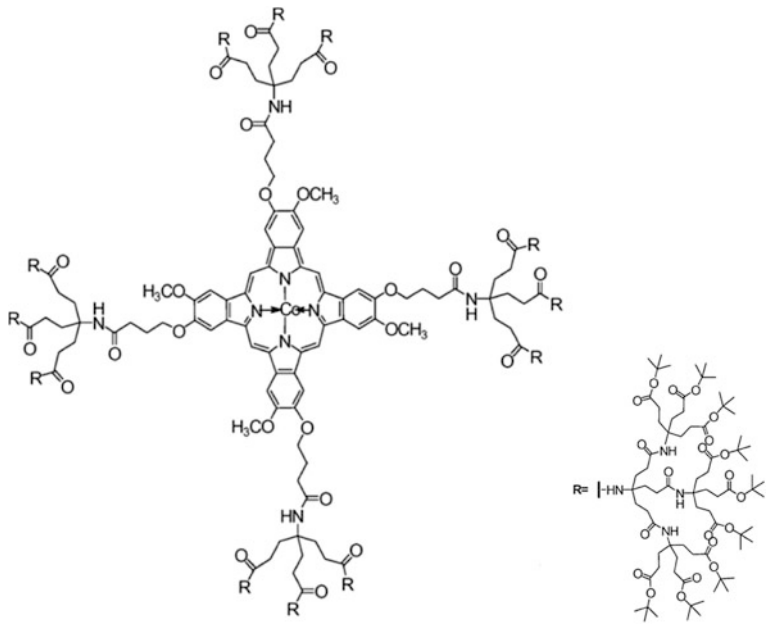

Fig. 5.39 M-Pc dendrimer possessing Newkome-type dendrons

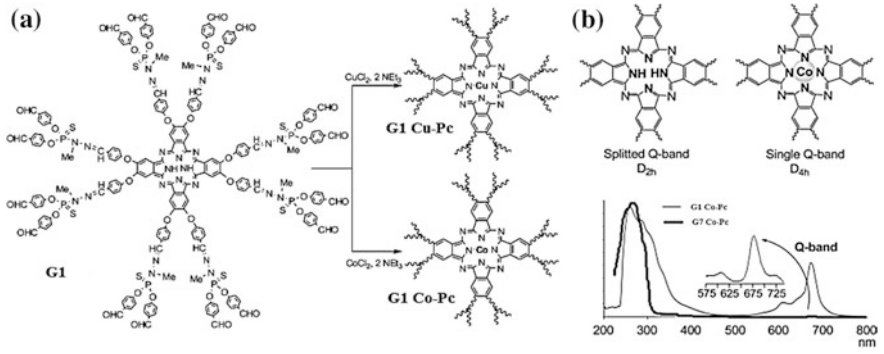

Fig. 5.40 **a** Synthesis of dendrimers having a Pc as core and the corresponding copper and cobalt complexes. **b** (top) Symmetry of free-base and complexed Pc cores, and spectroscopic consequences. (bottom) UV/Vis spectra of the G1 and G7 of the Co-Pc; both spectra are normalized to have the same intensity at 268 nm. The insert is an enlargement of the area of the Q-band of G7 Co-Pc in THF

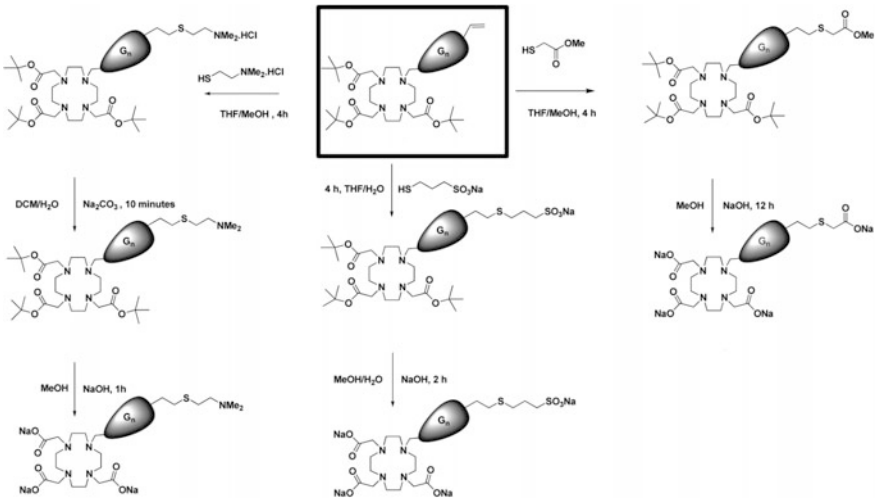

Scheme 5.15 Synthesis of neutral (amine or ester) and ionic (ammonium, carboxylate, or sulfonate)-terminated dendrons with protected and unprotected DO3A at the focal point

DO3A ligand at the focal point (Scheme 5.15) [277]. The presence of the dendron branches modifies the chelation capacity of the macrocyclic ring with respect to that of monomer DOTA ligand. In this situation, one can keep the periphery for the desired biomedical application while adding a new function at the focal point, normally as a radiolabeling moiety.

As a typical example, we note a readily and rapidly accessible triazine dendrimer prepared in four steps with 23% overall yield to give a structure showing four maleimide fragments and DOTA [278]. The functionalization of the chelating DOTA group with gadolinium was also accomplished easily.

In another interesting example, the Arg-Gly-Asp (RGD) peptide dendrimers were conjugated with a DOTA moiety and radiolabeled with ^{111}In to evaluate the in vitro receptor binding characteristics and in vivo tumor targeting properties [279]. The monovalent, divalent, and tetravalent dendrimers (Fig. 5.41) were radiolabeled by dissolving these compounds in an NH_4OAc buffer of pH 6.0 and 22.2–37 MBq $^{111}InCl_3$ was added to each of the reaction mixtures. The radiochemical yield was more than 98% with a specific activity of 7.4 MBq μg^{-1} for monovalent (corresponding to 13.6 GBq μmol^{-1}) and divalent (22.7 GBq μmol^{-1}) ^{111}In-labeled dendrimers and was 80% for ^{111}In-labeled tetravalent dendrimer (43.3 GBq μmol^{-1}).

Of considerable interest is PAMAM G5-Gd-BnDOTA dendrimer synthesized in order to develop a clinically applicable analog [280]. Its main advantages are the greater inherent stability of the macrocyclic complex of Gd-BnDOTA under in vivo conditions, slightly smaller overall size, and ability to uniquely prepare a preformed Gd(III) chelate to attach to the dendrimer. Promising is the use of DAB core instead of en core because the slightly longer spacer will produce fewer cavities or defects

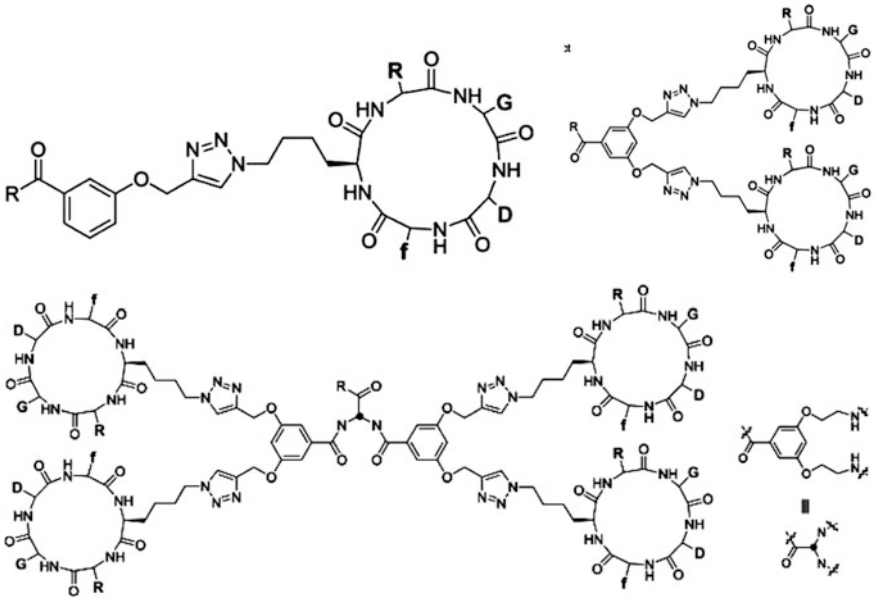

Fig. 5.41 Synthesis of the mono-, di- and tetravalent cyclo-peptide DOTA-conjugated dendrimers (R = DOTA-EtNH)

on the surface of the dendrimer into force less packed branches, and therefore more reproducible batch-to-batch production.

The conjugation of Gd-DOTA chelates to the PEG cored PLL dendrimer leads to a macromolecular MRI contrast agent for the differentiation of human breast cancer from benign soft tissue (Fig. 5.42a). No acute adverse effect was observed for this diagnostic agent in a long-term clinical trail [281]. It should be also noted the using the PAMAM framework to obtain a series of multivalent lanthanide(III)-glyco-conjugates, possessing DOTA monoamide functionalized chelators (Fig. 5.42b) [100]. The relaxivity of the Gd(III) chelates of the glycodendrimer in solution had a low value due to restrictions imposed by the flexibility and molecular weight of the dendrimer. At the same time, the lectin-glycoconjugated interaction was capable of retarding the tumbling rate considerably, therefore increasing the relaxivity of the Gd(III) chelates.

Of great interest is the relaxometric characterization of the fully loaded conjugate, containing 16 gadolinium chelates Gd-DO3AP^{ABn} based on monophosphinated DOTA-like ligand, where H_4DO3AP^{ABn} is 1,4,7,10-tetraazacyclododecane-4,7, 10-triacetic-1-{methyl[(4-aminophenyl) methyl] phosphinic acid}, on the surface of a G2 PAMAM dendrimer (Scheme 5.16) [282]. The corresponding Gd(III) chelate was synthesized by mixing the conjugate with a twofold excess of $GdCl_3$ at pH 7.

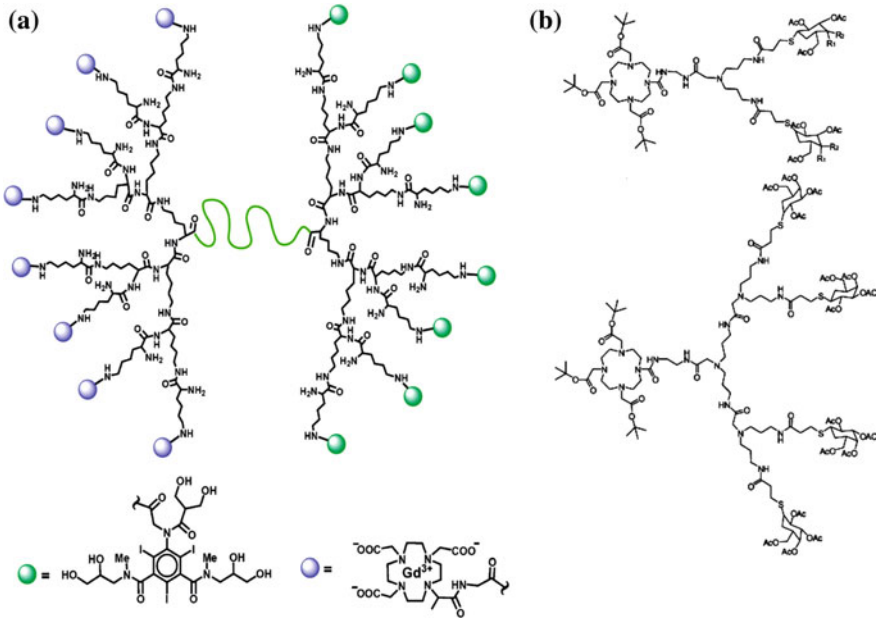

Fig. 5.42 **a** PEG-cored PLL dendrimers as MRI contrast agents. The green line represents PEG chain. **b** DOTA-Glycoconjugate ligands for lanthanide(III) chelation

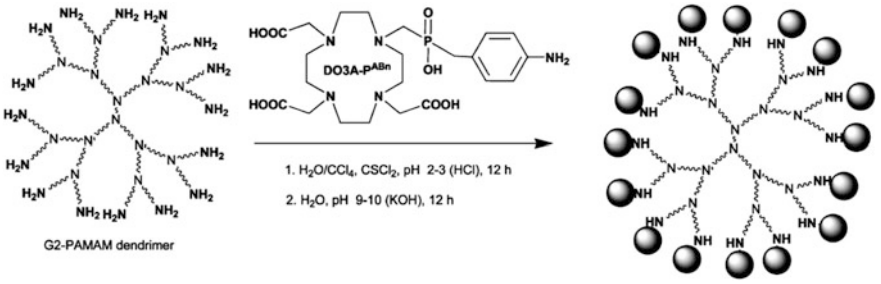

Scheme 5.16 Reaction sequence leading to the full-loaded G2-PAMAM dendritic conjugate

It is important that the proton relaxivity of this system was found to be pH dependent and, at pH = 6, it increased to ca. 24.8 mM^{-1} s^{-1}.

It should be noted G0 and G2 PPI dendrimers functionalized Yb(III)-DOTAM as pH-sensitive paramagnetic chemical exchange saturation transfer (CEST) agent [283].

5.4 Metal Chelate Star Polymers

One of the significant drawbacks of the MCDs is that their synthesis has usually required cumbersome multiple condensation reactions to increase the generation (molecular weight), which was even more complicated when a chelating functionality or metal chelate unit was introduced into the structure. As a similar 3D MCD, the metal chelates with hyperbranched polymers are the attracting alternative materials, because the synthesis is by simple addition polymerization, which is easy to prepare macromolecules with various chelating functionalities or metal chelate units through copolymerizations of functional monomers.

The simplest metal chelates with hyperbranched polymers are so-called star PMCs with more than three arms linked with the core. The undoubted advantages of star PMCs are simpler synthetic methodologies and a large number of terminal metal chelate units within a single polymer. As a typical example, we note star PMCs prepared by the modification of the different parts of star polymers using CRP method [284–292]. It is important that the size of star PMC can be tuned over a wide range by controlling the synthesis conditions.

The synthetic strategy of the star PMCs is based on the combination of star polymer synthesis and the coordination chemistry of metal chelates. There are two general methods for the synthesis of star PMCs: the «arm-first» and «core-first» methods (Scheme 5.17) [293]. Each of these has a select set of advantages and disadvantages inherently attached, and so care must be taken when planning the desired properties or targeted application for the star PMC prior to deciding which approach to employ. Advances in living/controlled polymerization methods have greatly improved the

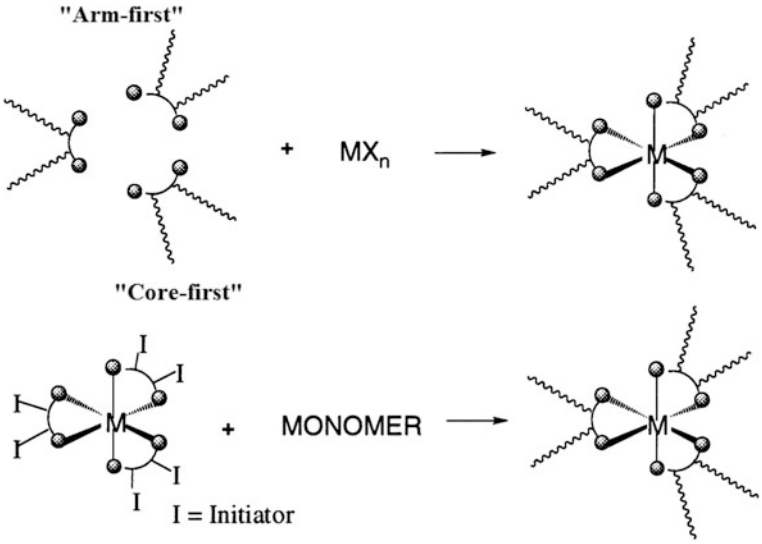

Scheme 5.17 Scheme presentation of «arm-first» and «core-first» methods

accessibility to star PMCs, with libraries of metal chelate stars of different size and/or functionality now able to be prepared for detailed assessment of structure-property relationships.

The «arm-first» method is based on MX_n chelation with the polymers containing terminal chelating fragments for preparing star PMCs. The different star PMCs including miktoarm star ones can be prepared by this method using various metal compounds and modifying polymer arms alone and their terminal fragments.

At the same time, «core-first» approach uses a metal chelate initiator for living polymerizations and, thus, becomes the core of the formed star PMC. This synthetic methodology allows to preparing star block PMCs and regulating number of arms.

5.4.1 «Arm-First» Method

The most frequently used ligand to prepare star PMCs is bpy. This ligand forms bis- or tris-chelates with a large variety of metal ions, and is an ideal candidate for the preparation of multiarm metal chelate stars because bpy functionalized at the 4- and/or 4′-position can be rather easily prepared. Thus, star iron(II) tris(bpy)-PMCs based on PS, PMMA, PCL, poly (DL-lactic acid) of different molecular weights with 3, 4, 5, or 6 arms can in principle be synthesized according to the functionality of the bpy used [294]. Iron tris(bpy)-chelate star formation is facile for macroligands <15,000; however, both the rate and extent of chelation are polymer dependent and decrease with increasing molecular weight.

The various star PMCs were prepared based on chelation of bpy-terminated PEO with Ru(II) [295] or Os(II) [296] ions. The star PMC obtained had a higher molecular weight than the pre-polymer and showed a narrow PDI. In the case of a Ni(II) or a Co(II) chelates, however, the star PMC is dissociated into three linear prepolymers under the conditions of GPC measurement.

Macromolecular PEG-containing iron tris(bpy)-chelates, presenting hydroxyl end groups for further modification as bioconjugates, copolymers, or cross-linking agents, were prepared via anionic ROP of ethylene oxide from hydroxyl-containing bpy initiators and subsequent chelation to iron(II) (Fig. 5.43a) [297]. Study of chelation of the bpy-centered PEGs with molecular weights from 4000 to 17,000 and low PDI (<1.1) to iron(II) sulfate revealed unexpected air sensitivity unlike iron tris(bpy)-LMC. In particular, red-violet aqueous solutions of $[Fe(bpyPEG_2)_3]^{2+}$ begin to bleach within hours when exposed to air and under argon, the chromophores are stable (Fig. 5.43b). Fe-PMCs are slower to form and faster to degrade in air with increasing molecular weight of $bpyPEG_2$.

$BpyPEG_2$ macroligands modified with methacrylate groups were also chelated with $FeSO_4$ to produce star PMCs [298]. In this case spontaneous gelation of iron (II) tris(bpy)-chelate PEG methacrylate was observed without the addition of a cross-linking agent. It is interesting that treatment of preformed hydrogels of chelating macroligands with aqueous solutions of $FeSO_4$, $CuBr_2$, and $CoCl_2$ also produced materials with color changes indicative of complexation.

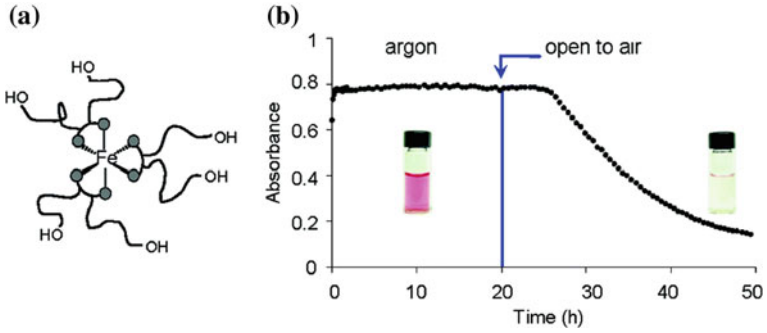

Fig. 5.43 Structure of $[Fe(bpyPEG_2)_3]^{2+}$ chelate with hydroxyl end groups (**a**). Rate comparison of $[Fe(bpyPEG_2)_3](SO_4)$ complexation in water under argon followed (after 20 h) by degradation under air for sample prepared from $bpyPEG_2$ macroligand of molecular weight M_n = 6200 (**b**)

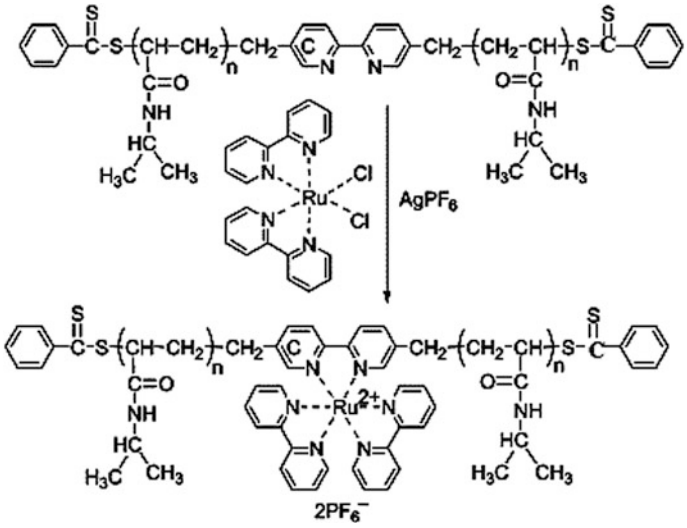

Scheme 5.18 Schematic representation for preparation of tris(bpy)Ru(II)-chelate poly(NIPAM) thermosensitive star polymers

«Arm-first» method was also employed for star PMCs with various arms including PS, PMMA, poly (propylene glycol), PCL, polylactides, and their block-copolymers [299–301]. Thus, macroligands $bpyPMMA_n$ (n = 1 or 2) were chelated to Fe(II) and Ru(II) with formation of star PMCs with one to six chains emanating from the central core, as well as different heteroarm star products [302]. Bpy-centered poly (NIPAM) polymers with controlled molecular weight and low PDI were chelated with ruthenium ion to produce thermosensitive star PMCs with well-defined structure (Scheme 5.18) [303].

Estimated CEs for formation of the Fe(II) and Ru(II) chelate stars, biocompatible polyesters, polylactides, PCL, and various copolymer analogues (M_n = 20,000–240,000 and 6000–30,000 for Fe and Ru chelates, accordingly) were high [300]. CE refers to the ratio of the extinction coefficient determined from λ_{max} for the PMC with that of Fe(II) and Ru(II) bpy-LMCs. Thin films of the red-violet colored iron-chelate stars exhibited reversible, thermochromic bleaching. Solutions and films of the polymers decolorize in response to some stimuli (heat, acid, bases, peroxides, ammonia), suggesting interesting possibilities for their use in qualitative and quantitative assays.

Narrow dispersity PS with bpy binding sites ($bpyPS_2$) were chelated to Ru precursor complexes, RuL_2Cl_2 (L = bpy, phen) or $Ru(DMSO)_4Cl_2$, to form star Ru-PMCs, $[Ru(bpyPS_n)_3]^{2+}$, with three and six arms, respectively [293]. More versatile were sequences involving chelation of 2 equiv of a $bpyPS_n$, followed by association of another ligand with the Ru(II) center (four-arm stars $[Ru(bpyPS_2)_2(L)]^{2+}$, where L = bpy, phen, 4,4′-bis(hydroxymethyl)-bpy, and 4,4′-bis(tricosanyl)-bpy) [304]. The determining factors of the reactivity at the Ru center are the CPL molecular weight, the position of the bpy donor in the PS chain, and solvent polarity. Homo-block star Ru-PMCs, $[Ru(bpyPS)_2(bpyPS_2)]^{2+}$ and $[Ru(bpyPS_2)_2(bpyPS)]^{2+}$, were synthesized by using two different kinds of $bpyPS_n$ macroligands.

The method has further permitted the synthesis of heteroarmed star PMCs [301]. Bis(bpy)Ru chelates were prepared with macroligands bearing one or two PS chains and then a second type of bpy-macroligand, bearing one or two PMMA chains, was attached to the bis-chelates, yielding hetero-arm star PMCs with 3 or 6 arms.

The bpy end-functionalized PS and poly (NIPAM)) polymers were used as macroligands for the preparation of star PMCs [305]. In this case, hydrophobic PS macroligand combined with hydrophiphilic poly (NIPAM) was chelated with Ru ions to produce amphiphilic star Ru-PMCs (Fig. 5.44).

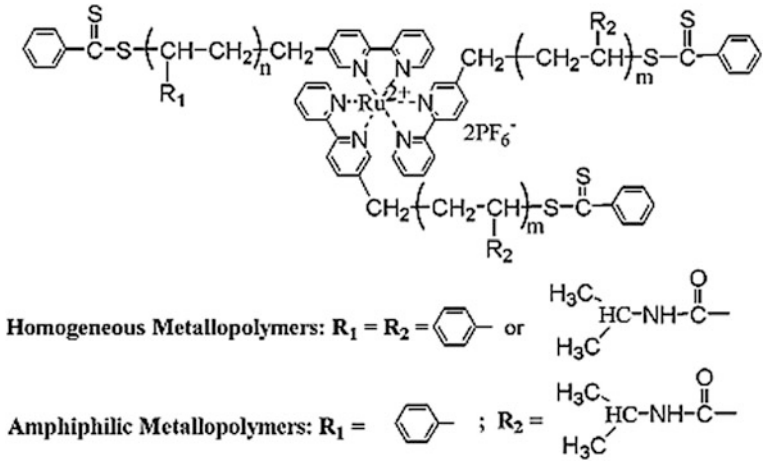

Fig. 5.44 Structure of star-shaped tris(bpy)-ruthenium-cored PMCs

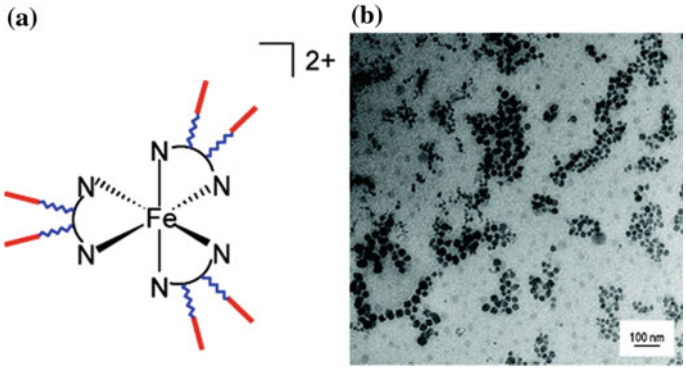

Fig. 5.45 **a** Schematic representation of star tris(bpy)-Fe(II) block-PMC: *N–N* bpy, zigzag PEG, straight poly(lactide). **b** TEM images of star Fe-PMC nanoparticles (M_n = 37,000)

It is important that the prepared amphiphilic star PMCs are able to form micelles in water, which morphology is determined by the polymer concentration and the hydrophilic poly (NIPAM) block length [306].

Bpy-centered block copolymers incorporating biocompatible PEG and poly (lactide) polymers with Fe(II) ions form star PMCs (Fig. 5.45a) [307]. Micelle-like nanoparticles of block copolymer macroligands and star Fe-PMCs were prepared via nanoprecipitation. The presence of spheroid particles (chelating macroligands, 111–253 nm in diameter; Fe-chelates, 37–75 nm in diameter) is shown (Fig. 5.45b). Halolike regions surrounding the nanoparticles and a distribution of lighter particles between the nanoparticles are observed, indicating that a fraction of the polymer is dissolved in the nanoparticle dispersion and aggregates during solvent evaporation.

The macroligands bpy(PMMA-PS)$_2$ and bpy(PS-PMMA)$_2$ were chelated with Fe(II) to yield six-arm star PMCs [308, 309]. However, for bpy[PCL-poly(*tert*-butyl acrylate)]2 and bpy[poly(lactic acid)-poly(*tert*-butyl acrylate)]2 macroligands, only bis(bpy)-chelates were formed. This is associated with variations in chain conformation in the solvent mixture used, inducing steric hindrance around the metal chelating site. CE is determined by polymer molecular weight and composition. It should be noted that most macroligands form tris-chelates efficiently (CE = 0.95–1.00) for lower molecular weights (20,000–25,000). At the same time, CEs decrease with increasing the molecular weights (e.g., for M_n = 115,000 only 62% tris-chelate formation is observed). Energetic preferences of polymer-polymer versus polymer-solvent interactions also play a role.

Hetero-arm star PMCs can also be produced by the chelation of the bpy (PS-PCL) macroligand with Fe(II) or Pt(II) [310]. In another example, a stepwise Ru chelation method was developed for synthesis of miktoarm star block-PMCs (Scheme 5.19) [311]. In this case six-arm metal chelate stars were obtained by first forming a Ru bis-chelate with bpy bearing two PCL chains as macroligands, followed by chelation with a bpy bearing either two PS chains or two PEG chains.

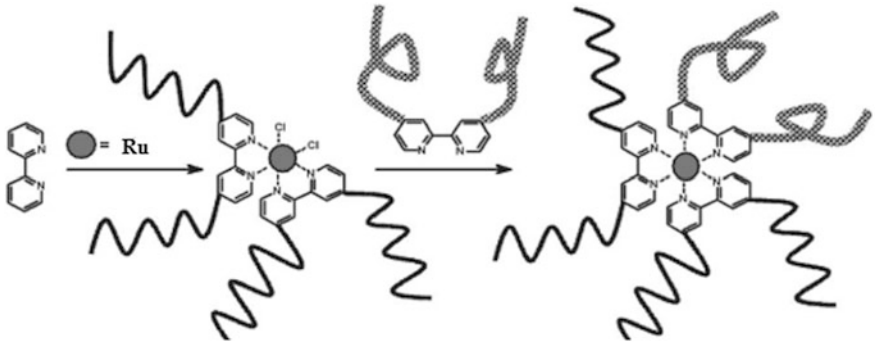

Scheme 5.19 Synthesis of hetero-arm metal chelate star polymers from bpy ligands

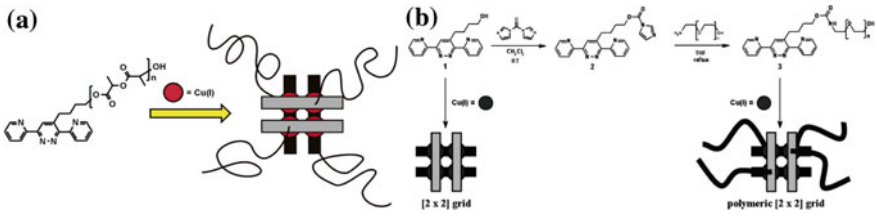

Fig. 5.46 **a** Schematic representation of the formation of polymeric grid-like complexes from the macroligands. **b** Schematic representation of the synthesis of PEG-DPP via activation of hydroxyl-DPP with CDI followed by coupling with α-hydroxy-ω-amino-PEG (top). The formation of grid-like [2 × 2] metal chelates upon addition of Cu(I) is also shown (bottom)

Four-arm stars were prepared by chelation to a Ru-bpy bis-chelate bearing one PS chain on each bpy, a bpy bearing either two poly (lactic acid) chains or two PEG chains.

Well-defined bpy-centered triblock and pentablock macroligands with low PDI were chelated with c $FeCl_2$ for preparation of star iron-PMCs [Fe{bpy(PEG-PCL)$_2$}$_3$]Cl_2, [Fe{bpy(PEG-PCL-L-poly(lactide))$_2$}$_3$]Cl_2, and [Fe{bpy(PEG-PCL-D,L-poly(lactide))$_2$}$_3$]Cl_2 with six diblock and three-block arms [312].

Among other chelating polymers, we note a poly (L-lactide) functionalized DPP which forms star polymeric [2 × 2] grids upon the addition of Cu(I) ions [313]. It is important that the chelation could be successfully performed in dichloromethane, thus, indicating that both the properties of the ligands (chelation) and the polymers (solubility) could be combined in one material since the Cu(I) grid of hydroxyl-DPP is insoluble in CH_2Cl_2. Besides, CPLs revealed strong cooperativity in the grid formation in the case of short polymer side-chains, the macroligands, whereas the larger CPLs formed polymeric [2 × 2] copper(I) grids without cooperativity [314].

This concept is expanded to metal chelate PCL-DPP (Fig. 5.46a) [315] and PEG-DPP star by end-functionalization of amine-containing PEG with DPP (Fig. 5.46b) [316].

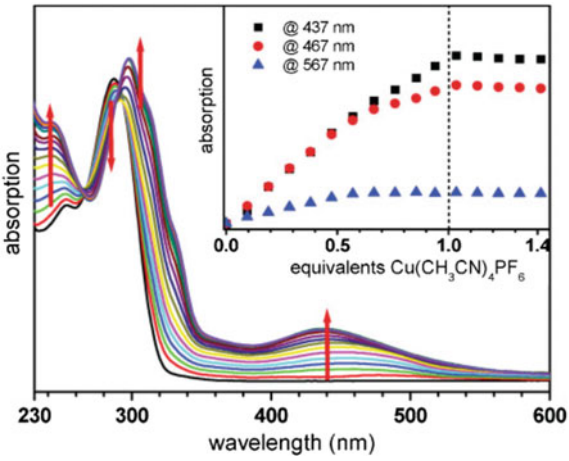

Fig. 5.47 UV-vis spectra obtained during the titration of $Cu(CH_3CN)_4(PF_6)$ to solutions of PEG-DPP in dichloromethane. The insets show the increase of absorption with the addition of copper ions

Addition of Cu(I) ions leads to the appearance of the characteristic MLCT band and the maximal absorption was reached at 1 equiv. of Cu(I) ions, which is associated with the formation of [2 × 2] Cu(I) grids (Fig. 5.47). Besides, the addition of 0.5 equiv. of Cu(I) ions resulted in a change in λ_{max} of the MLCT from 467 to 437 nm indicating that up to 0.5 equiv. of Cu(I), chelates containing two ligands and one Cu(I) ion are formed. Following addition of Cu(I) ions leads to the formation of the most stable structure, namely [2 × 2] grid-like chelates containing four ligands and four Cu(I) ions. Strong cooperativity is not observed in the grid formation due to sterical hindrance and/or entropic forces induced by the PEG-chains (Fig. 5.47, inset).

The self-diffusion dynamics of unentangled associating polymers based on four-arm PEG end-functionalized with tpy moieties chelated by Zn(II) in DMF (Fig. 5.48a) is measured by forced Rayleigh scattering at varying grating spacings ranging from 0.5 to 50 μm [317]. This model system is chosen for it's narrowly disperse molecular weight of the star polymer building blocks, its well-defined tpy-based sticker chemistry, and its robustly tunable strength of the metal-ligand bonds. Tracer diffusion of four-arm PEG polymers with just three associating arms is investigated through the same model transient network (Fig. 5.48b), providing insight into the diffusion mechanisms based on comparisons of self-diffusion and tracer diffusion.

Using 5-arm PEG polymer core with tpy end ligands on each arm (Fig. 5.49a), cross-linking network can be formed by introduction of different metal ions, including Mn(II), Fe(II), Co(II), Ni(II), Cu(II) and Zn(II) [318]. In particular, the increase of the π-π* band at 310 nm upon addition of Co(II) ions indicates the chelation (Fig. 5.49b). A similar behavior was found for the other investigated metal ions with π-π* bands in the region between 300 and 330 nm. However, no undesired effects such as precipitation were observed in the investigated concentration ranges.

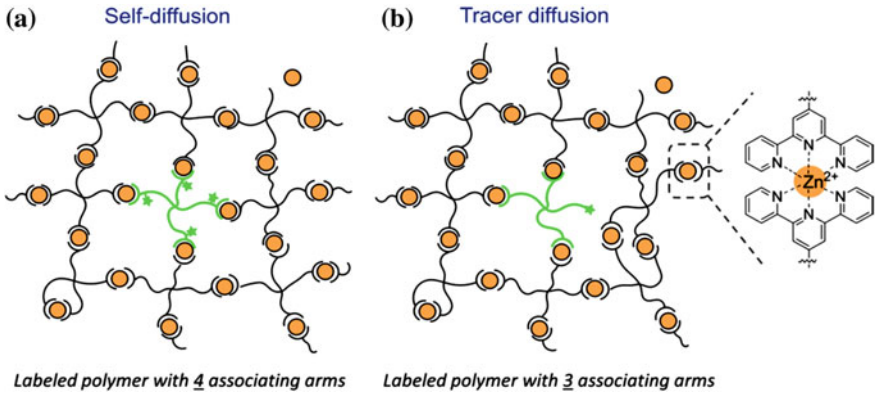

Fig. 5.48 Diffusion of fluorescently tagged four-arm PEG polymers with **a** four and **b** just three associating arms is probed in model transient networks formed by chelation between Zn(II) and tpy end-modified four-arm PEG polymers in (**a**) self-diffusion and (**b**) tracer diffusion configurations. Intramolecular primary loops and dangling chains are shown as two possible defects in the model transient networks. Green stars on the labeled polymers represent the locations of nitrobenzofurazan labels

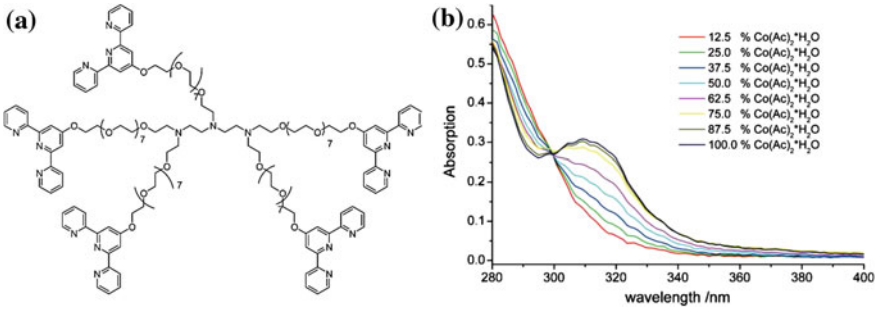

Fig. 5.49 **a** Structure of 5-arm PEG polymer core with tpy end ligands on each arm. **b** Chelation behavior of chelating macroligand with a variety of transition metal ions investigated in a parallel fashion in DMSO. The displayed spectra detail the case of Co(II) ions

The star PMC was obtained by coordination of *p*-(1,3-butanedionyl) phenyl-terminated PEO with Cr(III) ion [319]. It is important that the prepared star-shaped PMC exhibited film-forming properties, and the different star PMCs can be synthesized by coordination of this chelating macroligand with various transition metals.

Macroligands with β-diketone fragments were chelated to Eu, Fe, Cu and Ni metal ions to prepare star PMCs of various architectures (Fig. 5.50) [320]. «Arm-first» approach provides site-isolated PMCs with spectroscopic properties that correlate well with low molecular weight analogues. At the same time, the luminescence intensities of Eu-PMCs are substantially enhanced relative to $Eu(dbm)_3$

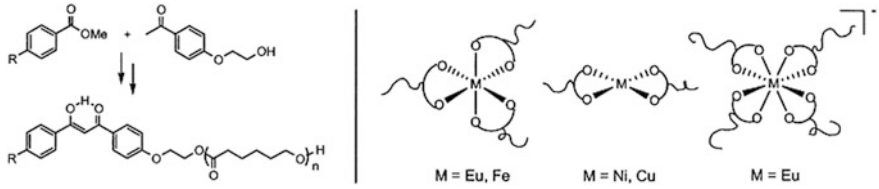

Fig. 5.50 Preparation of dbm initiators to generate dbm end-functionalized and dbm-centered PCL macroligands and structure of Eu, Fe, Cu and Ni metal chelate star polymers

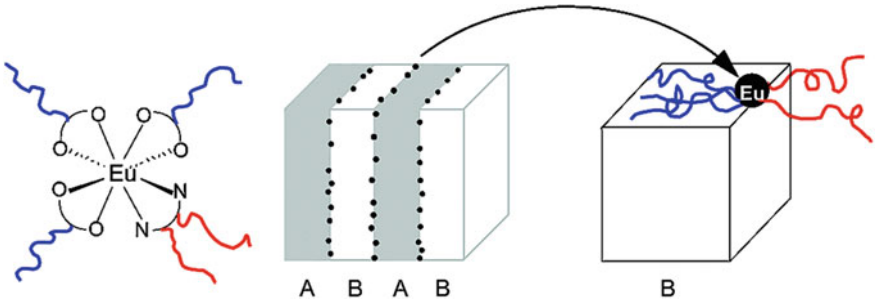

Fig. 5.51 A schematic representation of the lamellar morphology of a Eu[{dbm-poly(lactic acid)]$_3$}{bpy-(PCL}$_2$] block copolymer film (A = PCL, B = poly(lactic acid), filled circle = Eu center)

chelates. This is associated with the protective action of the polymer shell, determining luminescence quenching due to metal-metal interactions and access of water and other donor ligands to the metal site.

An Eu-chelate tri-armed star poly (lactic acid) was obtained by the «arm-first» approach using dbm-terminated poly (lactic acid) and $EuCl_3$ [321]. The three-armed star polymer was further turned into a five-armed one by addition of PCL containing the bpy fragment in the middle of the chain (Fig. 5.51). During transition from Eu $(dbm)_3$ solutions to Eu[dbm-poly(lactic acid)]$_3$ solutions to Eu[dbm-poly(lactic acid)]$_3$ films the increasing relative amounts of the longer lifetime component is observed due to the «polymer shell effect» and the decreasing aqua adducts known to shorten lifetimes. The sharpness of the feature at 579.7 nm, corresponding to the $^5D_0 \rightarrow {}^7F_0$ transition in the emission spectrum of PMC, lends further support for a homogeneous sample. This star PMC showed a lamellar morphology in thin films with the Eu(III) ions on the phase boundary. These microstructures containing Eu luminophores at the glassy poly (lactic acid)-crystalline PCL domain interfaces are modified by thermal treatment.

[Ln(dpa-PCL-PEG-$OCH_3)_3$]$(HNEt_3)_3$, where Ln = Eu(III), Tb(III), were synthesized by the chelation of an amphiphilic block copolymer of PEG-*b*-PCL methyl ether functionalized with a dipicolinic acid (dpa) fragment with lanthanide ions (Scheme 5.20) [322]. Micelle-like nanoparticles of star PMCs were prepared by

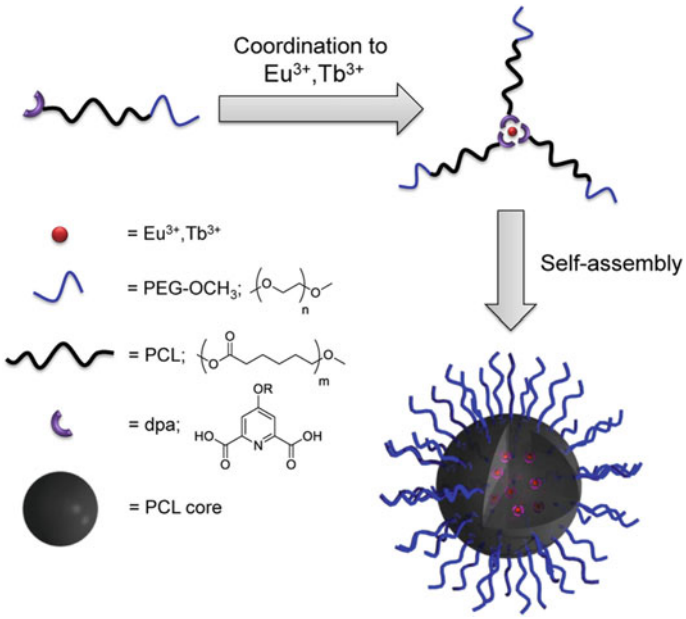

Scheme 5.20 Schematic representation for preparation of $[Ln(dpa\text{-}PCL\text{-}PEG\text{-}OCH_3)_3](HNEt_3)_3$ (Ln = Eu, Tb)

solvent displacement methods. The presence of solid sphere (<47 nm in diameter) and vesicle (>47 nm in diameter) morphologies was confirmed. The color of emission and morphology of the luminescent nanoparticles were tuned in a relatively straightforward approach by either changing the lanthanide ion or tuning the solution-assembly conditions, respectively.

The unique properties of star PMCs with a large number of functional arms make them suitable as fluorescent probes, contrast agents, and in vitro diagnostic systems [287, 323]. Star PMCs are highly desirable as MRI contrast agents owing to their well-defined architecture and potentially enhance MRI performance by reducing the rotational molecular tumbling rate (subsequently increasing the relaxivity). The results of the study of a series of MRI contrast agents based on star PMCs indicated the importance of the precise molecular location of Gd(III) in the optimization of MRI contrast at different magnetic field strengths [324, 325]. Thus, copolymers of oligoethylene glycol methyl ether acrylate and an activated ester monomer, pentafluorophenyl acrylate, were modified with the DO3A-tBu-NH_2 for the chelation of Gd(III) (Scheme 5.21) [324]. Star PMCs exhibited a substantially increased relaxivity in comparison to existing commercial Gd(III) MRI contrast agents.

Metal chelate based on DO3A-*t*Bu-NH_2 was also introduced into different parts (arms, cores, and end-groups) of the polymers using activated ester/amine nucleophilic substitutions, deprotected and chelated with Gd(III) [325]. In this case the precise placement of Gd(III) in the PMCs plays the determining role in optimizing

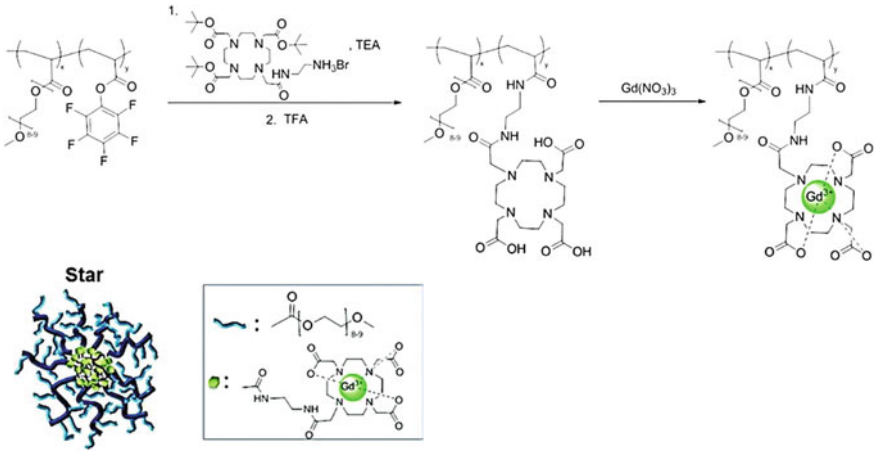

Scheme 5.21 General procedure for the preparation of metal chelate macromolecular star contrast agents

the performance of the PMCs as MRI contrast agents. The relaxivity varies from 11 to 22 mM^{-1} s^{-1}, 2–5 times higher than that of a commercial DOTA-Gd contrast agent when using a magnetic field strength of 0.47 T. Finally, the residence time of the coordinated water and the rotational correlation time of the final molecule were correlated with the polymeric structure.

Functionalization of 3D nanostructures having a PEG outer shell, a hydrophilic inner shell containing reactive functionalities, and a central hydrophobic core with a DOTA-ligand allows to chelating radioactive ^{64}Cu nuclei [323]. The biodistribution evaluation in normal rodents has shown a distinct correlation between the length of the PEG chains and the in vivo behavior of these nanostructures. Particularly, the cross-linked star PMCs with 2000 and 5000 PEG showed a much slower rate of blood clearance.

Of interest is the design of multifunctional drug delivery systems with bioimaging capabilities at the same time [326] as well as of multi-modality imaging [327] based on star polymers. Thus, acrylate star PMCs as fluorescence and MRI agents for multimodal imaging combining fluorescent and magnetic resonance features were developed (Fig. 5.52). Acrylate star polymers with hydrodynamic diameters of 10 ± 2 nm containing fluorene fragments as core units were functionalized with dopamine derivatives to chelate lanthanides such as Gd(III) and Eu (III) through the catechol moieties, which resulted in rapid water exchange of the highly hydrated star polymer. The in vitro and in vivo studies indicated that these multimodal imaging agents retained blue/red fluorescence and remarkable magnetic properties, with high relaxivity and high contrast features. The polymeric MRI agents based on a star architecture, where catechol chelates were fixed on the arms of stars, yielded contrast agents with a very high relaxivity (84 mM^{-1} s^{-1}) [328].

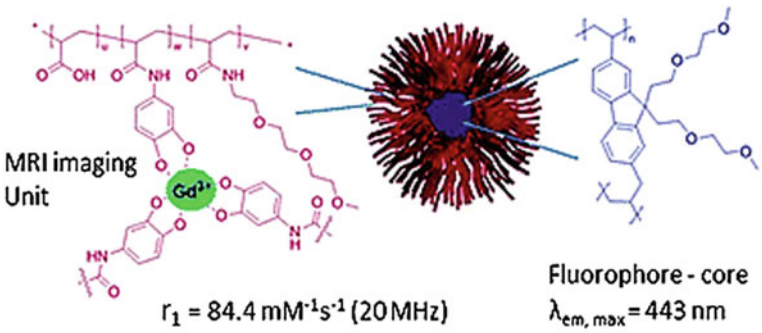

Fig. 5.52 Bimodal MRI star PMC imaging reagents

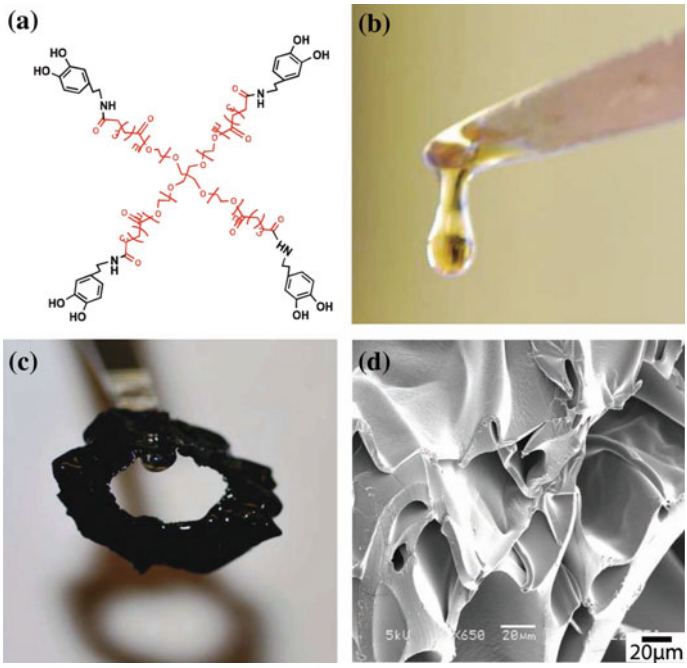

Fig. 5.53 **a** Chemical structure of PEG_4-dopamine (pentaerythritol-PEG_4 in red, dopamine in black). **b**, **c** Photograph of PEG_4-dopamine (20 mg) before (**b**) and after (**c**) the introduction of 2 M aqueous Fe(III) solution. **d** SEM image of the material in (**c**)

It should be noted a stiff injectable biodegradable elastomer based on a 4-arm PEG which was functionalized with dopamine terminal fragments (Fig. 5.53a). This chelating polymer was viscous and sticky (Fig. 5.53b). When PEG_4-dopamine was mixed with Fe(III) solution, a tough rubbery green-black polymer was formed within

a few seconds (Fig. 5.53c). The micrometer-scale morphology of this polymer (Fig. 5.53d) exhibited a rough surface with pores of different sizes and shapes [329].

5.4.2 «Core-First» Method

«Core-first» approach, which is faster, requires careful screening of initiator/catalyst/solvent compositions to find reaction conditions, for which polymerization is controlled [330, 331]. For example, tris(dialkylaminostyryl-bpy) M(II) chelates (M = Fe, Ru, Zn) are used as multifunctional metalloinitiators for the ATRP of MMA with CuBr/*N*-propyl-2-pyridylmethanimine as a catalytic system (Scheme 5.22) [332]. The polymerization rate strongly depends on the nature of the metalloinitiator : whereas a conversion of 94% was achieved after 4 h with Zn-initiator, only 50% conversion was reached when Ru-initiator was used. Kinetic curves of the polymerization exhibit a first-order behavior consistent with a living system. For the Fe and Ru chelates, an induction period of approximately 25 min is characteristic. The resulting star PMCs combine the optical properties of the monomers with good processability, which allow to preparing high optical quality thin films by the spin-coating method and thicknesses varying between 1 and 2 mm.

The bulk and solution (toluene) ATRP of MMA and methyl acrylate was performed using a Ru(II) tris(bpy) chelate bearing six α-bromoester initiating groups and $NiBr_2(PPh_3)_2$ and $NiBr_2(PBu_3)_2$ as catalysts resulting in well-defined polymers [333]. The molecular weight distributions of the PMMAs were narrow (toluene, PDI = 1.1–1.3; bulk, PDI < ∼1.3 at <50% conversion). This method allows to preparing Ru chelate PMMA stars with molecular weights ranging from 2800 to ∼350,000 (Table 5.2). It is interesting that the ε values were typically comparable to that of metalloinitiator (λ_{max} = 465 nm, ε = 16,607 M^{-1} cm^{-1}) and consistent with data for model structure containing a single Ru ion at the center.

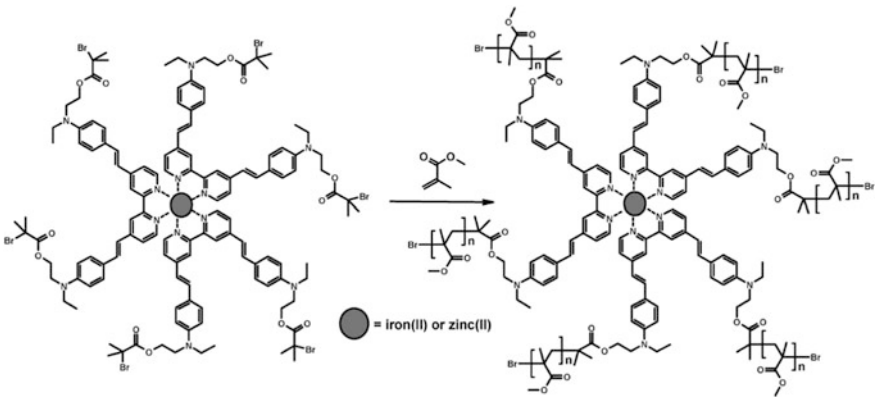

Scheme 5.22 Schematic representation of the synthesis of PMMA star PMCs

Table 5.2 Molecular weight and UV/vis data for a series of Ru chelate PMMA star polymers

$M_n^a \times 10^{-3}$	$M_w^a \times 10^{-3}$	PDI	$M_n(lin)^b \times 10^{-3}$	$M_w(lin)^b \times 10^{-3}$	PDI	$\varepsilon(465\ nm)^c$ ($M^{-1}\ cm^{-1}$)
11.8	12.3	1.04	9.4	10.7	1.12	17,200
54.0	57.7	1.07	42.4	46.9	1.10	18,800
74.7	81.8	1.09	64.8	74.7	1.15	19,300
114.1	123.6	1.08	90.6	102.4	1.13	20,100
116.9	129.3	1.11	102.5	125.1	1.22	19,300

[a]Molecular weight determined by GPC in $CHCl_3$ at 25 °C using multi-angle laser light scattering/refractive index detection
[b]Molecular weight determined by GPC in $CHCl_3$ at 25 °C using linear (lin) PMMA standards
[c]Molar extinction coefficient of the MLCT band determined using M_n(lin) to calculate sample concentration

The efficiency of initiation and controlled nature of these reactions are confirmed by low PDI of cleaved linear PMMA arms ($\sim$1.10–1.24) and $M_n^{star}/M_n^{arm} \approx 6$.

The poly(*N*-(ω′-alkylcarbazolyl) methacrylate) tris(bpy) bifunctional star Ru-PMCs were synthesized by ATRP of *N*-(ω′-alkylcarbazolyl) methacrylate in solution, where Ru chelates with one and three initiating sites acted as metalloinitiators with $NiBr_2(PPh_3)_2$ as a catalyst [334]. Electronic absorption and emission spectra of the formed PMCs indicate the chromophore presence within a single polymeric chain.

A hexafunctional Ru complex initiator, $[Ru\{bpy(CH_2Cl)_2\}_3](PF_6)_2$ was employed as initiator in the ATRP of St to form star polymers containing chelating fragments and chromophores at discrete positions in the polymer structures [335, 336]. A polymer product with narrow molecular weight distribution (M_n = 42,800, PDI = 1.10) is obtained using DMF as a solvent, when the reaction is quenched at $\sim$20% monomer conversion. Di- and tetrafunctional metalloinitiators with alkyl chains, $[Ru\{bpy(C_{13}H_{27})_2\}_n\{bpy(CH_2Cl)_2\}_{3-n}](PF_6)_2$ (n = 1, 2), showed improved initiation and molecular weights closer to targeted values. The preparation of well-defined metal chelate PS star polymers demonstrates the compatibility of the ATRP process with the cationic ruthenium initiators.

A quenchometric oxygen sensor based on a low PDI star PMC $[Ru(bpyPS_2)_3](PF_6)_2$ is obtained [337]. The incorporation of the oxygen sensing Ru chelate in the PS support allows to reaching much higher doping levels without microcrystallization of the chelate than traditional two-component sensors. However, the luminescence decays were still multiexponentials, indicating that sensor heterogeneity was not completely eliminated despite the narrow PDI (1.10).

Three-arm star PMC was prepared by the «core-first» approach using ATRP method [338]. This PMC included charged Ir chelate as the luminescent core and 2-(carbazol-9-yl) ethylmethacrylate as the arm repeat fragment. The prepared PMC shows a relatively low PDI of 1.30 with high thermal stability. It demonstrated effective inter- and intra-molecular energy transfer from the arm Cz fragment to the

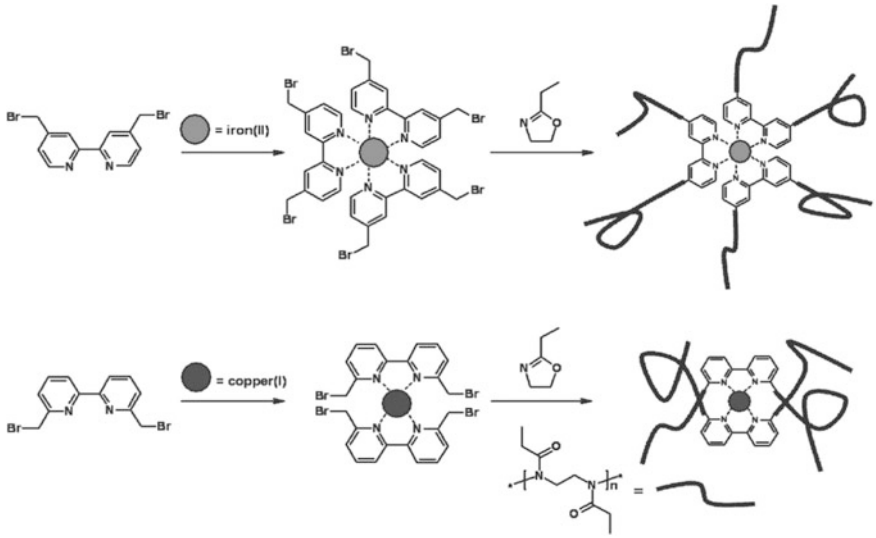

Scheme 5.23 Living ROP of 2-ethyl-2-oxazoline initiated with hexa-(halomethyl)tris(bpy) Fe(II) (top) and tetra-(halomethyl)bis(bpy) Cu(II) (bottom)

Ir chelate core in the host-guest system. It is important that good phosphorescent emission can be achieved at 565 nm by the design of the arm length.

A preformed Ru(II)bpy chelate was used as initiator for the direct polymerization of ε-caprolactone [339]. The resulting star PMCs showed both the electrochemical and optical properties of the Ru(II) chelate as well as the thermal properties of the polymers indicating the possibility of preparation of the materials with a novel combination of properties via the «core-first» method.

Metal chelate star polyoxazoline with six arms was prepared by living ROP of 2-ethyl-2-oxazoline initiated with di-, tetra- and hexa-(halomethyl)tris(bpy) Fe(II) and Ru(II) [340, 341] chelates as initiators resulting in well-defined star PMCs (Scheme 5.23, top). Dechelation of these star Fe(II)-PMCs was performed by reaction with potassium carbonate resulting in the free poly(2-ethyl-2-oxazoline) bpy macroligands. The decoloring of the polymer films was observed at 210 °C indicative of thermal dechelation, whereby the violet color of the Fe(II) chelate returned upon cooling. These metalloinitiators are also suitable for the polymerization of several other 2-oxazoline monomers including 2-methyl-, 2-phenyl- and 2-undecyl-2-oxazoline [342]. Samples were subjected to chemical cleavage in aqueous K_2CO_3 to generate metal-free bpy-centered polyoxazolines, which chelate to Fe(II), regenerating the $[Fe(bpy)_3]^{2+}$ chromophores. These experiments produce polymers with reasonably narrow molecular weight distributions ($\sim$1.1–1.5).

The cationic ROP of 2-ethyl-2-oxazoline with bis(bromomethyl)bpy Cu(I) initiators results in well-defined metal chelate four-arm star poly(2-ethyl-2-oxazoline) with central 6,6′-disubstituted bpy unit (Scheme 5.23, bottom) [343]. The living character of the polymerization was demonstrated with the linear relationship

between the M_w and the [monomer]/[initiator] ratio as well as in the synthesis of block copolymers. Thus, a metal chelate poly (2-ethyl-2-oxazoline-*b*-2-nonyl-2-oxazoline) star block copolymer was synthesized utilizing the same bis(bpy) Cu(I) initiator [344].

Amphiphilic six-arm star block-PMCs were prepared by the sequential addition of two different oxazoline monomers to the hexafunctional metalloinitiator, [Fe(4,4′-bis-(chloromethyl)-bpy)$_3$](PF$_6$)$_2$ [345]. The first block was made of the hydrophilic 2-ethyl-2-oxazoline, and the second, hydrophobic, block of either 2-phenyl-2-oxazoline or 2-undecyl-2-oxazoline. The star block-PMCs exhibit narrow molecular weight distributions (PDIs < 1.1) and molecular weights close to targeted values and T_g and T_m values that correlate well with those observed for the respective homopolymers. It was found that the hydrophilic poly (2-ethyl-2-oxazoline) block forms cylindrical microdomains in a matrix of hydrophobic block of poly (2-undecyl-2-oxazoline) [346].

A six-arm star PMC was prepared by a combination of ROP and ATRP [304]. At first, the polymerization of D,L-lactide by ROP using [Ru{bpy(CH$_2$OH)$_2$}$_3$](PF$_6$)$_2$ as hexafunctional initiator was carried out. Then, the hydroxyl terminal groups were turned to bromoesters, and tert-butyl acrylate was polymerized by ATRP. Finally, conversion of poly(tert-butyl acrylate) to PAA via hydrolysis affords water-soluble polymers, [Ru(bpyPAA$_2$)$_3$]$^{2+}$ and [Ru{bpy(C$_{13}$H$_{27}$)$_2$}(bpyPAA$_2$)$_2$]$^{2+}$ and the amphiphilic star polymer [Ru{bpy(D,L-polylactide)-PAA)$_2$}$_3$)](PF$_6$)$_2$.

Hexa(dithiobenzoate)-functionalized Ru(II) tris(bpy) chelate was used as chain transfer agents for the RAFT polymerization of St to obtain well-defined star light-harvesting block-PMCs containing an energy cascade of chromophores from the periphery to the core [347, 348]. RAFT polymerization of St functionalized coumarin monomers permits to introduce the first block with an average length of two St-coumarin units into each arm [348]. Then, the prepared polymer was used as a macro-RAFT agent for the polymerization of acenaphthylene to synthesizing the star diblock-PMC with a narrow PDI and an average length of 36 acenaphthenyl repeat fragments in each arm. A third block was introduced for synthesis a star triblock-PMC with an average length of 44 NIPAM repeat fragments in each arm (Fig. 5.54). It was demonstrated that the energy transfer proceeds mainly through a stepwise energy cascade from the initially excited acenaphthyl fragments to the coumarin chromophores and hence to the Ru(II) chelate core.

It should be noted numerous examples of the use of tpy metal chelates as metalloinitiators for star PMC preparation [349]. Thus, Fe(II) and Co(II) chelates of mono- and bis(bromomethyl)tpy were applied as initiators for the cationic ROP of 2-ethyl-2-oxazoline resulting in defined hydrophilic polymers with a central chelate unit and star-like architectures [350–352]. The living character of the polymerization allows an exact control of the molecular weight as well as the incorporation of additional (chelating) units at the polymer chain ends. Dechelation of both the Fe(II) and Co(II) star PMCs was carried out by refluxing the PMC with potassium carbonate in acetonitrile leading to the tpy-containing poly (2-ethyl-2-oxazoline). Rechelation of the CPLs with Fe(II) ions was effective up to 94%. Besides, an

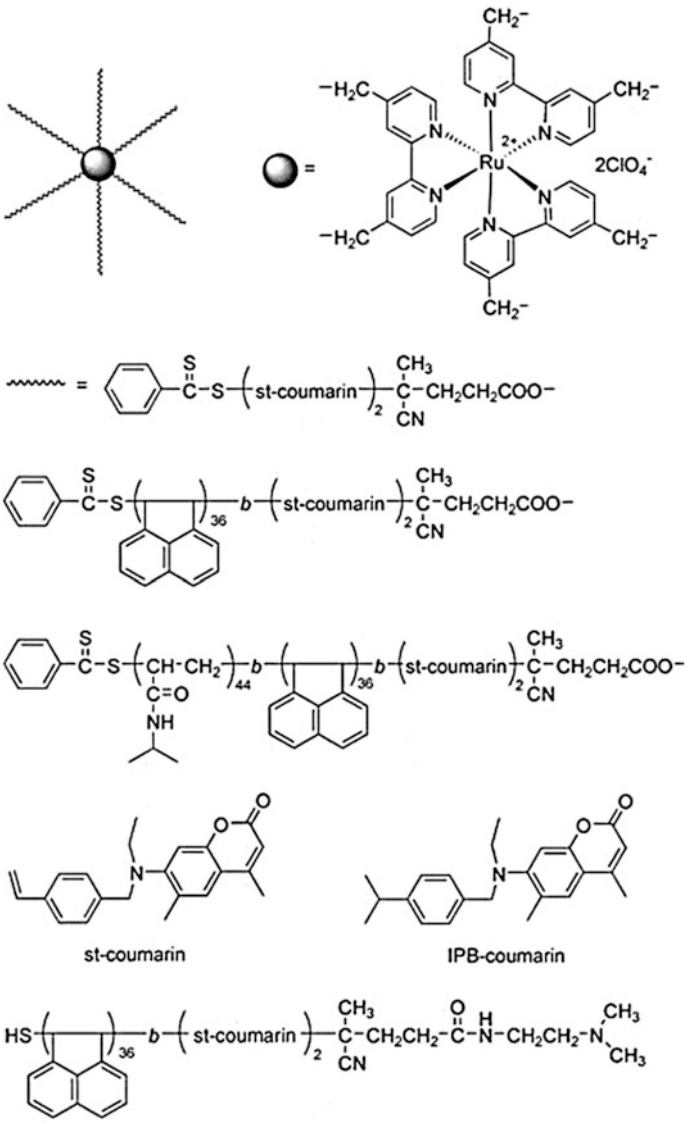

Fig. 5.54 Star light-harvesting PMCs

increase in viscosity was observed upon rechelation due to the coupling of the polymer chains by the metal chelation.

Of interest are amphiphilic PMCs containing a tri-arm or tetra-arm, conjugated, rigid core and flexible PEG coil blocks [353]. The synthesis of the PMCs includes the formation of heteroleptic bis-tpy Ru(II) chelates between the tpy-containing rigid cores and mono-tpy containing PEG chains. It should be noted the synthesis of

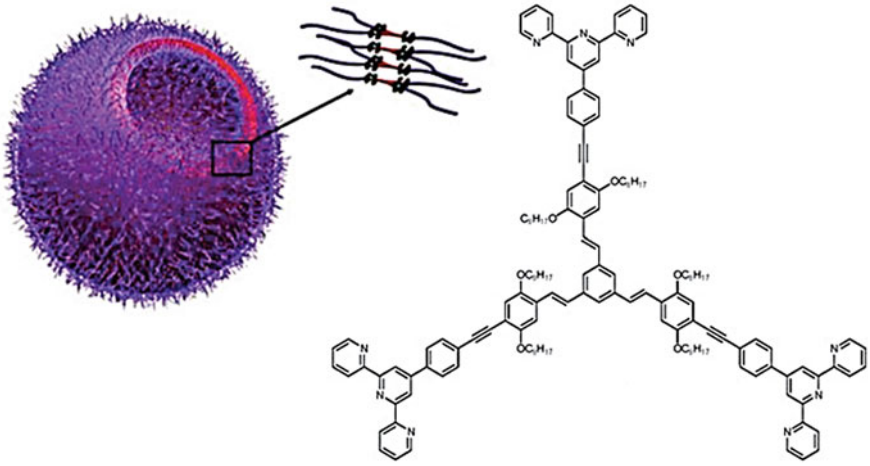

Fig. 5.55 Schematic representation of a vesicle formed from a tri-arm metal chelate star copolymer in acetone

the tri- and tetra-arm star block-PMCs by first preparing the PEG-Ru(II) monochelate with its following interaction with the tpy-containing rigid core. The self-organization in selective solvents leads to well-defined vesicles with thin walls for the tri-arm derivative in acetone and acetone/water mixtures in which the vesicular wall is formed by the rigid cores and both its inner and outer surfaces are decorated with the PEG blocks (Fig. 5.55).

The chelate $Fe(dbmOH)_3$ was used as an initiator in lactide polymerization [354]. Short reaction times (10 min) were noted with this trifunctional metalloinitiator and $Sn(Oct)_2$, and high molecular weights were achievable. Besides, reactions with $Sn(Oct)_2$ were controlled to high monomer conversion. Fe(III) tris(dbm) chelates play multiple roles in the synthesis and properties of poly (lactic acid) star PMCs. In particular, iron chelate acts as a dbm protecting group, a ROP initiator, catalyst and activating group, and as responsive fragments (i.e., chromophores, reactive centers) in the formed PMCs.

The same $Fe(dbmOH)_3$ chelate initiated ROP of D,L-lactide in the absence of additional catalysts (Fig. 5.56a) [355]. As a result, the $Fe(dbmOH)_3$-mediated ROP of D,L-lactide was fast and highly efficient, and it afforded well-defined tri-arm star PMCs in excellent purity and yield (Fig. 5.56b, c). It should be noted high quality control of molecular weight (PDI < 1.1) at ~60–70% conversion. Besides, demetalation by diluted HCl leads to dbm-functionalized polylactide CPLs for other metals chelation.

Star oxime palladacycle complexes were prepared from star-shaped oxime-based ligands and lithium tetrachloropalladate in methanol (Fig. 5.57a) [356]. Indeed, a brown solid quickly precipitated due to the formation of cross-linkages among star-shaped fragments. SEM images exhibited that the solids include micrometer particles with the individual scales about 0.5–5 mm (Fig. 5.57b). It was calculated

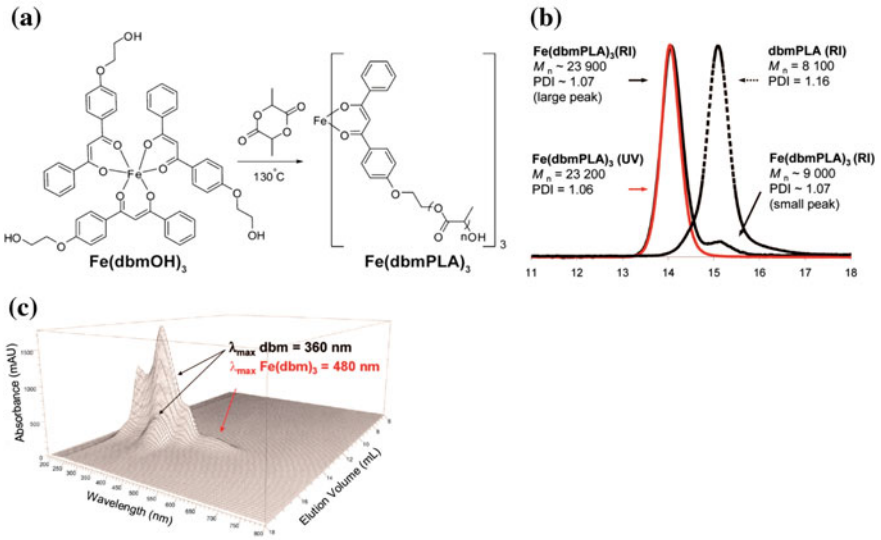

Fig. 5.56 **a** Schematic illustration for the synthesis of Fe(dbm-(poly (lactide acid))$_3$ three-arm star polymer. **b** GPC overlay of star PMC and the corresponding dbm-(poly (lactide acid) macroligand obtained after demetalation by acid treatment. **c** 3D GPC plot of metal chelate star polymer from a UV-vis diode-array detector [PLA is poly (lactide acid)]

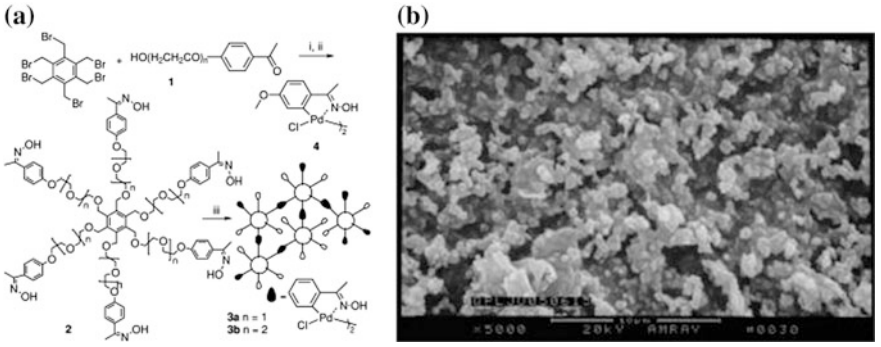

Fig. 5.57 Synthesis (**a**) and SEM image (**b**) of self-supported star-shaped oxime-palladacycles

that the Pd-loading was 1.98–2.03 mmol Pd × g^{-1} and about 48.2–55.2% oxime ligands were coordinated with Pd through chloro-bridges (molar ratio of Pd/N).

Various functional four-arm star PMCs were synthesized via ROPs of rac-β-butyrolactone, ε-caprolactone, rac-lactide acid, and allyl- or propargyl-functionalized trimethylene carbonates using tetrahydroxyl-functionalized tetraphenylethene/salan lutetium chelate as the initiator/catalyst (Fig. 5.58a) [357]. The prepared star AIE functional PMCs can be cast into thin solid films or devices by spin coating under

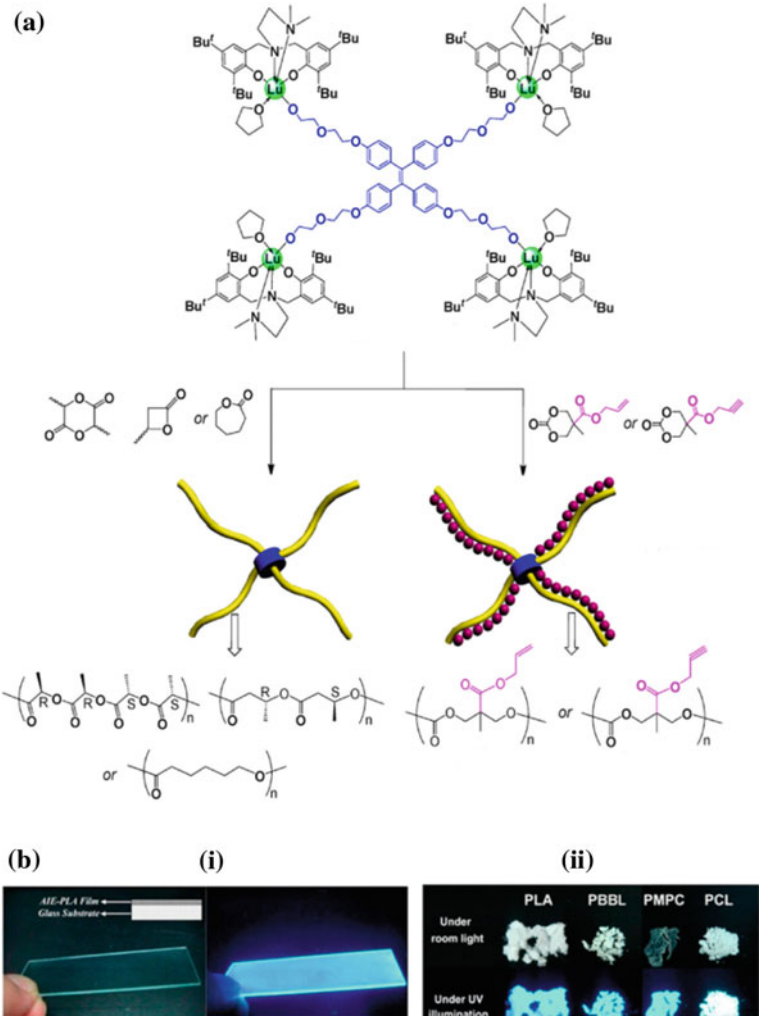

Fig. 5.58 **a** Schematic illustration for the synthesis of four-armed star AIE-active biocompatible polymers using salan lutetium alkoxide chelates. **b** Photographs of (i) AIE-active poly (lactide acid)-coated glass substrate taken under room light and UV illumination, and (ii) star luminogenic biocompatible polymers under room light and UV illumination

simple conditions (Fig. 5.58b). It is important that click functionalities (i.e., C=C and C≡C bonds) can be conveniently installed into the arm segments of the stars via (co) polymerization of functional monomers with pendent allyl or propargyl moieties.

It should be noted other cores used for «core-first» star PMC synthesis, for example different M-Pp (e.g., Zn [358, 359], Sn [360, 361], and Pd [362]). Many of these M-Pp star polymers are of interest because of the photocatalytic abilities of the core, with benefits derived from the polymeric arms including increased

solubility characteristics and improved recoverability, as well as potential modulation of the photoactivity or fluorescence intensity when the use of stimuli-responsive polymers is employed. The incorporation of copper during the polymerization of monomer hinders subsequent chelation of other metals. It is important that only a limited number of metals inside the Pp core can be used due to the interaction of these metals with the copper catalyst. In addition, removing the copper from the Pp core is difficult and often leads to the decomposition of the polymer.

Thus, the synthesis of star poly (2-ethyl-2-oxazoline) containing a Pp core starting from alkyne-functionalized Pp and azide-functionalized poly (2-ethyl-2-oxazoline) via CuAAC was developed [363]. The Pp core was further chelate Cu or Fe within the central cavity. For Cu chelate, the introduction of the metal ion proceeds through a one-pot reaction during the CuAAC reaction for fixing the azide-containing poly (2-ethyl-2-oxazoline) arms.

Of interest is using ATRP catalyzed by transition metals for the synthesis of well-defined Pp polymers. However, only some metal-containing (Zn(II) [364], Pd (II) [365]) Pp initiators were used for the preparation of star PMCs by ATRP. Unfortunately, attempts to synthesize polymers with free-base Pp using ATRP was unsuccessful due to a complexation of Cu(II) (formed by the Cu(I) catalyst) by the Pp core during the polymerization [364]. As a typical example, we note four-arm M-Pp star polymer of St and alkyl (meth)acrylates prepared from tetrabromo Pp-based initiators via ATRP because the coordination of zinc ion and Pp initiator allows avoiding copper ion as catalyst into Pp in star polymers [364]. Zn(II) 10,15,20-tetrakis(4-(2-methyl-2-bromopropoxy) phenyl)-21H,23H-porphine was used as an initiator in the ATRP of MMA, leading to the Zn-Pp-core star-PMMA. It should be noted using Pd(II) 10,15,20-tetrakis(4-(2-methyl-2-bromopropoxy) phenyl)-21H,23H-porphine as an initiator in the ATRP of MMA, however, the polymerization was completely inhibited. Star polymers containing M-Pp-core were prepared by *trans*-metalation of the Zn-Pp or by metal incorporation into the free-base Pp, for example, by heating the Pp-core star polymers in $PdCl_2$ or $PtCl_2$ solution.

The polymerization of St-type monomer 9-(4-vinylbenzyl)-9H-carbazole and methacrylate-type monomer 2-(9H-carbazole-9-yl)-ethyl methacrylate leads to M-Pp star polymers respectively via ATRP with participation of zinc 5,10,15,20-tetrakis(4-(2-methyl-2-bromopropoxy) phenyl)-Pp as an initiator [358]. PDI of M-Pp star polymers are relatively narrow (PDI = 1.09–1.32), that suggest a «living» polymerization process (Table 5.3). It is important that the content of Zn-Pp in the star PMCs depends on the arm length and the flexible arms effectively impede π-π stacking, thus preventing aggregation and fluorescent self-quenching in the solid state. In contrast to the initial monomers showing blue light emission, red light emission is observed in the emission spectra of M-Pp star polymers in the solid state, indicating the effective energy transfer from the Cz to the Zn-Pp core. At the same time, emission spectra of M-Pp star polymers in DMF solution exhibit weak red light emission and strong UV light emission at 350–400 nm that is associated with inefficient energy transfer from the Cz to the Zn-Pp core.

Table 5.3 Monomer, reaction time, molecular weight parameters and monomer conversion of the star PMCs made by ATRP

Monomer	Time (h)	Conversion (%)	M_n, GPC	M_w/M_n
St-type	1	3.4	7600	1.12
St-type	2	5.1	9200	1.09
St-type	3	7.3	15,800	1.18
St-type	4	8.7	17,900	1.23
St-type	5	11.7	24,700	1.25
St-type	6	14.1	30,100	1.20
St-type	7	15.3	32,900	1.24
Methacrylate-type	2	5.4	9300	1.32

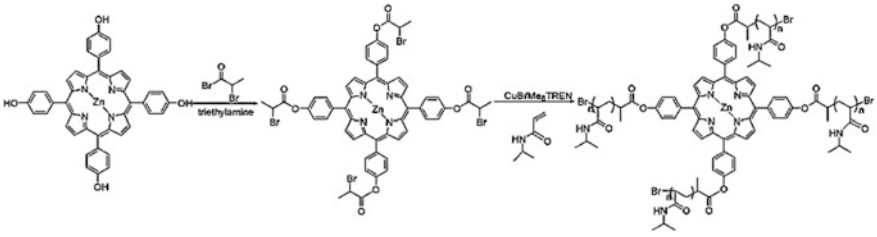

Scheme 5.24 Synthesis route of metal chelate star polymer with Zn-Pp core

A well-defined star poly (NIPAM) with Zn-Pp as the core was synthesized by ATRP with Zn(II)-*meso*-tetra(*p*-bromopropionylphenyl)-Pp as the initiator, and CuBr/tris(2-(dimethylamino) ethyl) amine as the catalytic system for 12 h at 60 °C (Scheme 5.24) [359]. The PDI was narrow and the polymerization was well controlled. The result exhibited lower value of lower critical solution temperatures for the aqueous solutions of M-Pp star polymers as compared to that of poly (NIPAM) homopolymer, which arose from the incorporation of the hydrophobic Pp core.

It should be noted free-base Pp cored star polymers and amphiphilic star block copolymers with controlled molecular weights and narrow PDI prepared by RAFT polymerization of the monomers containing *N*,*N*-dimethylacrylamide and St [366]. The formed polymers aggregated into star-like or flower-like micelles and their optical response to Zn(II) ions was a function of micellar structures. In particular, the formation of a Zn-Pp complex leads to the substantial UV-vis spectral changes within 17 h for Pp-[poly (*N*,*N*-dimethylacrylamide)$_{96}$-PS$_{33}$]$_4$ flower-like micelles (Fig. 5.59a). At the same time, for Pp-[PS$_{34}$-poly (*N*,*N*-dimethylacrylamide)$_{239}$]$_4$ star micelles the unchanged UV-vis absorption is characteristic after three days, which indicates an absence of Zn(II) coordination with Pp trapped in the micelle core (Fig. 5.59b).

Using of Sn(Oct)$_2$ as a catalyst in the synthesis of the free-base Pp star polymers leads to Sn incorporation into Pp core [360, 361]. Thus, Sn-containing star amphiphilic

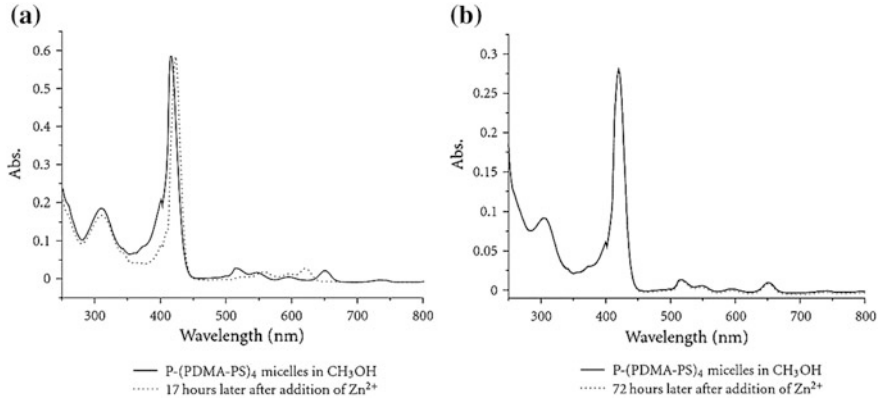

Fig. 5.59 UV-vis spectra of the micelles in methanol in the absence and in the presence of Zn (II) (5×10^{-4} M). **a** Pp-[poly (*N*,*N*-dimethylacrylamide)$_{96}$-PS$_{33}$]$_4$ micelles. **b** Pp-[PS$_{34}$-poly (*N*, *N*-dimethylacrylamide)$_{239}$]$_4$ micelles

PCL-*b*-poly [oligo (ethylene glycol) methyl ether methacrylate] with Pp core was synthesized by combination of ROP and ATRP (Scheme 5.25). The M-Pp star polymer can easily self-assemble into micelles in aqueous solution and the micelles can reversibly swell and shrink in response to external temperature. It should be noted that π-stacking and hydrophobic interactions in aqueous media leads to the aggregation of M-Pp and the resulting reduce in effectiveness of photodynamic effect.

The star CPL with Sn-Pp core was used for the preparation of the star CPL containing adamantyl terminal fragments with Sn-Pp core using DCC reaction with adamantaneacetic acid (Fig. 5.60a) [361]. The successful preparation of targeted star CPL confirms by disappearance of the signal at 3,65 ppm assigned to the methylene protons next to the terminal hydroxyl groups and appearance of the new peaks at 2.05 ppm (l), 1.96 ppm (j), and 1.65 ppm (peaks k, m were overlapped by peak g) assigned to adamantyl group in ^{1}H NMR spectrum (Fig. 5.60b).

Star diblock-PMCs were prepared via ATRP from a Pd-Pp macroinitiator (Scheme 5.26) [365]. It is interesting that the formed PMCs include the central Pd-Pp surrounded by a hydrophobic block of poly (butyl acrylate) and terminal hydrophilic block of poly (oligoethyleneglycol monomethylether monomethacrylate).

Of interest are star block copolymers with a hydrophilic pH sensitive shell and photosensitive hydrophobic core structure prepared by Cu-based ATRP [362]. At first, a multi-functionalized initiator containing Pd-Pp was used for the preparation of photosensitive *n*-butyl acrylate star PMC, which then was polymerized with *N*,*N*′-dimethylamino ethyl methacrylate or *tert*-butyl acrylate to synthesize the star block PMCs (Fig. 5.61). It is important that the prepared PMCs are characterized by well-defined molecular weights with narrow polydispersities (PDI < 1.23).

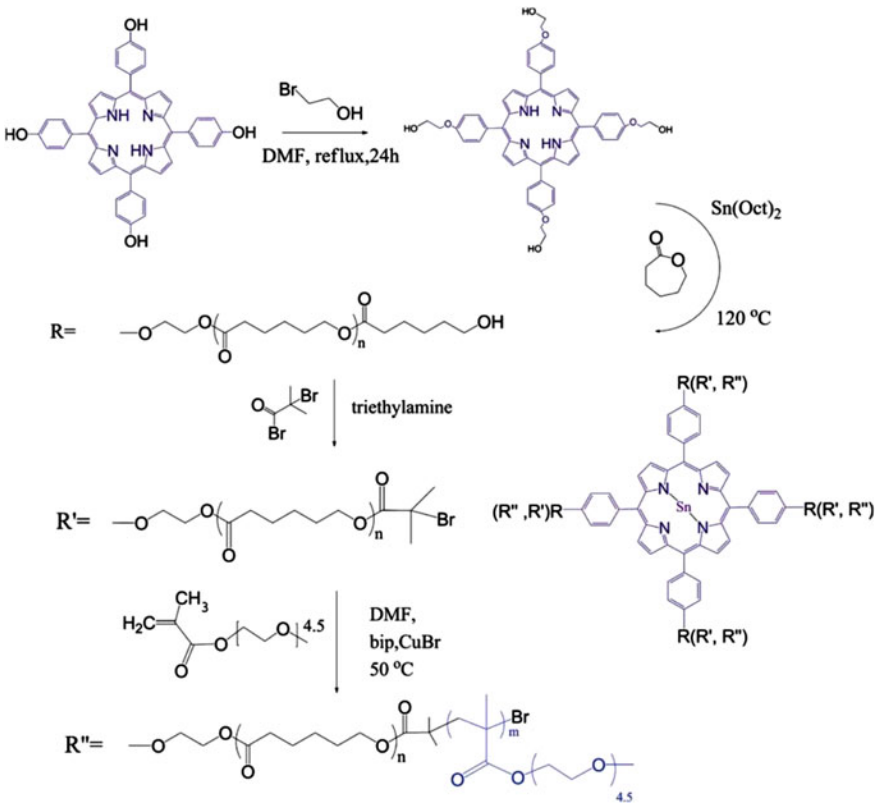

Scheme 5.25 Synthesis of Sn-containing star amphiphilic copolymers by the combination of ROP and ATRP

The hydroxyl-terminated star-shaped PCL with eight arms and different arm length ([M]/[I] = 30, 60, 90) with an initiator core of 2,3,9,10,16,17,23,24-octakis (3-hydroxypropylmercapto)-Pc-Zn(II) was prepared by the bulk ROP of ε-caprolactone (Fig. 5.62, top) [367]. The intrinsic viscosity and M_w of star PMCs (0.09–0.112 and 4542–6064, respectively) depend on concentration of polymer compounds and the [M]/[I] ratio. The addition of $AgNO_3$ causes the aggregation of the polymers and a slight shift in the electronic spectra is observed with the addition of $Hg(NO_3)_2$. At the same time, the addition of methanol and $Pb(NO_3)_2$ did not lead to any shift or optical change in the electronic spectra.

The «core-first» approach was used to the preparation of the M-Pc star polymer, with Zn-Pc as the core and poly (NIPAM) as the arms, via ATRP using Zn(II) tetra-(2-chloropropionylamido)-Pc as the initiator (Fig. 5.62, bottom) [368]. The thermo-responsive PMC has low PDI and photocatalytic activity. The introduction of the Pc core leads to increasing the lower critical solution temperatures for the M-Pc star polymer aqueous solutions.

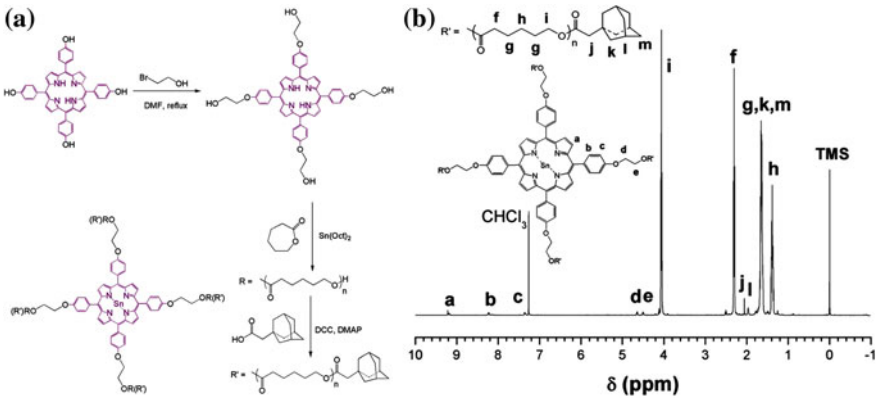

Fig. 5.60 **a** Synthesis and **b** ^{1}H NMR spectrum of adamantyl groups-terminated star PCL with Sn-Pp core

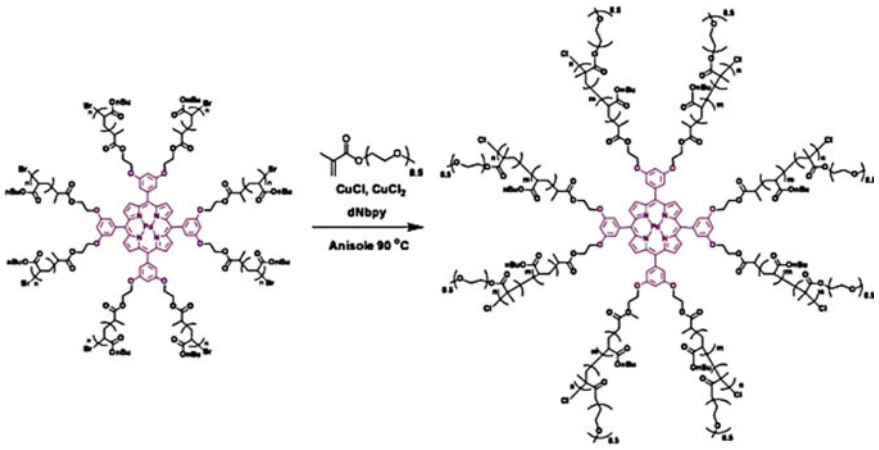

Scheme 5.26 Schematic representation of the synthesis of a diblock star polymer containing a Pd-Pp core, a hydrophobic interior block and a hydrophilic exterior block

5.4.3 Click-to-Chelate Approach

A new method called click-to-chelate approach to introduce chelating moieties on polymers using a 1,2,3-triazole ring as a coordinating functionality, which is easily prepared by CuAAC, was developed [369–371]. This method is a promising approach to incorporate bpy-like chelating fragment to macromolecules due to the excellent feasibility of azide substitution and click chemistry. Thus, a series of AB_2-, ABC-, $(AB)_2$-, A_2B_2- and ABCD-type miktoarm Ru(II)-PMCs was prepared by a click-to-chelate approach, which involved at first the chelation of $Ru(II)(DMSO)_4Cl_2$ by a

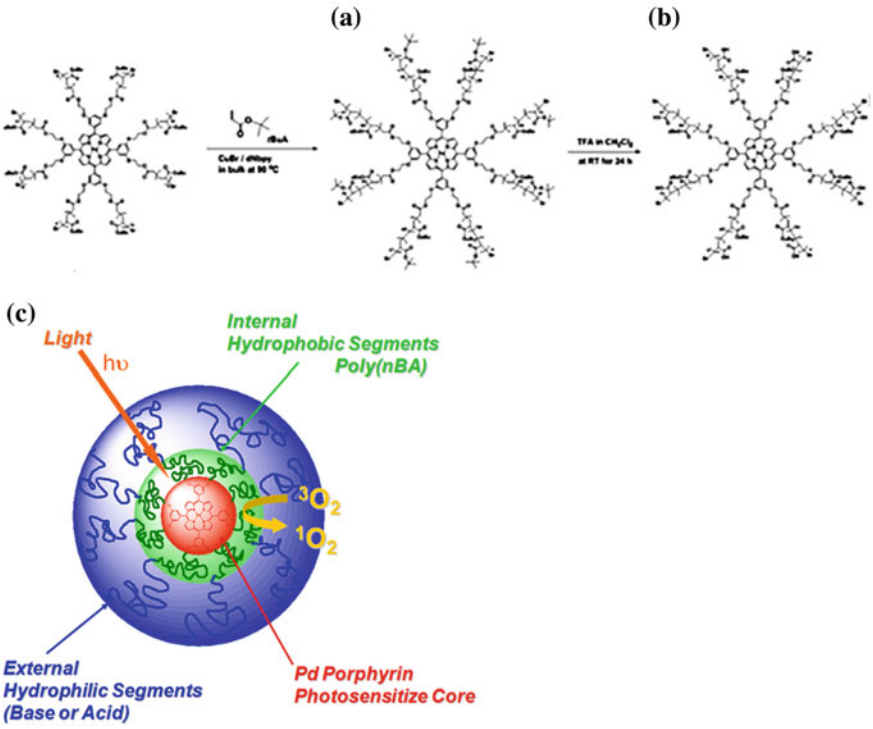

Fig. 5.61 Synthesis of poly (*n*-butyl acrylate)-*b*-poly (*N*,*N*′-dimethylamino ethyl methacrylate) (**a**) or of poly (*n*-butyl acrylate))-*b*-PAA (**b**) star PMCs from poly (*n*-butyl acrylate) star polymer macroinitiator by Cu-catalyzed living radical polymerization in bulk at 90 °C under argon. Structure of amphiphilic star block copolymer photosensitizers for photooxidation reactions (**c**)

polymer-substituted 2-(1H-1,2,3-triazol-4-yl)pyridine or 2,6-bis(1H-1,2,3-triazol-4-yl)pyridine to obtain a stable polymer Ru(II) *mono*-complex, and the chelation of the formed PMC with another polymer-substituted similar chelating ligands to afford the miktoarm Ru(II)-PMCs [372].

Of interest is using the click-to-chelate approach to incorporate chelating fragment in PS and chelation of Ru(II) ions to prepare 3-arm and 4-arm star-branched PS Ru(II) chelates [373]. The CuAAC of PS-N_3 with 2-ethynylpyridine or 2,6-diethynylpyridine leads to 2-(1H-1,2,3-triazol-4-yl) pyridine or 2,6-bis(1H-1,2,3-triazol-4-yl) pyridine ligands containing one or two PS chains at the first-position of the triazole rings. Star Ru(II)-PMCs as yellow solids were prepared by conventional procedure by heating of chelating macroligands with $RuCl_3$ with following addition of $NaPF_6$. The M_n of these chelates were equal to 6740 and 10,400, respectively, which correspond to 3-arm and 4-arm star-branched PS Ru(II) chelates.

It should be noted the preparation of 3-, 4-, 5-, 6-, 7-, 8-, 9-, 10-, 11-, and 12-armed star poly (styrene oxide)) (PSO) Ru(II) chelates by a click-to-chelate method including the combination of the click reaction and stepwise chelation of

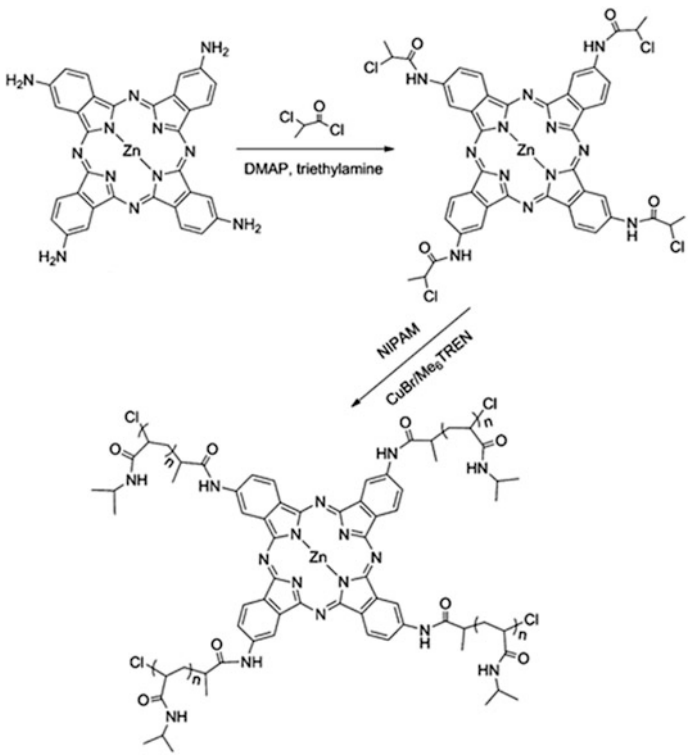

Fig. 5.62 Synthesis of star shaped PCL compounds with a Zn-Pc core (top) and synthetic route for the Zn-Pc star polymer (bottom)

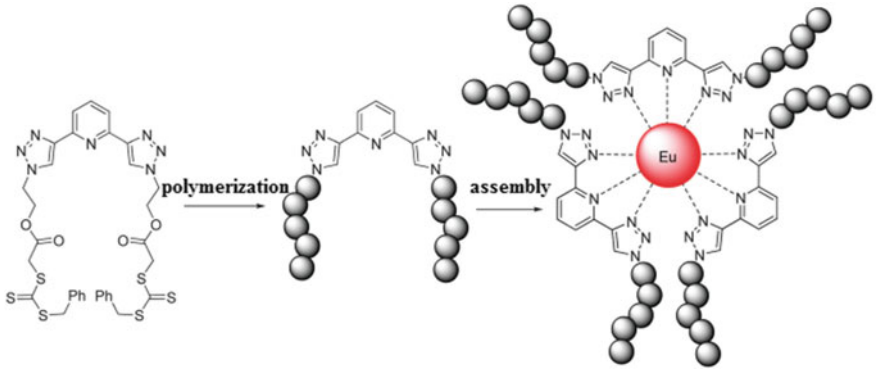

Fig. 5.63 Illustration of the polymerization-assembly strategy leading to formation of 6-arm star-branched PMC templated by Eu(III)

$Ru(II)(DMSO)_4Cl_2$ by 2-(1-PSO_n-1,2,3-triazol-4-yl) pyridine or 2-(1-PSO_m-1,2,3-triazol-4-yl)-6-(1-PSO_n-1,2,3-triazol-4-yl) pyridine (m, n = 1, 2, or 3) [374].

A click-to-chelate approach, including the click reaction of poly (NIPAM) with 2,6-diethynylpyridine to prepare the btp CPL and the following chelation of $RuCl_3$, was used to the preparation of the four-arm star poly (NIPAM) Ru chelate [375]. The study of the thermoresponsive properties of the PMCs demonstrated the effects of the polymer terminal and core linkage and constituents of the four-arm star poly (NIPAM) Ru chelate on the T_c.

A combination of metal chelation, RAFT and click chemistry was used to obtain of star polymers with the terdentate btp core [376]. RAFT polymerization (e.g. with St or MMA) with following chelation of Ru(II) or Eu(III) ions led to 4- or 6-arm star PMCs (Fig. 5.63). Interestingly, metal chelation is accompanied by significant increasing a hydrodynamic diameter of ca. 2 nm of initial CPL (indicating single polymer chains) to 180 nm (for the Ru analogue) and 240 nm (for the Eu analogue).

5.5 Metal Chelates with Hyperbranched Polymers

At present, great attention is given to the PMCs based on hyperbranched polymers [39, 377–381]. Undoubted advantages of these CPLs as compared on the dendrimer ligands are low cost, better accessibility of chelating fragments, similar properties, and the possibility of large-scale synthesis [382]. Of no small importance is the fact that some hyperbranched CPLs are commercially available.

Widely ubiquitous platform for creating hyperbranched CPLs is soluble hyperbranched polyglycerol (PG), an aliphatic polyether polyol, which is prepared by anionic ROP of glycidol [383]. A distinctive feature of PG is a chemically stable polymer chain allowing easily to modifying terminal functional groups. As a typical example, we note the transformation of the end hydroxyl groups of PG to form diethylamine or di-*n*-pentylamine substituted hyperbranched CPLs [384].

It should be noted the using Cu(I) chelation in situ with hyperbranched CPLs PG-triamine and PG-tetramine for the preparation of the catalysts for ATRP of MMA or St [385].

Of interest is the method of the modification of PG derivatives with ethylethylene diamine [386, 387]. For example, the fixing hydrophilic PEG chains to amine-containing fragments leads to a core-multishell architecture (ligand II) or to the PG core for core-random shell structure (ligand III) (Fig. 5.64). Besides, PG fully modified by trimethylethylene diamine (ligand I) was used as a reference system. These efficient Cu-chelating hyperbranched polymers have a low toxicity and high water solubility as well as bind high amounts of Cu(II), which makes them good candidates for balancing Cu levels in neurodegenerative diseases. In this case, the determining factor to control the binding degree, the chelation strength, and the release profile of copper is the spatial organization of the core-shell structure. It should be noted that the hyperbranched CPL II is the most promising system for Cu chelation and release.

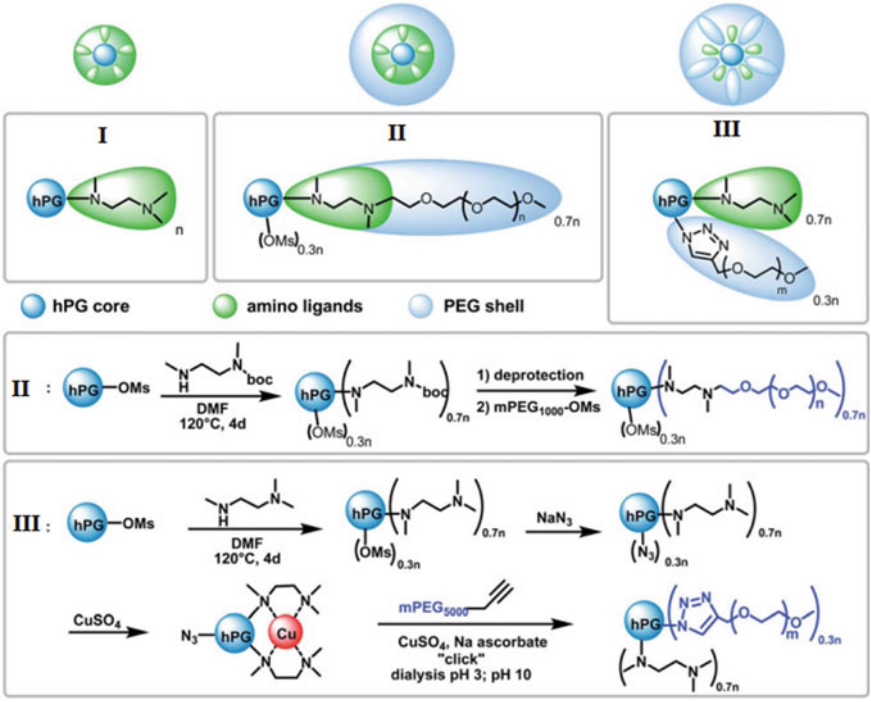

Fig. 5.64 Structure and synthesis scheme of ligands I, II and III (hPG is hyperbranched PG)

The hyperbranched CPL was synthesized by the interaction of trimethylethylene diamine possessing strong chelating ability to Cu(II) ions with hyperbranched PG [387]. The CPL links Cu(II) ions in the similar way as PEI (Fig. 5.65), however the formed Cu-PMC have a four times lower cytotoxicity. Besides, the chelation in the outer shell of the CPL based on PG core promotes the intracellular Cu release. At the same time, CPL based on PEI core links Cu(II) ions by amines in the core of the hyperbranched polymer, hindering the release of Cu.

The similar PG-based Cu-chelating ligands were prepared by covalent attachment of the *N*-methyl-*N*-picolylglycine amide, 2,6-Py-dicarboxylic acid monoamide, and cyclam tetraacetic acid, to the hyperbranched PG (M_w = 16,800) with amide bonds [388]. Among these CPLs, the cyclam-containing CPL shows the highest chelation capacity (29 Cu ions/polymer), lowest cytotoxicity, and best stability with respect to pH and EDTA.

Of interest are hyperbranched polyamines with s-triazine fragments (Fig. 5.66a), which link metal ions and are metal ion sensors. In particular, a decrease in the intensity of fluorescence of the these CPLs with the increase of Cu(II) concentration is observed in contrast to other metal ions (Fig. 5.66b) [389, 390]. Such selectivity for Cu(II) can be explained by the square planar spatial organization of Cu(II) chelate, while other metal chelates have octahedral structures.

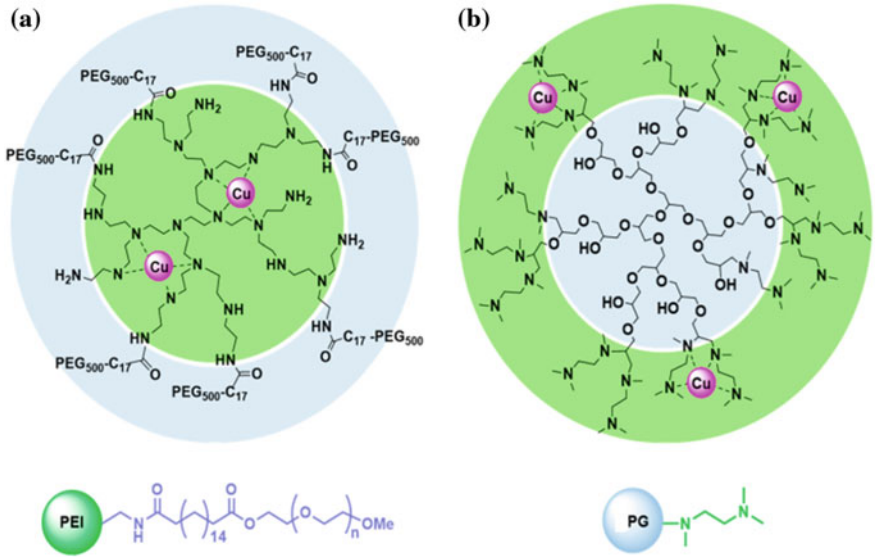

Fig. 5.65 Structures and Cu(II) chelation of the different hyperbranched architectures: **a** complexes Cu(II) inside the PEI core; **b** macroligand based on PEG core stabilizes Cu(II) ions in its amino ligand shell

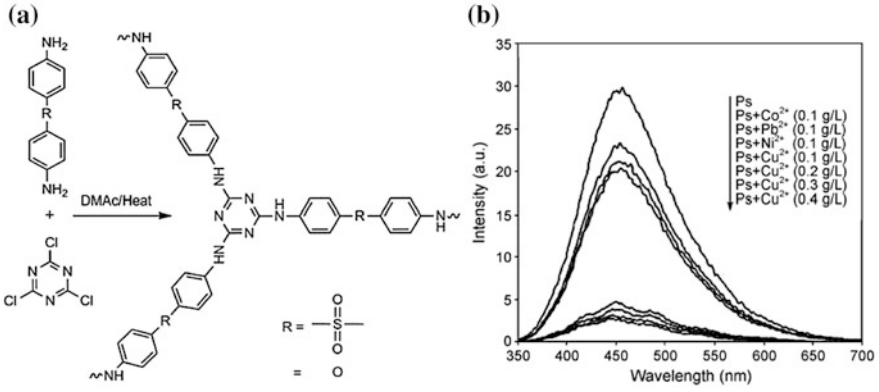

Fig. 5.66 Synthesis (**a**) and effect of metal ions on fluorescence (**b**) of hyperbranched polyamines

It should be noted the hyperbranched PEI with terminal amino or carbohydrate fragments (Scheme 5.27) which form the complexes with metal salts ($CuSO_4$, $HAuCl_4$, H_2PtCl_6, or $AgNO_3$) [391]. It turned out that the chelation capacity of the hyperbranched CPL is close to that of a G4 PAMAM dendrimer, although its molecular weight is only half of latter. Apparently, the hyperbranched CPL can link

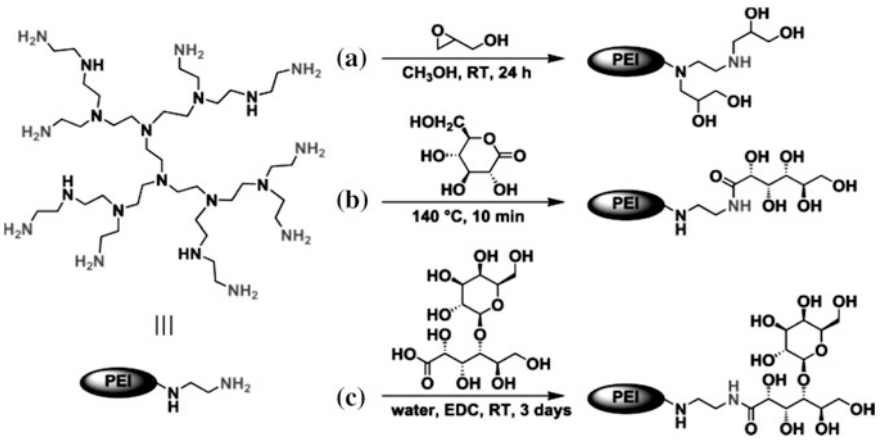

Scheme 5.27 Functionalization of hyperbranched PEI with **a** glycidol, **b** gluconic acid, and **c** lactobionic acid

metal ions by the internal chelating fragments. It is interesting that chelation capacity of the CPLs did not substantially change after the modification of the polymer ligand by gluconamide.

Hyperbranched PAMAM-*gr*-PTFE microfiltration membranes adsorbed 1.42 g m^{-2} Cu(II) ions from aqueous solution, with up to 90% desorption under acidic conditions and highly preserved adsorption capacity for Cu(II) ions with re-using cycles (Fig. 5.67) [392]. The results clearly indicate that hyperbranched PAMAM-*gr*-PTFE membrane is stable under the adsorption-desorption operating conditions and demonstrates its reusability in this environmental application.

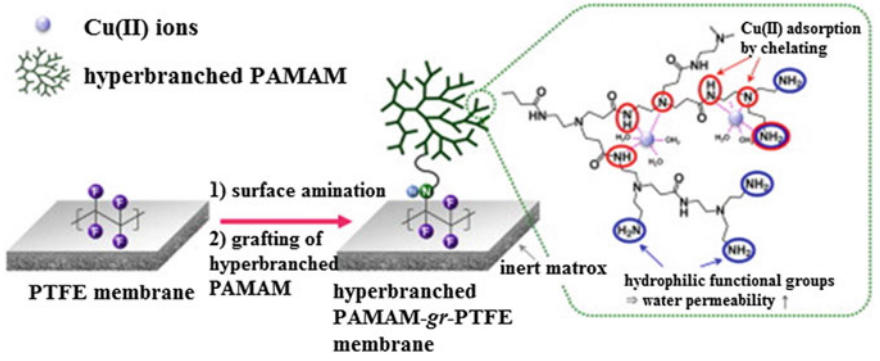

Fig. 5.67 Schematic illustration of the procedure used for the preparation of hyperbranched PAMAM-gr-PTFE microfiltration membranes for Cu(II) chelation

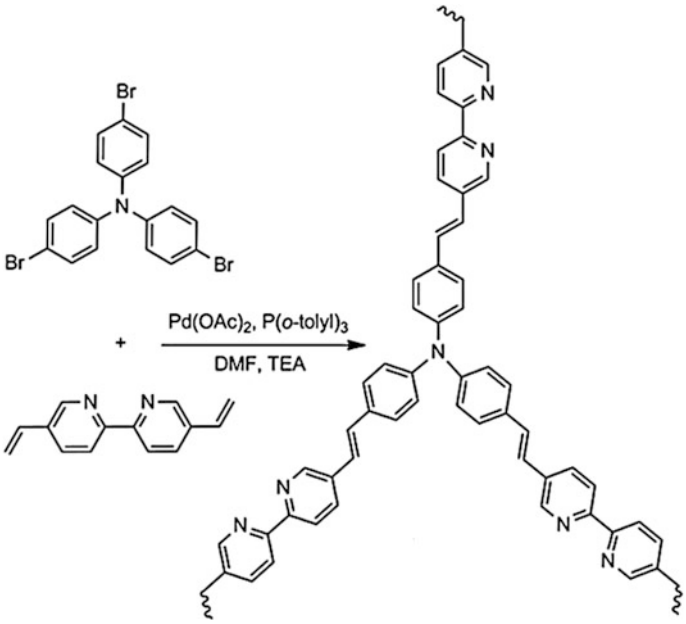

Scheme 5.28 The synthetic route of hyperbranched copolymer containing triphenylamine and divinyl-bpy units by Heck coupling reaction

Table 5.4 The K_{SV} of different metal ions

Ions	Co(II)	Ni(II)	Fe(II)	Mn(II)	Zn(II)
K_{SV} (M^{-1})	1.29×10^6	1.78×10^6	6.8×10^4	3.2×10^5	1.1×10^5

An amphiphilic derivative based on hyperbranched PAMAM was applied to the preparation of functional polysulfone membrane with heavy metal ion chelation [393]. It should be noted that the prepared membranes could provide high chelating capacity, effective regeneration of adsorption ability, and chemically inert matrices, which were the essential requirements in removing heavy metal ions from water.

A fluorescent hyperbranched copolymer with M_n of 1895 and M_w of 2315 containing triphenylamine and divinyl-bpy chelating fragments was prepared via the Heck cross-coupling reaction (Scheme 5.28) [394, 395].

Interestingly, hyperbranched copolymer has the higher K_{SV} for metal ions in comparison with similar linear polymer (Table 5.4). For example, for Mn(II), the K_{SV} of hyperbranched copolymer were equal to 3.2×10^5 M^{-1} that is 32 times high then that of linear analogue due to the «superamplified effect» of hyperbranched copolymer.

Of interest is a hyperbranched chelating aromatic polyamide with DB of 52% based on bifunctional 2,2′-diamino-4,4′-bithiazole and trifunctional 1,3,5-benzenetricarbonyl trichloride (Scheme 5.29) [396]. Two kinds of hyperbranched PMCs were synthesized

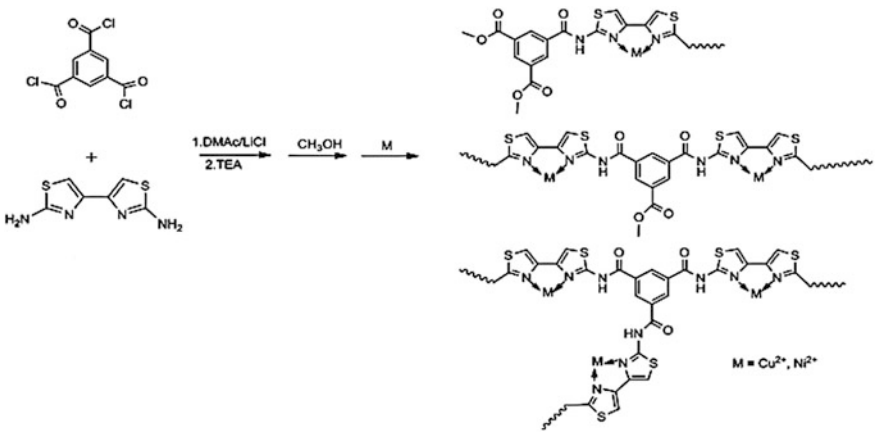

Scheme 5.29 The route of polymers' synthesis and preparation of metal chelate hyperbranched polymers

by the interaction of the hyperbranched CPL with Cu(II) and Ni(II) ions with the yields of 64.3 and 68.5%, respectively. It is important that PMCs were soft ferromagnets having Curie-Weiss temperature at 102 and 53 K, respectively.

The similar conjugated hyperbranched CPL based on 1,3,5-benzenetricarboxaldehyde and 2,2′-diamino-4,4′-bithiazole forms PMCs with Co(II) and Sm(III) ions [397]. In this case, the magnetic hysteresis loops the Co- and Sm-PMCs have the typical «S» shape at 5 K with the Curie-Weiss temperature T_θ = 96 and 41 K, respectively. It is important that the prepared PMCs are also soft ferromagnets.

It should be noted two conjugated hyperbranched polymer fluorescent sensors with benzochalcogendiazole and triazole chelating fragments (Fig. 5.68) [398]. It is interesting that benzoselenadiazole-based CPL has higher sensitivity and selectivity with detection limit of 2.4 nM.

Of interest is fluorescence sensor based on a hyperbranched poly (phenylene sulfide) with $M_w = 6 \times 10^3$ to 1×10^5 [399]. It is important that the K_{SV} is equal to 1.443×10^4 mL g^{-1} and the quenching efficiency is 20% at Cu(II) concentration of about 10 ppm.

It should be noted that Cu(II) and Fe(III) ions have substantial effect on fluorescence quenching of hyperbranched poly (hydroxyl ether) modified by *p-N*, *N*-dimethylaminobenzaldehyde [400]. For example, increasing the concentration of $Fe(NO_3)_3$ leads to a decrease of the intensity of the peak at 360 nm of the hyperbranched CPL with appearance of a new peak at 420 nm (Fig. 5.69a). This is explained by «complex quenching effect» . At the same time, the addition of Ni $(NO_3)_2$ and $Co(NO_3)_2$ does not lead to substantial change of the fluorescence intensity (Fig. 5.69b).

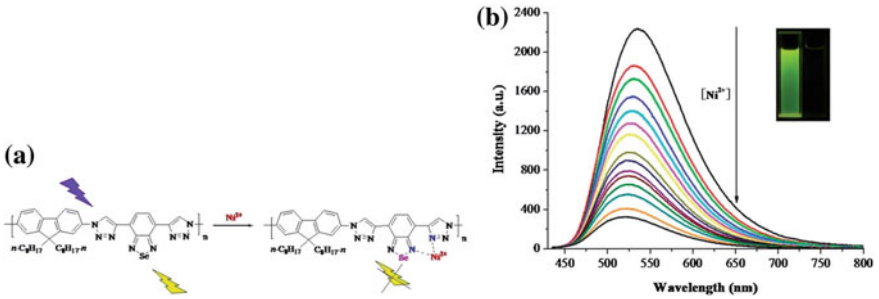

Fig. 5.68 Possible benzoselenadiazole-based polymer nickel ion detection mechanism (**a**). Fluorescence spectra of benzoselenadiazole-based polymer with increasing concentrations of Ni(II) (0, 0.2, 0.4, 0.6, 0.8, 1, 1.2, 1.4, 1.6, 1.8, 2.0, 2.5, 3.0, 4.0, 5.0 mmol L^{-1}) (λ_{ex} = 425 nm). Inset: visible fluorescence of benzoselenadiazole-based polymer before (left) and after (right) the addition of Ni(II) (5.0 mmol L^{-1}) under a 365 nm UV lamp (**b**)

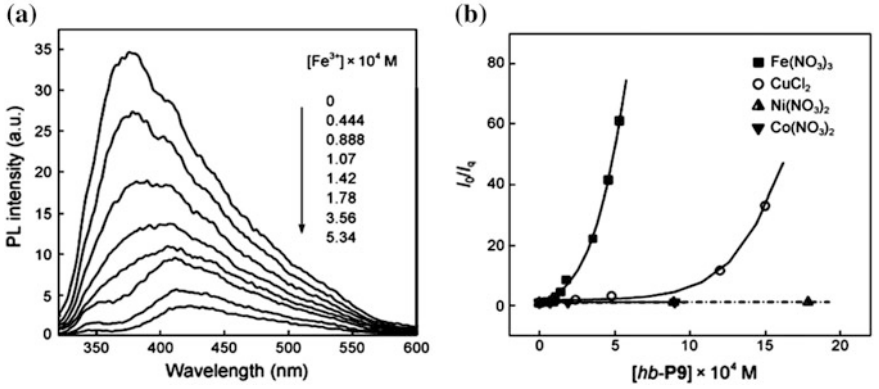

Fig. 5.69 **a** Quenching effect of $Fe(NO_3)_3$ on the fluorescence of hyperbranched polymer. **b** Stern-Volmer plots of hyperbranched polymer quenched by various quenchers in ethanol solution, c = 3.01 × 10^{-3} g mL^{-1}, λ_{ex} = 310 nm

A «complex quenching effect» was also shown in the case of fluorescent hyperbranched poly (sulfone-amine) modified by *N*,*N*′-dimethylaminoaniline [401]. It is important to emphasize that Ag(I), Cu(II) and Fe(III) ions quenched fluorescence in contrast to alkali and alkaline earth metal ions.

It should be noted the dual (thermal and metal ion) stimuli-responsiveness of oligo (ethylene glycol)-terminated hyperbranched poly (triazole) prepared by CuAAC [402]. It is important that the metal ion nature has substantial effect on the cloud point of hyperbranched polymer solution.

Of interest is the preparation of heterogeneous Pd catalysts using a hyperbranched poly (phenylacetylene) with side alkyne fragments (Fig. 5.70) [403].

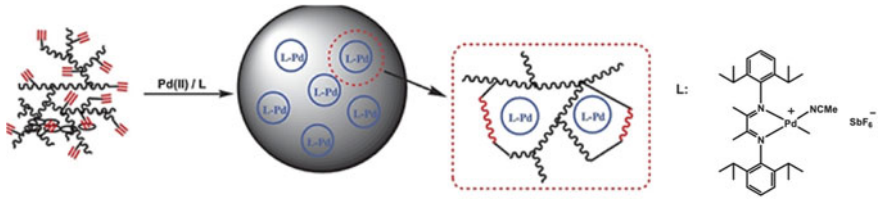

Fig. 5.70 Synthesis of heterogeneous Pd catalysts containing Pd chelate by Pd-catalyzed cross-linking of hyperbranched poly (phenylacetylene)

Under the action of Pd(II) diimine chelate, the cross-linking of the initial polymer and simultaneous linking metal compound into the cross-linked polymer matrix is carried out.

Three graphene oxide-hyperbranched PEI gels were used for Pb(II) adsorption which is determined by such parameters as Pb(II) concentration, pH value, contact time, the amino group concentration and the cross-link density [404]. The prepared CPL showed high adsorption capacity of 438.6 mg g^{-1} for Pb(II) ions.

Of interest is using carbo-BINAP and glutaroyl-AMINAP (methylene amino-substituted BINAP) functionalized hyperbranched PEI, as soluble carriers in the Cu-catalyzed hydrosilylation of acetophenone [405].

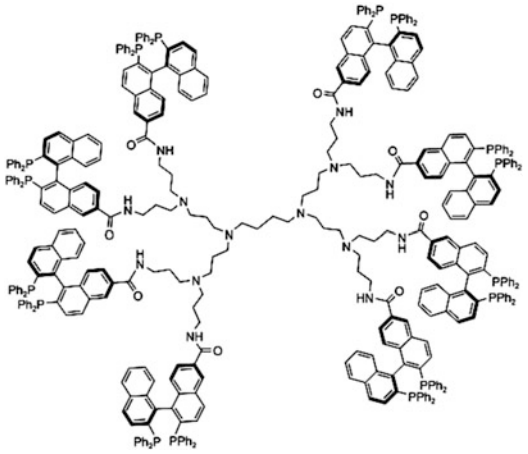

Cationic hyperbranched pyrphos-Rh(nbd) chelates have been synthesized using hyperbranched PEI containing on average 9–139 chelating fragments [142]. All hyperbranched metal chelates have been obtained in excellent yields of between 88 and 99%. It is important that the initial chelate nodes retain their spatial configuration, although the symmetry of the hyperbranched PMCs is much lower due to their PDI.

Of considerable interest is various pincer complexes attached to hyperbranched polymers [406, 407]. As a typical example, we note pincer-metal complexes fixed on a hyperbranched polyethers based on racemic hyperbranched PG (M_n = 2000) as well as chiral hyperbranched (−)-PG (M_n = 3000) and (+)-PG (M_n = 5500) [408, 409]. It should be noted that core-shell structures and a small size-distribution (15–20 nm) are characteristic for these PMCs, and thickness of the corona correlates with the content of pincer-Pt fragments.

In another interesting example, a hyperbranched carbosilane was functionalized with aryl diamine [$C_6H_3(CH_2NMe_2)_2$-2,6]-(NCN)-Pd(II) complex, using a lithiation-transmetalation method [410].

The hyperbranched conjugated polymers based on substituted *p*-phenylenes as the host fragments with *fac*-Ir(ppy)$_3$ or Ir(III) bi(2-tolyl-pyridine)acac as a light-emitting unit was synthesized by Yamamoto polycondensation [411]. For all the obtained hyperbranched PMCs, the efficient energy transfer from poly (*p*-phenylene) fragments to the Ir-complex was shown. It is interesting that Ir complex completely quenched EL emission from poly (*p*-phenylene) fragments.

It should be noted green-light-emitting hyperbranched PMC containing *fac*-Ir(ppy)$_3$ core and 3,6-Cz-*co*-2,6-Py branch [412] as well as PMCs with the 3,6-Cz-*co*-2,8-dioctyldibenzothiophene-S,S-dioxide-3,7-diyl as the main chain [413]. The emission color of the hyperbranched PMCs changes during the transition from *fac*-Ir(ppy)$_3$ fragments to other Ir chelates. In particular, hyperbranched PMCs containing an Ir chelate core and fluorene-*alt*-Cz branches are red light-emitted [414]. The other red-emitting hyperbranched PMCs contain polyfluorene and poly (fluorene-alt-Cz) branches and the Ir chelate [(L′)$_2$IrL] core (where L′ is 1-phenylisoquinoline and L is 3-(pyridin-2-yl)-1H-1,2,4-triazole) [415]. It is important that the same Ir complex was used to preparation of the hyperbranched π-conjugated light-emitting polymers [416–418].

Of interest are hyperbranched PMCs containing chlorotricarbonyl Rh(I) bis(stilbazoylimino)acenaphthene chelates [419]. It is important that the multilayer films for photovoltaic cells can be prepared from these PMCs.

PG-supported salen analogues were synthesized for the incorporation of Cr(II) ion in situ with subsequent air oxidation to the Cr(III) chelates (Scheme 5.30) [420]. The same route was used for the preparation of other hyperbranched Cr(III) salen chelates with subsequent substitution of the counter-anion Cl to SbF_6 using $AgSbF_6$.

It should be noted hyperbranched chromium chelate based on a PG-fixed unsymmetrical salen ligand used as catalyst for asymmetric Diels-Alder reactions [420].

Hyperbranched PG-fixed salen forms red PG-salen-Co(II) after the interaction with $Co(OAc)_2$ under inert atmosphere (Scheme 5.31) [421]. Then, the Co(II) chelate will oxidized into the Co(III) chelate, and a color changes from red to dark brown. The similar PG-fixed Mn-salen was synthesized by reacting hyperbranched ligand with Mn(II) ions. According to elemental analysis, 54 and 71% of salen sites are occupied by cobalt and manganese, respectively.

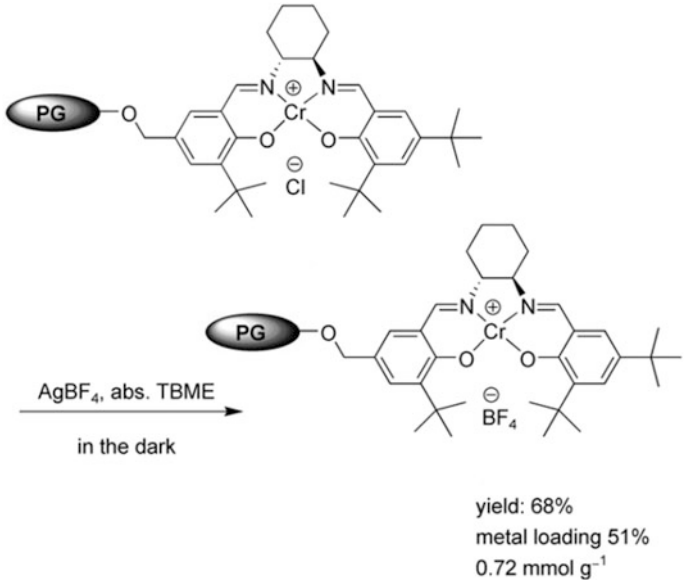

Scheme 5.30 Synthesis of a PG-supported chromium(III) salen complex with tetrafluoroborate counter-anions

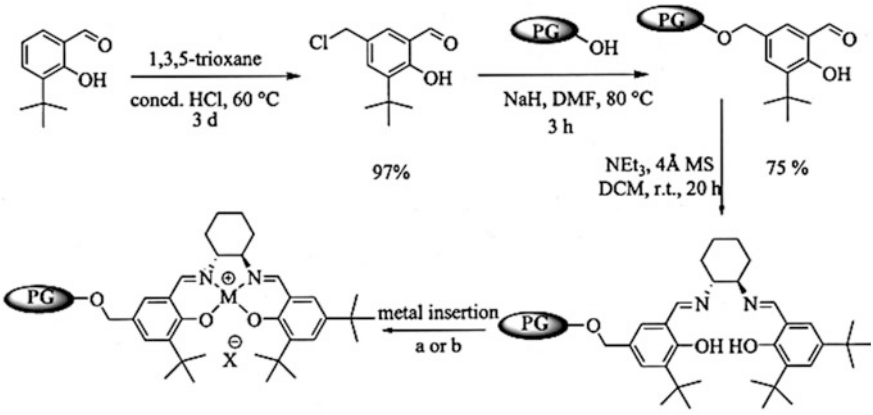

Scheme 5.31 Preparation of PG-supported Co- and Mn-salen chelates

The same PG-supported Mn-salen chelate is used as a catalyst in the epoxidation of 6-cyano-2,2-dimethylchromene [422].

Of considerable interest are the symmetrical hyperbranched (pyrrolidine-salen)-Cr(III) PMCs with spacers of different lengths (Fig. 5.71, top), which showed a positive dendritic effect in the asymmetric ring-opening of *meso*-epoxides [423].

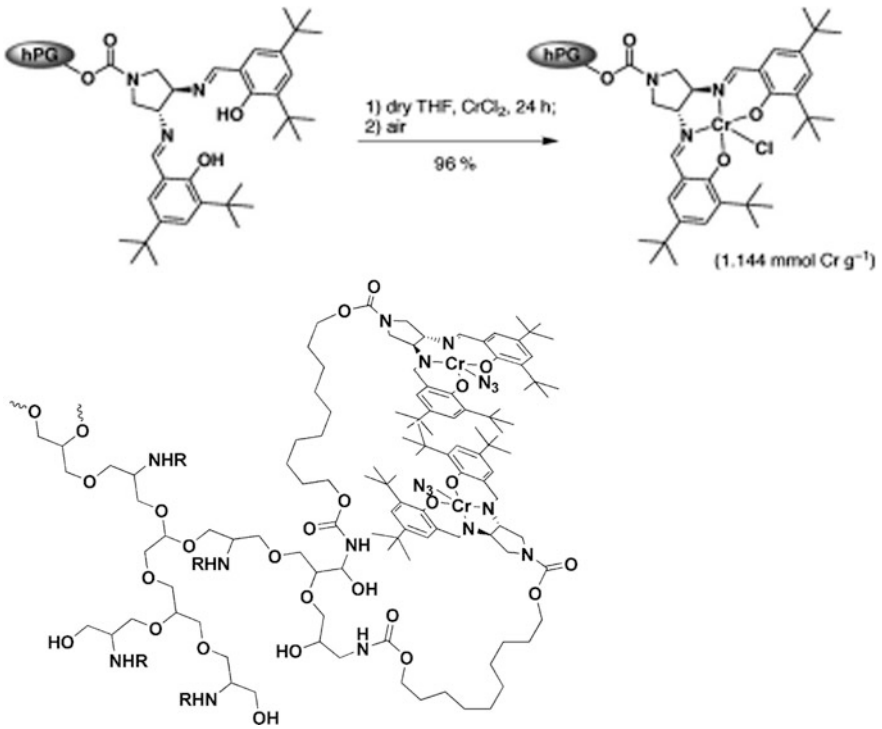

Fig. 5.71 Synthesis of PG-C1-CrCl (top). Possible back-folding mechanism for the favored head-to-tail orientation with a C10 spacer (bottom)

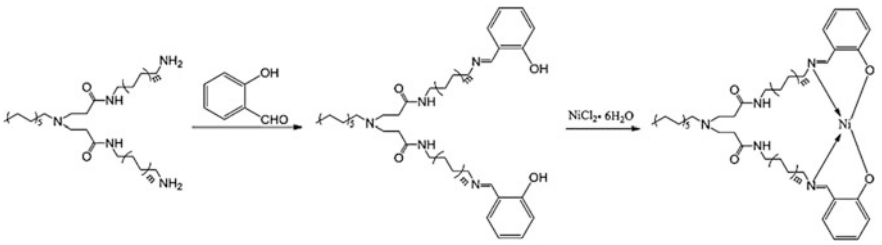

Scheme 5.32 Synthesis of hyperbranched ligand and nickel chelate

It is important that long spacers promote the favored head-to-tail orientation of two molecules (Fig. 5.71, bottom).

The hyperbranched salicylaldimine nickel chelates were synthesized by the Schiff's base and the chelation reactions with G1 hyperbranched macromolecules, salicyladehyde and nickel chloride hexahydrate as materials by employing two-step synthesis and one-pot synthesis, respectively (Scheme 5.32) [424, 425]. All nickel

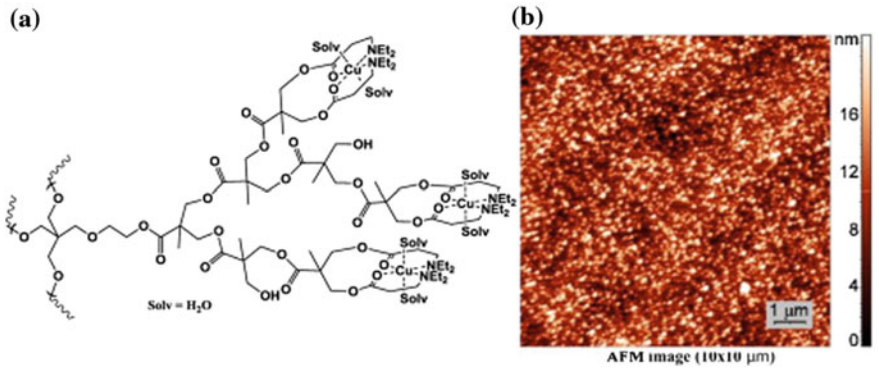

Fig. 5.72 **a** Scheme of synthesis of G2 and G3 copper(II) chelates of amine-modified hyperbranched polyesters ligands. **b** AFM image (10 × 10 μm) of the G3 Cu(II) chelate

chelates, activated with MAO, exhibited high activities for ethylene oligomerization and good selectivities for the longer chain oligomers produced.

It should be noted the fixing Hoveyda-Grubbs type I and II metathesis catalysts onto hyperbranched PG with a degree of functionalization of 3.85% [426].

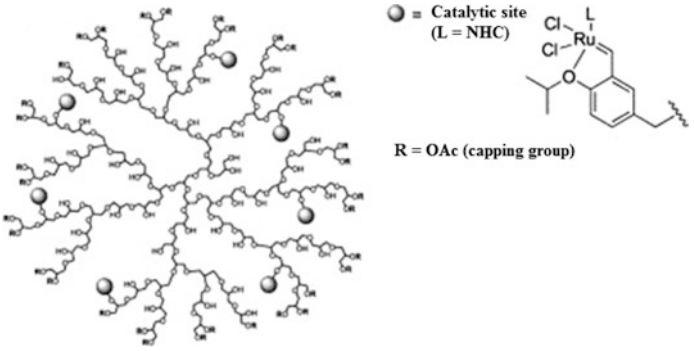

The polynuclear copper(II) chelates with hyperbranched G2 and G3 polyesters carrying end (3-diethylamino) propionate units were synthesized (Fig. 5.72a) [427]. A chelate node has composition $CuN_2O_2Solv_2$ where Solv is H_2O or DMSO. We note the preparation of a thin film composed of nanoparticles by dropping the solution of Cu(II)-PMC in methanol on the highly oriented pyrolytic graphite surface. The mean square roughness for 10 × 10 μm scan is 4 nm, variation in height is 20 nm (Fig. 5.72b).

Hyperbranched poly(ester-amide) Sm(III)-PMC was obtained by coordinating Sm(III) ions to hyperbranched CPL via a dissolution-distillation process [428]. The study of ^{13}C NMR spectra (Fig. 5.73a, b) shown disappearance of the peaks at 175.71 and 175.15 ppm assigned to the –CO–OH group and –CO–O– structure of

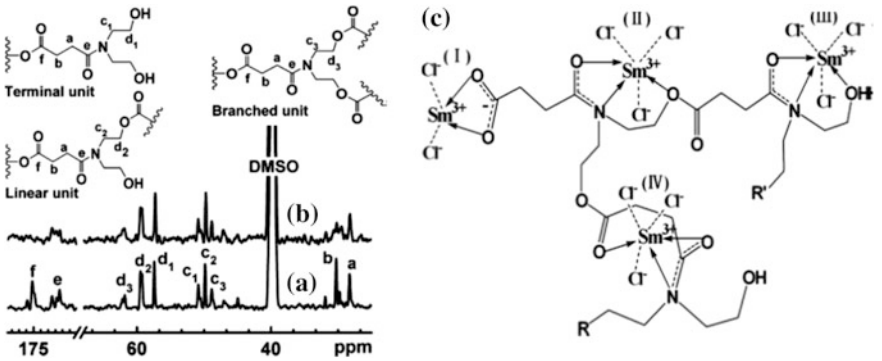

Fig. 5.73 ^{13}C NMR spectra of **a** hyperbranched poly (ester-amide) and **b** Sm(III)-hyperbranched poly(ester-amide) complex. Modes of chelation of hyperbranched poly (ester-amide) ligand with Sm(III) ions (**c**)

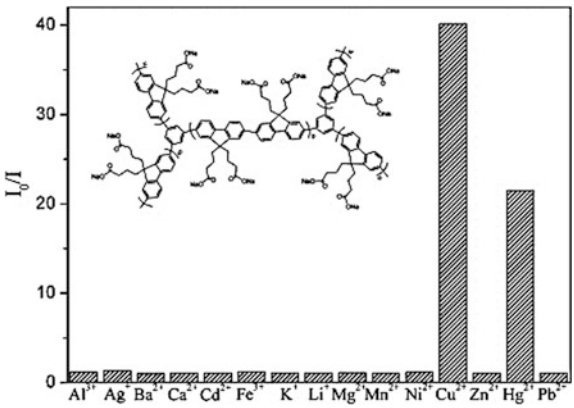

Fig. 5.74 The fluorescence response of hyperbranched polyfluorenes upon titration of various metal ions ([metal ion] = 50 × 10^{-6} M) at pH 7.0 in 10 mM NaH_2PO_4–Na_2HPO_4 buffer solution

the CPL after chelation of Sm(III) ions. Other peaks, those of –COOH group, –CO–RN–CH_2– structure and –CH_2–OH group, are downfield shifted or upfield shifted due to the participation of the oxygen and nitrogen atoms in chelation (Fig. 5.73c).

Hyperbranched polyfluorenes containing carboxylate fragments showed high selectivity toward Hg(II) and Cu(II) ions in aqueous solution with the K_{sv} of 0.8 × 10^6 M^{-1} and 3.11 × 10^6 M^{-1}, respectively (Fig. 5.74) [429].

Of interest is studying adsorption of metal ions by the hyperbranched polyesters based on 2,2-bis(hydroxymethyl)propionic acid and triethanol amine (Table 5.5), in which the ester groups and terminal hydroxyl groups take part in chelation [430]. The extent of binding (EOB)is determined by the number of moles of a metal ion linked per mole of CPL. It is important that the maximum EOB followed the order G2 < G3 < G4 < G5 for all metal ions. It should be noted that chelating ability of the prepared CPLs is better than that of Boltorn ones.

Table 5.5 The EOB of G2, G3, G4 and G5 for the metal ions

Metal ion	Efficiency of binding									
	G2	RSD (%)	G3	RSD (%)	G4	RSD (%)	G5	RSD (%)	Boltorn H30	RSD (%)
Cu(II)	4.5	2.8	10.1	1.2	18.0	1.2	26.1	1.0	10.8	2.5
Fe(III)	4.0	3.2	9.0	1.4	18.0	0.7	25.0	1.0	9.4	3.8
Pb(II)	3.5	4.5	8.0	3.2	16.0	1.5	20.0	1.1	9.1	2.9
Co(II)	2.4	4.6	7.0	1.0	15.6	1.7	22.4	1.0	7.8	3.1
Ni(II)	2.0	4.6	4.0	3.3	10.9	0.9	21.2	1.1	5.4	1.9
Cd(II)	2.0	4.7	7.0	1.6	14.0	2.5	22.5	0.9	8.3	2.7
Zn(II)	0.6	5.9	1.7	4.8	4.5	2.8	6.8	1.7	2.3	2.0

Table 5.6 Characterization and EOB values for Cd(II) ion of all prepared polymers

Sample	^{1}H NMR M_n g mol^{-1}	Number of (OH) mole/mole	Number of (COOH) mole/mole	EOB for Cd (II) ion
G1-OH	590	6	–	1
G2-OH	1170	11	–	2
G3-OH	1900	17	–	3
G4-OH	3200	28	–	5
G1-COOH	1457	–	10	4
G2-COOH	2760	–	18	8
G3-COOH	4653	–	32	14
G4-COOH	7100	–	44	20

The aliphatic hyperbranched polyesters based on 1,3,5-tris(2-hydroxyethyl) cyanuric acid with terminal hydroxyl and aromatic carboxylic groups were used for removal of heavy metal ions from waste water [431–433]. The increasing generation of the CPLs leads to an increase of their chelating ability, irrespective of the nature of end fragments (Table 5.6). It is interesting that two carboxyl fragments take part in chelation of one Cd(II) ion in the case of carboxyl containing polymers, whereas four OH groups coordinated with each Cd(II) ion for hydroxyl containing CPLs.

The carboxyl-terminated hyperbranched oligomer (M_w = 2125 and narrow PDI = 1.21) containing citric acid fragments was used to the absorption of chrome and reduce chromium emission [434]. It is interesting that prepared PMC retained chelation ability of citric acid that led to the formation of stable PMCs.

It should be noted biomedical applications of hyperbranched PMCs, for example, in bioimaging and contrast agents having reduced toxicity, prolonged plasma half-life, enhanced stability, and improved targeting specificity [435, 436]. In particular, hyperbranched conjugated polyelectrolyte was subsequently reacted with DTPA dianhydride in anhydrous DMSO at room temperature overnight to afford

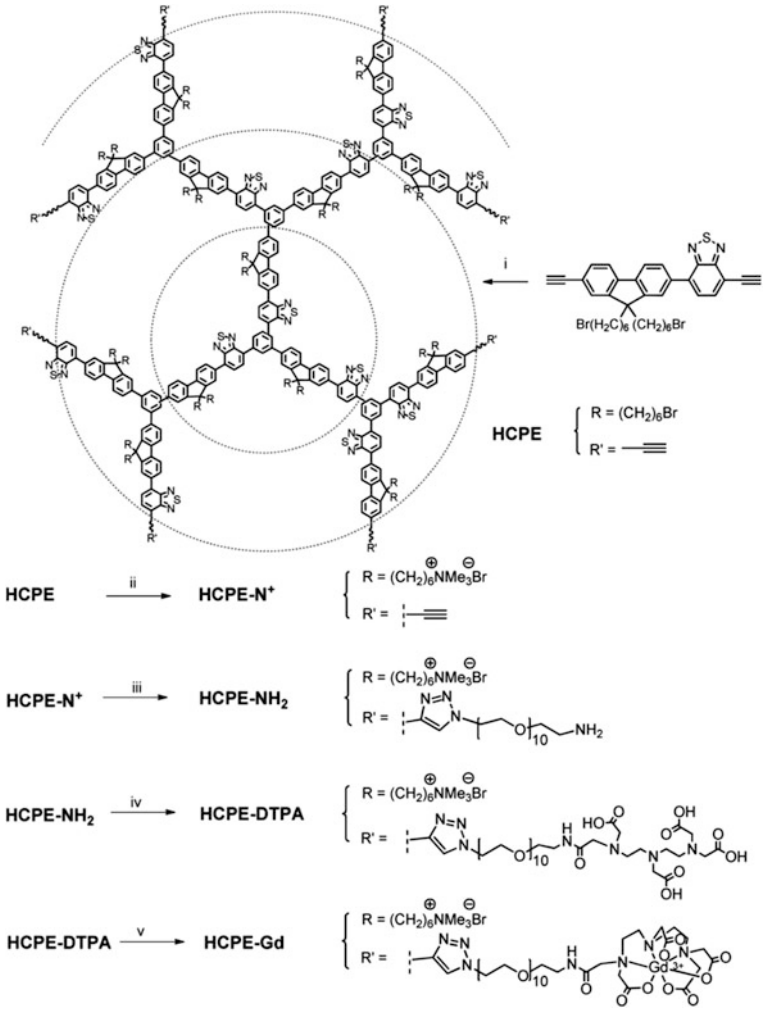

Scheme 5.33 Synthetic route to Gd-DTPA hyperbranched polymer

DTPA-containing hyperbranched polymer in 92% yield (Scheme 5.33) [437]. The final product Gd-DTPA hyperbranched polymer was obtained by chelation of Gd (III) to the DTPA moieties of the hyperbranched polymer. The prepared Gd-DTPA hyperbranched polymer is an efficient dual-modal (optical/MR) imaging agent for in vivo cancer diagnosis.

Numerous studies have been devoted to macrocyclic complexes with hyperbranched polymers, in particular, M-Pp [438]. In a typical example, iron was inserted within the Pp core by reacting hyperbranched polymer with $FeCl_2$. The solution was refluxed for 4 h and subsequently exposed to air to convert the Fe(II)-Pp to the Fe(III)-Pp hyperbranched polymer [439]. Fe-Pp hyperbranched polymer

was fractionated to prepare three different PMCs with M_n = 5400, 10,000 and 16,000, corresponding to the G2, G3 and G4 dendrimers.

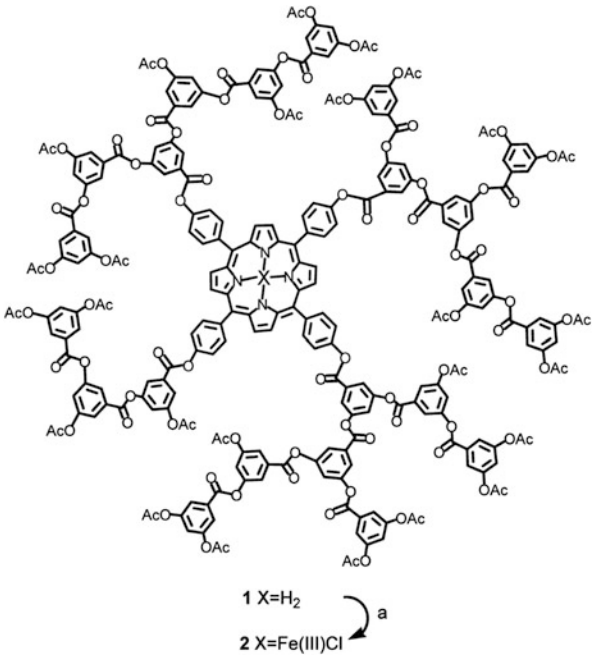

Hyperbranched poly (arylene ether ketones) containing M-Pp were synthesized by mixing of the ligand and excesses metal chlorides ($MgCl_2 \cdot 6H_2O$, $ZnCl_2$ or $MnCl_2 \cdot 4H_2O$) in the mixed solvent of $CHCl_3$ and DMF (yield 96%) [440]. It is important that dendritic architecture allowed for maximum dispersion of the chromophores, avoided aggregation, more optical limiting property was obtained. Besides, they retained the excellent properties of the materials, particularly in thermal stability.

It should be noted a narrowly dispersed tetra (acetoxyphenyl)-Pp cored hyperbranched polymer containing chelating and catalytic sites [441]. The interaction of the CPL and zinc acetate leads to the Zn-Pp hyperbranched polymer, which had a very similar molecular weight (11,710) to the initial Pp cored polymer (11,306).

A hyperbranched poly (aryl ester) with molecular weights between 4500 and 30 000 that possesses a number of free-base Pp units within its globular structure was synthesized [442]. The number of free-base Pp increased with molecular weight with the largest polymer containing $\sim$6 Pp. Metalation was carried out into the internal free-base Pp without harming or damaging the polymeric backbone. For example, Zn-Pp hyperbranched poly (aryl ester) was prepared by mixing of the Pp cored hyperbranched polymer with excess $Zn(OAc)_2 \cdot 3H_2O$ at room temperature for 30 min (yield 72%) (Scheme 5.34). As iron is slightly larger than zinc, a more

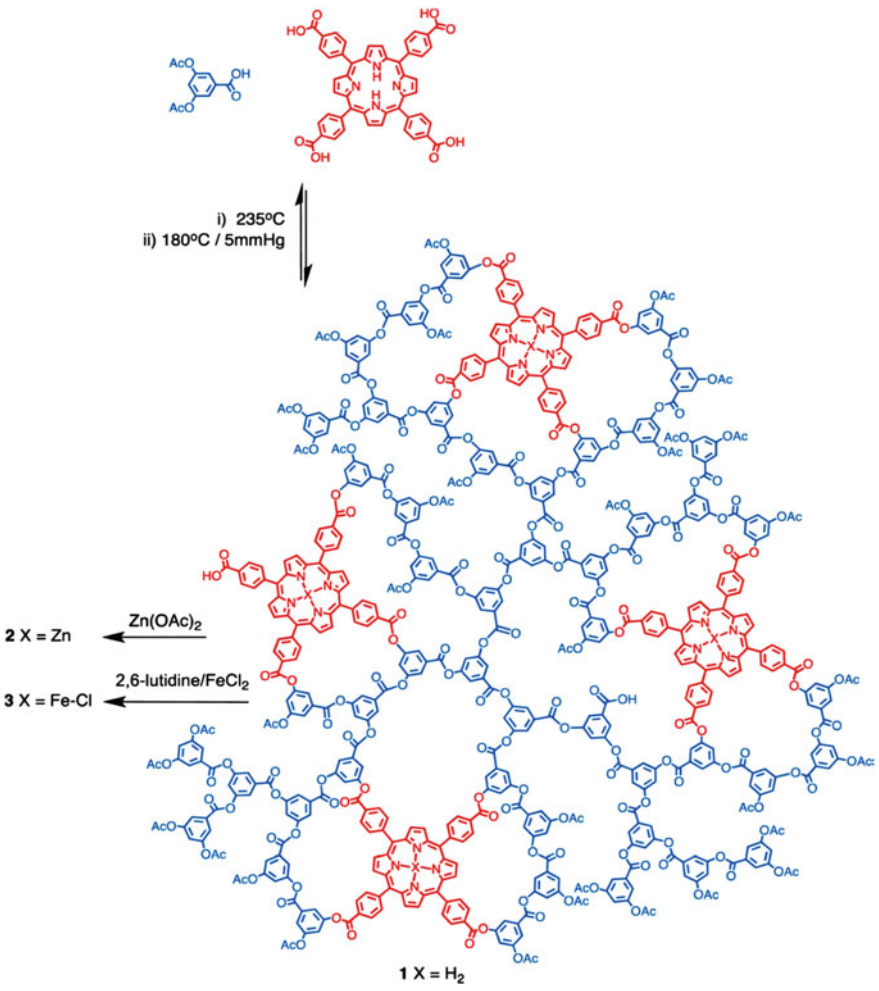

Scheme 5.34 Synthesis of multi-Pp hyperbranched poly (3,5-diacetoxybenzoic acid)

rigorous reaction procedure was required. In particular, the initial Pp cored polymer was dissolved in THF, and an excess of $FeCl_2$ was added together with 2,6-lutidine (yield 75%). It is important that the zinc- and iron-containing hyperbranched polymers confirmed that metalation had not destroyed or damaged the polymer: the M_n of both products remained unchanged, although the PDI was slightly reduced due to the additional purification step that also removed small oligomers.

It should be noted the one-stage preparation of a Fe(II)-Pp hyperbranched polymer similar the natural heme-based proteins [443]. Incorporation of iron was reached by the interaction of free-base Pp cored CPL and $FeBr_2$ with consequent oxidation to form Fe(III)-Pp cored PMC with values of 16,650 and 2.08 for M_n and PDI respectively.

Of interest is the preparation of pyridine-cored hyperbranched polymer by the polymerization of 3,5-diacetoxybenzoic acid followed by coordination of Zn-Pp (Scheme 5.35) [444].

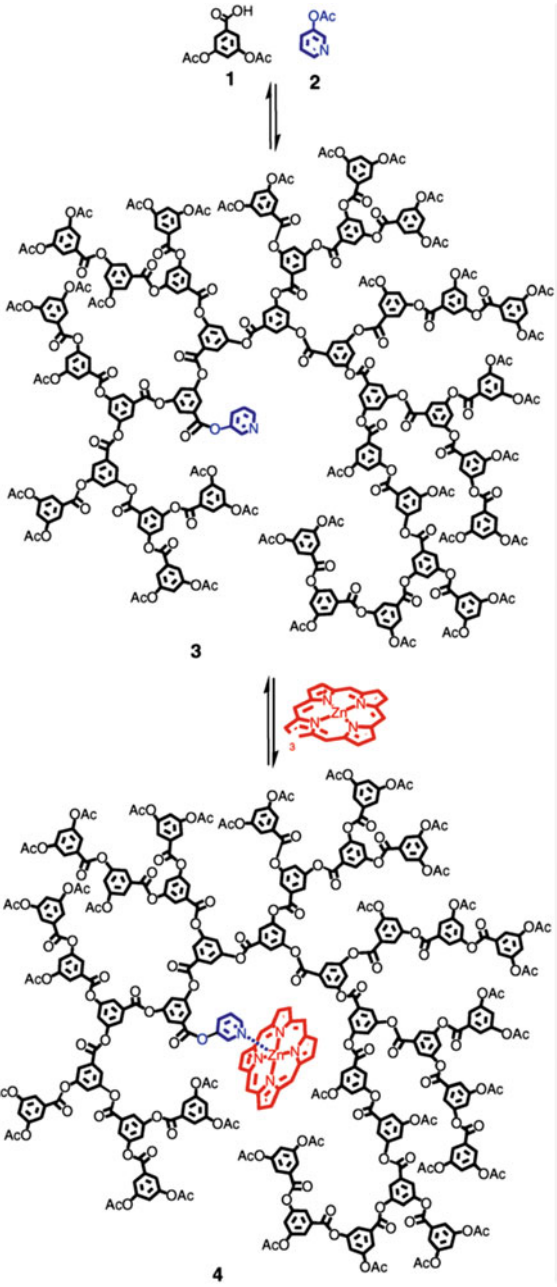

Scheme 5.35 Synthesis of the Py-cored hyperbranched polymer and its Zn-Pp complex

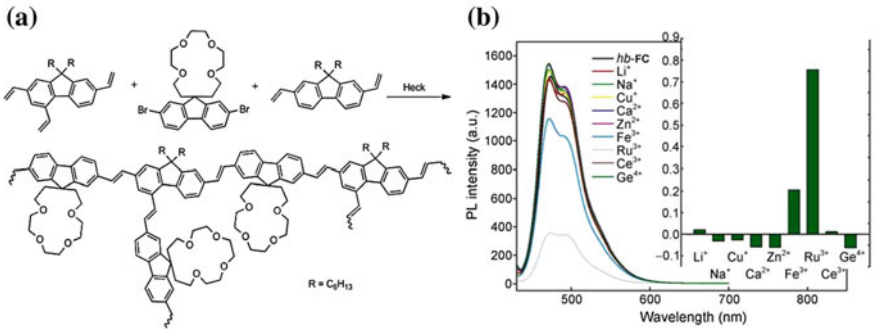

Fig. 5.75 **a** Synthesis of fluorescent hyperbranched polymers by Heck coupling copolymerization. **b** Photoluminescence spectra of fluorescent hyperbranched polymers in the presence of various metal cations. λ_{ex} = 423 nm, c = 10^{-6} M in DMF/H_2O = 9/1 (v/v), [ions] = 2.2 × 10^{-4} M. Inset figure is the photoluminescence spectra response profile by adding different metal cations

A range of M-Pc hyperbranched polymers was prepared using template method [445–448].

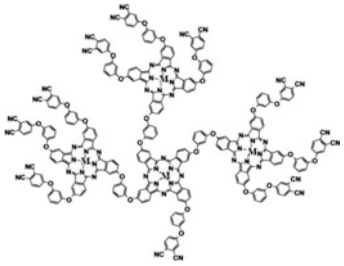

In a typical example, 1,3-bis(3,4-dicyanophenoxy) benzene or its mixture with $Ti(OC_4H_9)_4$ or $Cu(acac)_2$, in 1-pentanol in the presence of DBU, was heated at 90 to 110 °C for 2 to 4 h under a slow stream of nitrogen. The dark green powder was dried in the air for 6 h and then kept under vacuum for another 12 h [448]. A soluble Cu-Pc hyperbranched polymer was synthesized by Cu fusion technique from 1,2-bis(3,4-dicyanophenoxy) benzene and CuCl [446]. It should be noted the preparation of high-performance programmable memory devices [447] and organic-inorganic hybrid solar cells [448] based on M-Pc hyperbranched polymers.

Of considerable interest is using stimulus-responsive fluorescent hyperbranched CPLs as metal sensors [449]. As a typical example, we note metal ions responsive fluorescent hyperbranched polymers with 15-crown-4 fragments (Fig. 5.75a) [450]. Binding of crown ether receptor with conjugated polymer main chain leads to amplified fluorescence spectral change in the presence of different metal ions (Fig. 5.75b). In particular, the fluorescent hyperbranched polymers exhibit selective

fluorescence quenching toward Fe(III) and Ru(III), with the K_{sv} of 2×10^4 and 1.9×10^4 M^{-1}, respectively.

The PL intensity of another fluorescent hyperbranched polymer containing 18-crown-6 fragment was quenched by Cu(II), Ag(I), Ni(II) and Na(I) ions, whereas K(I) addition led to the emission enhancing without a noticeable absorption change [451]. Such behavior is explained by the strong coordination of K(I) with crown fragments due perfect size matching.

References

1. A.S. Abd-El-Aziz, I. Manners, *Frontiers in Transition-Metal Containing Polymers* (Wiley, NY, 2007)
2. S. Campagna, P. Ceroni, F. Puntoriero (eds.), *Designing Dendrimers* (Wiley, Hoboken, 2012)
3. L.H. Gade (ed.), *Dendrimer Catalysis* (Springer, Berlin, Heidelberg, NY, 2006)
4. Y. Cheng (ed.), *Dendrimer-based Drug Delivery Systems: From Theory to Practice* (Wiley, Hoboken, New Jersey, 2012)
5. U.S. Schubert, H. Hofmeier, G.R. Newkome, *Modern Terpyridine Chemistry* (Wiley-VCH Verlag GmbH & Co. KGaA, Weinheim, 2006)
6. D.A. Tomalia, J.B. Christensen, U. Boas, *Dendrimers, Dendrons, and Dendritic Polymers: Discovery, Applications, and the Future* (Cambridge University Press, Cambridge, 2012)
7. F. Vögtle, G. Richardt, N. Werner, *Dendrimer Chemistry: Concepts, Syntheses, Properties, Applications* (Wiley, Weinheim, 2009)
8. R. Andrés, E. de Jesus, J.C. Flores, New J. Chem. **31**, 1161 (2007)
9. I. Angurell, O. Rossell, M. Seco, Inorg. Chim. Acta, Part A **409**, 2 (2014)
10. D. Astruc, E. Boisselier, C. Ornelas, Chem. Rev. **110**, 1857 (2010)
11. D. Astruc, R. Ciganda, C. Deraedt, S. Gatard, L. Liang, N. Li, C. Ornelas, A. Rapakousiou, J. Ruiz, D. Wang, Y. Wang, P. Zhao, Synlett **26**, 1437 (2015)
12. D. Astruc, J. Ruiz, J. Inorg. Organomet. Polym. **25**, 2 (2015)
13. A.-M. Caminade, A. Ouali, R. Laurent, J.-P. Majoral, Inorg. Chim. Acta **431**, 3 (2015)
14. A.-M. Caminade, A. Ouali, R. Laurent, C.-O. Turrin, J.-P. Majoral, Chem. Soc. Rev. **44**, 3890 (2015)
15. E. de Jesus, J.C. Flores, Ind. Eng. Chem. Res. **47**, 7968 (2008)
16. F. Figueira, P.M.R. Pereira, S. Silva, J.A.S. Cavaleiro, J.P.C. Tome, Curr. Org. Synth. **11**, 110 (2014)
17. S.-H. Hwang, C.D. Shreiner, C.N. Moorefield, G.R. Newkome, New J. Chem. **31**, 1192 (2007)
18. W. Huang, Curr. Trends Surf. Sci. Catal. **1**, 65 (2014)
19. D.-L. Jiang, T. Aida, Prog. Polym. Sci. **39**, 403 (2005)
20. R.S. Kalhapure, M.K. Kathiravan, K.G. Akamanchi, T. Govender, Pharm. Dev. Technol. **20**, 22 (2015)
21. W.-S. Li, T. Aida, Chem. Rev. **109**, 6047 (2009)
22. F. Martinez-Olid, J.M. Benito, J.C. Flores, E. de Jesus, Isr. J. Chem. **49**, 99 (2009)
23. D. Méry, D. Astruc, Coord. Chem. Rev. **250**, 1965 (2006)
24. Z. Qiao, X. Shi, Prog. Polym. Sci. **44**, 1 (2015)
25. J.N.H. Reek, S. Arevalo, R. van Heerbeeck, P.C.J. Kamer, P.W.N.M. van Leeuwen, Adv. Catal. **49**, 71 (2006)
26. L. Xu, L.-J. Chen, H.-B. Yang, Chem. Commun. **50**, 5156 (2014)

27. X. Wang, G. Guérin, H. Wang, Y. Wang, I. Manners, M.A. Winnik, Science **317**, 644 (2007)
28. H. Frauenrath, Prog. Polym. Sci. **30**, 325 (2005)
29. D.A. Tomalia, Soft Matter **6**, 456 (2010)
30. N. Satoh, T. Nakashima, K. Kamikura, K. Yamamoto, Nat. Nanotechnol. **3**, 106 (2008)
31. K. Yamamoto, T. Imaoka, W.-J. Chun, O. Enoki, H. Katoh, M. Takenaga, A. Sonoi, Nat. Chem. **1**, 397 (2009)
32. M.S. Diallo, L. Balogh, S. Christie, P. Swaminathan, X. Shi, W.A. Goddard III, J.H. Johnson Jr., Dendritic nanoscale chelating agents: synthesis, characterization and environmental applications, in *Nanotechnology and the Environment*, vol. 890, Sect. VI, Ch. 7, ed. by B. Karn, T. Masciangioli, W.-X. Zhang, (Oxford University Press, NY, 2004), p. 238 (ACS Symp. Ser.)
33. C.N.R. Rao, A. Müller, A.K. Cheetham, dendrimers and their use as nanoscale sensors, in *Nanomaterials Chemistry: Recent Developments and New Directions*, ed. by N. Jayaraman (Wiley-VCH Verlag GmbH & Co. KGaA, Weinheim, 2007)
34. D. Astruc (ed.), *Dendrimers and Nanoscience* (Elsevier/C.R. Chimie, Paris, 2003)
35. A.-M. Caminade, R. Laurent, A. Ouali, J.-P. Majoral, Inorg. Chim. Acta **409**, 68 (2014)
36. F.G. Zhao, W.S. Li, Sci. Chin. Chem. **54**, 286 (2011)
37. R.W.J. Scott, O.M. Wilson, R.M. Crooks, J. Phys. Chem. B **109**, 692 (2005)
38. W. Lesniak, A.U. Bielinska, L.P. Balogh, Nano Lett. **5**, 2123 (2005)
39. X. Huang, S. Zheng, I. Kim, J. Nanosci. Nanotechnol. **14**, 1631 (2014)
40. Y. Shirota, H. Kageyama, Chem. Rev. **107**, 953 (2007)
41. R.W. Saalfrank, A. Scheurer (eds.), *Chemistry of Nanocontainers* (Springer, Berlin, Heidelberg, 2012)
42. V. Balzani, E. Marchi, M. Semeraro, Rendiconti Lincei **21**, 91 (2010)
43. V. Balzani, A. Credi, M. Venturi, *Molecular Devices and Machines—A Journey into the Nano World* (Wiley-VCH Verlag GmbH & Co, Weinheim, 2003)
44. B. Champin, P. Mobian, J.-P. Sauvage, Chem. Soc. Rev. **36**, 358 (2007)
45. D. Astruc, P. Zhao, L. Liang, A. Rapakousiou, R. Djeda, A. Diallo, T. Kusamoto, J. Ruiz, C. Ornelas, J. Inorg. Organomet. Polym. **23**, 41 (2013)
46. Y.-H. Tang, A.Y.-T. Huang, P.-Y. Chen, H.-T. Chen, C.-L. Kao, Curr. Pharm. Design **17**, 2308 (2011)
47. D.A. Tomalia, New J. Chem. **36**, 264 (2012)
48. B.M. Rosen, D.A. Wilson, C.J. Wilson, M. Peterca, B.C. Won, C. Huang, L.R. Lipski, X. Zeng, G. Ungar, P.A. Heiney, V. Percec, J. Am. Chem. Soc. **131**, 17500 (2009)
49. D.A. Tomalia, S.N. Khanna, Chem. Rev. **116**, 2705 (2016)
50. R.S. Bagul, N. Jayaraman, Inorg. Chim. Acta. Part A **409**, 34 (2014)
51. A.M. Caminade, A. Hameau, J.P. Majoral, Chem. Eur. J. **15**, 9270 (2009)
52. A.W. Kleij, A. Ford, J.T.B.H. Jastrzebski, G. van Koten, Dendritic polymer applications: catalysts, in*: Dendrimers and Other Dendritic Polymers* (Wiley, West Sussex, UK, 2001)
53. J. Wang, H. Wang, C. Li, H. Li, Acta Petrolei Sinica (Petroleum Processing Section) **29**, 920 (2013)
54. S.A. Chavan, W. Maes, L.E.M. Gevers, J. Wahlen, I.F.J. Vankelecom, P.A. Jacobs, W. Dehaen, D.E. De Vos, Chem. Eur. J. **11**, 6754 (2005)
55. D. Wang, C. Deraedt, J. Ruiz, D. Astruc, Acc. Chem. Res. **48**, 1871 (2015)
56. P. Govender, A.K. Renfrew, C.M. Clavel, P.J. Dyson, B. Therrien, G.S. Smith, Dalton Trans. **40**, 1158 (2011)
57. P. Govender, B. Therrien, G.S. Smith, Eur. J. Inorg. Chem. **2012**, 2853 (2012)
58. N.C. Antonels, J.R. Moss, G.S. Smith, J. Organomet. Chem. **696**, 2003 (2011)
59. L.P. Sadowski, P.E. Edem, J.F. Valliant, A. Adronov, Macromol. Biosci. **14**, 1475 (2016)
60. C. Ghobril, G. Lamanna, M. Kueny-Stotz, A. Garofalo, C. Billotey, D. Felder-Flesch, New J. Chem. **36**, 310 (2012)
61. A. Parat, C. Bordeianu, H. Dib, A. Garofalo, A. Walter, S. Bégin-Colin, D. Felder-Flesch, Nanomedicine **10**, 977 (2015)

62. R.K. Tekade, P.V. Kumar, N.K. Jain, Chem. Rev. **109**, 49 (2009)
63. M.A. Oar, J.M. Serin, W.R. Dichtel, J.M.J. Fréchet, T.Y. Ohulchanskyy, P.N. Prasad, Chem. Mater. **17**, 2267 (2005)
64. A. Valente, M.H. Garcia, Inorganics **2**, 96 (2014)
65. V. Gajbhiye, V.K. Palanirajan, R.K. Tekade, N.K. Jain, J. Pharm. Pharmacol. **61**, 989 (2009)
66. A.B. Nepomnyashchii, M.A. Alpuche-Aviles, S. Pan, D. Zhan, F.-R.F. Fan, A.J. Bard, J. Electroanal. Chem. **621**, 286 (2008)
67. A. Tsuda, M.A. Alam, T. Harada, T. Yamaguchi, N. Ishii, Angew. Chem. Int. Ed. **46**, 8198 (2007)
68. D.-I. Lee, T. Goodson III, J. Phys. Chem. B **110**, 25582 (2006)
69. Y. Li, A. Rizzo, M. Salerno, M. Mazzeo, C. Huo, Y. Wang, K. Li, R. Cingolani, G. Gigli, Appl. Phys. Lett. **89**, 061125 (2006)
70. J.B. Oh, Y.H. Kim, M.K. Nah, H.K.J. Kim, J. Lumin. **111**, 255 (2005)
71. A.S. Mahadevi, G.N. Sastry, Chem. Rev. **116**, 2775 (2016)
72. L. Babel, T.N.Y. Hoang, L. Guénée, C. Besnard, T.A. Wesolowski, M. Humbert-Droz, C. Piguet, Chem. Eur. J. **22**, 8113 (2016)
73. W. Jiang, K. Nowosinski, N.L. Löw, E.V. Dzyuba, F. Klautzsch, A. Schäfer, J. Huuskonen, K. Rissanen, C.A. Schalley, J. Am. Chem. Soc. **134**, 1860 (2012)
74. M. Brewis, M. Helliwell, N.B. McKeown, Tetrahedron **59**, 3863 (2003)
75. M. Brewis, M. Helliwell, N.B. McKeown, S. Reynolds, A. Shawcross, Tetrahedron Lett. **42**, 813 (2001)
76. J.M. Benito, E. de Jesús, F.J. de La Mata, J.C. Flores, R. Gómez, Chem. Commun. 5217 (2005)
77. J.M. Benito, E. de Jesús, F.J. de la Mata, J.C. Flores, R. Gómez, P. Gómez-Sal, Organometallics **25**, 3876 (2006)
78. J.M. Benito, E. de Jesús, F.J. de la Mata, J.C. Flores, R. Gómez, Organometallics **25**, 3045 (2006)
79. G. Smith, R. Chen, S. Mapolie, J. Organomet. Chem. **673**, 111 (2003)
80. G.S. Smith, S.F. Mapolie, J. Mol. Catal. A Chem. **213**, 187 (2004)
81. B.C. Makhubela, A.M. Jardine, G. Westman, G.S. Smith, Dalton Trans. **41**, 10715 (2012)
82. X. Zhao, A.C.J. Loo, P.P.-F. Lee, T.T.Y. Tan, C.K. Chu, J. Inorg. Biochem. **104**, 105 (2010)
83. A. Ouali, R. Laurent, A.M. Caminade, J.P. Majoral, M. Taillefer, J. Am. Chem. Soc. **128**, 15990 (2006)
84. N. El Brahmi, S. El Kazzouli, S.M. Mignani, E.M. Essassi, G. Aubert, R. Laurent, A.M. Caminade, M.M. Bousmina, T. Cresteil, J.P. Majoral, Mol. Pharm. **10**, 1459 (2013)
85. T. Ahamad, S.M. Alshehri, S.F. Mapolie, Catal. Lett. **138**, 171 (2010)
86. L. Liang, J. Ruiz, D. Astruc, Adv. Synth. Catal. **353**, 3434 (2011)
87. U. Stebani, G. Lattermann, M. Wittenberg, J.H. Wendorff, Angew. Chem. Int. Ed. **35**, 1858 (1996)
88. U. Stebani, G. Lattermann, Adv. Mater. **7**, 578 (1995)
89. M.C. Parrot, S.R. Benhabbour, C. Saab, J.A. Lemon, S. Parker, J.F. Valliant, A. Andrianoov, J. Am. Chem. Soc. **131**, 2906 (2009)
90. A. Parat, D. Kryza, F. Degoul, J. Taleb, C. Viallard, M. Janier, A. Garofalo, P. Bonazza, L. Heinrich-Balard, R. Cohen, E. Miot-Noirault, J.-M. Chezal, C. Billotey, D. Felder-Flesch, J. Mater. Chem. B **3**, 2560 (2015)
91. C.-L. Kao, Y.-H. Tang, Y.C. Lina, L.-T. Chiu, H.-T. Chen, S.C.N. Hsu, K.-C. Hsieh, C.-Y. Lu, Y.-L. Chen, Nanomedicine. NBM **7**, 273 (2011)
92. A. Patri, C.N. Moorefield, G.R. Newkome, e-Journal **84**, 1023 (2012)
93. P. Geotti-Bianchini, T. Darbre, J.-L. Reymond, Org. Biomol. Chem. **11**, 344 (2013)
94. N.A. Uhlich, P. Sommer, C. Bühr, S. Schürch, J.-L. Reymond, T. Darbre, Chem. Commun. 6237 (2009)
95. A. Jahier, S. Nlate, J. Organomet. Chem. **694**, 637 (2009)
96. P. Govender, S. Pai, U. Schatzschneider, G.S. Smith, Inorg. Chem. **52**, 5470 (2013)

97. K.Y. Zhang, H.-W. Liu, T.T.-H. Fong, X.-G. Chen, K.K.-W. Lo, Inorg. Chem. **49**, 5432 (2010)
98. R. Roy, J.M. Kim, Tetrahedron **59**, 3881 (2003)
99. T. Muraki, K.-I. Fujita, M. Kujime, J. Org. Chem. **72**, 7863 (2007)
100. J.P. André, C.F.G.C. Geraldes, J.A. Martins, A.E. Merbach, M.I.M. Prata, A.C. Santos, J.J.P. de Lima, É. Tóth, Chem. Eur. J. **10**, 5804 (2004)
101. U.S. Schubert, A. Winter, G.R. Newkome (eds.), *Terpyridine-based Materials. For Catalytic, Optoelectronic and Life Science Applications* (Wiley-VCH, Weinheim, 2011)
102. S. Glazier, J.A. Barron, P.L. Houston, H.D. Abruña, J. Phys. Chem. B **106**, 9993 (2002)
103. H. Stephan, G. Geipel, G. Bernhard, P. Comba, G. Rajaraman, U. Hahn, F. Vogtle, Eur. J. Inorg. Chem. **2005**, 4501 (2005)
104. U. Hahn, F. Vögtle, G. De Paoli, M. Staffilani, L. De Cola, Eur. J. Inorg. Chem. **2009**, 2639 (2009)
105. U. Luning, J.P.W. Eggert, K. Hagemann, Eur. J. Org. Chem. **2006**, 2747 (2006)
106. A. Astruc, Nat. Chem. **4**, 255 (2012)
107. H.F. Chow, I.Y.K. Chan, P.S. Fung, T.K.K. Mong, M.F. Nongrum, Tetrahedron **57**, 1565 (2001)
108. E.C. Constable, C.E. Housecroft, M. Neuburger, S. Schaffner, L.J. Scherer, Dalton Trans. 2635 (2004)
109. M. Kimura, T. Shiba, T. Muto, K. Hanabusa, H. Shirai, Chem. Commun. 11 (2000)
110. A. Joester, V. Gramlich, F. Diederich, Helv. Chim. Acta **87**, 2896 (2004)
111. A. Mishra, E. Mena-Osteritz, P. Bäuerle, Beilstein J. Org. Chem. **9**, 866 (2013)
112. G.R. Newkome, E. He, L.A. Godinez, G.R. Baker, J. Am. Chem. Soc. **122**, 9993 (2000)
113. H. Jiang, S.J. Lee, W. Lin, J. Chem. Soc. Dalton Trans. 3429 (2002)
114. G.R. Newkome, K.S. Yoo, C.N. Moorefield, Chem. Commun. 2164 (2002)
115. G.D. Storrier, K. Takada, H.D. Abruna, Langmuir **15**, 872 (1999)
116. R. Satapathy, M. Ramesh, H. Padhy, I.-H. Chiang, C.-W. Chu, K.-H. Wei, H.-C. Lin, Polym. Chem. **5**, 5423 (2014)
117. J.-C.G. Bünzli, C. Piguet, Chem. Soc. Rev. **34**, 1048 (2005)
118. C. Piguet, J.-C.G. Bünzli, B. Donnio, D. Guillon, Chem. Commun. 3755 (2006)
119. A. Pucci, B. Donnio, in *Metal-Containing Liquid Crystals, in Handbook of Liquid Crystals*, ed. by J.W. Goodby, P.J. Collings, T. Kato, C. Tschierske, H. Gleeson, P. Raynes (Wiley-VCH Verlag GmbH & Co, Weinheim, 2014)
120. A. Terazzi, B. Bocquet, S. Campidelli, B. Donnio, D. Guillon, R. Deschenaux, C. Piguet, Chem. Commun. 2922 (2006)
121. T.B. Jensen, E. Terazzi, K.L. Buchwalder, L. Guénée, H. Nozary, K. Schenk, B. Heinrich, B. Donnio, D. Guillon, C. Piguet, Inorg. Chem. **49**, 8601 (2010)
122. K. Binnemans, in *Molecular Materials*, ed. by D.W. Bruce, D. O'Hare, R.J. Walton (Wiley, Weinheim, 2010)
123. A. Perrier, M. Keller, A.-M. Caminade, J.-P. Majoral, A. Oualli, Green Chem. **15**, 2075 (2013)
124. A. Sánchez-Méndez, E. de Jesús, J.C. Flores, P. Gómez-Sal, Eur. J. Inorg. Chem. **2010**, 141 (2010)
125. M. Gaab, S. Bellemin-Laponnaz, L.H. Gade, Chem. Eur. J. **15**, 5450 (2009)
126. A. Gissibl, C. Padie, M. Hager, F. Jaroschik, R. Rasappan, E. Cuevas-Yanez, C.O. Turrin, A.M. Caminade, J.P. Majoral, O. Reiser, Org. Lett. **9**, 2895 (2007)
127. D. Wang, D. Denux, J. Ruiz, D. Astruc, Adv. Synth. Catal. **355**, 129 (2013)
128. M. Koprowski, R.M. Sebastian, V. Maraval, M. Zablocka, V. Cadierno, B. Donnadieu, A. Igau, A.M. Caminade, J.P. Majoral, Organometallics **21**, 4680 (2002)
129. J.P. Byrne, J.A. Kitchen, T. Gunnlaugsson, Chem. Soc. Rev. **43**, 5302 (2014)
130. A. Xu, H.U. Kim, J.-H. Kim, B.J. Jung, A.C. Grimsdale, D.-H. Hwang, Progr. Polym. Sci. **47**, 92 (2015)
131. J.W. Levell, W.-Y. Lai, R.J. Borthwick, P.L. Burn, S.-C. Lo, I.D.W. Samuel, New J. Chem. **36**, 407 (2012)

132. M. Dasgupta, P.M. Brad, A.K. Kakkar, Coord. Chem. Rev. **233–234**, 223 (2002)
133. A.-M. Caminade, J.-P. Majoral, Molecules **21**, 538 (2016)
134. A.-M. Caminade, A. Ouali, R. Laurent, C.-O. Turrin, J.-P. Majoral, Coord. Chem. Rev. **308**, 478 (2016)
135. M. Tristany, R. Laurent, H. Dib, L. Gonsalvi, M. Peruzzini, J.P. Majoral, A.M. Caminade, Inorg. Chim. Acta **409**, 121 (2014)
136. A.-M. Caminade, A. Hameau, J.-P. Majoral, Dalton Trans. **45**, 1810 (2016)
137. R. Laurent, A.M. Caminade, J.P. Majoral, Tetrahedron Lett. **46**, 6503 (2005)
138. E. Badetti, G. Franc, J.-P. Majoral, A.-M. Caminade, R.M. Sebastián, M. Moreno-Mañas, Eur. J. Org. Chem. **2011**, 1256 (2011)
139. B. Ma, Z. Ding, J. Liu, Y. He, Q.-H. Fan, Chem. Asian J. **8**, 1101 (2013)
140. L. Routaboul, S. Vincendeau, C.O. Turrin, A.M. Caminade, J.P. Majoral, J.C. Daran, E. Manoury, J. Organomet. Chem. **692**, 1064 (2007)
141. P. Servin, R. Laurent, A. Romerosa, M. Peruzzini, J.P. Majoral, A.M. Caminade, Organometallics **27**, 2066 (2008)
142. J.K. Kassube, L.H. Gade, Adv. Synth. Catal. **351**, 739 (2009)
143. J. Yu, T.V. RajanBabu, J.R. Parquette, J. Am. Chem. Soc. **130**, 7845 (2008)
144. J. Lemo, K. Heuzé, D. Astruc, Org. Lett. **7**, 2253 (2005)
145. G. Engel, L.H. Gade, Chem. Eur. J. **8**, 4319 (2002)
146. V. Maraval, R. Laurent, B. Donnadieu, A.M. Caminade, J.P. Majoral, Phosphorus. Sulfur Silicon Relat. Elem. **184**, 1612 (2009)
147. E. Alonso, D. Astruc, J. Am. Chem. Soc. **122**, 3222 (2000)
148. V. Maraval, R. Laurent, A.-M. Caminade, J.-P. Majoral, Organometallics **19**, 4025 (2000)
149. K. Heuze, D. Mery, D. Gauss, J.-C. Blais, D. Astruc, Chem. Eur. J. **10**, 3936 (2004)
150. R.S. Bagul, N. Jayaraman, J. Organomet. Chem. **701**, 27 (2012)
151. S. Gatard, S. Nlate, E. Cloutet, G. Bravic, J.-C. Blais, D. Astruc, Angew. Chem. Int. Ed. **42**, 452 (2003)
152. G. Franc, C.O. Turrin, E. Cavero, J.P. Costes, C. Duhayon, A.M. Caminade, J.P. Majoral, Eur. J. Org. Chem. 4290 (2009)
153. Z.-J. Wang, G.-J. Deng, Y. Li, Y.-M. He, W.-J. Tang, Q.-H. Fan, Org. Lett. **9**, 1243 (2007)
154. J. Liu, Y. Feng, B. Ma, Y.-M. He, Q.-H. Fan, Eur. J. Org. Chem. **2012**, 6737 (2012)
155. B. Ma, T. Miao, Y. Sun, Y. He, J. Liu, Y. Feng, H. Chen, Q.-H. Fan, Chem. Eur. J. **20**, 9969 (2014)
156. Y.-Y. Huang, X. Yang, Y. Feng, F. Verpoort, Q.-H. Fan, J. Mol. Catal. A Chem. **393**, 150 (2014)
157. J. Liu, B. Ma, Y. Feng, Y. He, Q.-H. Fan, Inorg. Chim. Acta **409**, 106 (2014)
158. S.C. Bourque, H. Alper, L.E. Manzer, P. Arya, J. Am. Chem. Soc. **122**, 956 (2000)
159. S.-M. Lu, H. Alper, J. Am. Chem. Soc. **125**, 13126 (2003)
160. S.-M. Lu, H. Alper, J. Am. Chem. Soc. **127**, 14776 (2005)
161. S.-M. Lu, H. Alper, Chem. Eur. J. **13**, 5908 (2007)
162. P.P. Zweni, H. Alper, Adv. Synth. Catal. **346**, 849 (2004)
163. J.P.K. Reynhardt, Y. Yang, A. Sayari, H. Alper, Adv. Funct. Mater. **15**, 1641 (2005)
164. I. Angurell, E. Puig, O. Rossell, M. Seco, P. Ǵomez-Sal, A. Martin. J. Organomet. Chem. **716**, 129 (2012)
165. R. Chanthateyanonth, H. Alper, Adv. Synth. Catal. **346**, 1375 (2004)
166. N.J.M. Pijnenburg, H.P. Dijkstra, G. van Koten, R.J.M.K. Gebbink, Dalton Trans. **40**, 8896 (2011)
167. N.J.M. Pijnenburg, M. Lutz, M.A. Siegler, A. Spek, G. van Koten, R.J.M.K. Gebbink, New J. Chem. **35**, 2356 (2011)
168. P. Arya, N.V. Rao, J. Singkhonrat, H. Alper, S.C. Bourque, L.E. Manzer, J. Org. Chem. **65**, 1881 (2000)
169. B.M.J.M. Suijkerbuijk, L.J. Shu, R.J.M. Klein Gebbink, A.D. Schlüter, G. van Koten, Organometallics **22**, 4175 (2003)

170. A. Bergamini, E. Marchi, P. Ceroni, in *Advanced Fluorescence Reporters in Chemistry and Biology II*, ed. by A.P. Demchenko (Springer, Berlin, Heidelberg, 2010)
171. I. Grabchev, J.-M. Chovelon, X. Qian, New J. Chem. **27**, 337 (2003)
172. I. Grabchev, J.-M. Chovelon, V. Bojinov, G. Ivanova, Tetrahedron **48**, 9591 (2003)
173. I. Grabchev, J.-P. Soumillion, B. Muls, G. Ivanova, Photochem. Photobiol. Sci. **3**, 1032 (2004)
174. I. Grabchev, D. Staneva, V. Bojinov, R. Betcheva, V. Gregoriou, Spectrochim. Acta. Part A Mol. Biomol. Spectr. **70**, 532 (2008)
175. S. Sali, I. Grabchev, J.-M. Chovelon, G. Ivanova, Spectrochim. Acta. Part A Mol. Biomol. Spectr. **65**, 591 (2006)
176. S. Yordanova, I. Grabchev, S. Stoyanov, V. Milusheva, I. Petkov, Inorg. Chim. Acta **409**, 89 (2014)
177. I. Grabchev, S. Dumas, J.-M. Chovelon, A. Nedelcheva, Tetrahedron **64**, 2113 (2008)
178. J.P. Cross, M. Lauz, P.D. Badger, S. Petoud, J. Am. Chem. Soc. **126**, 16278 (2004)
179. V. Balzani, P. Ceroni, S. Gestermann, C. Kauffmann, M. Gorka, F. Vögtle, Chem. Commun. 853 (2000)
180. F. Vögtle, S. Gestermann, C. Kauffmann, P. Ceroni, V. Vicinelli, V. Balzani, J. Am. Chem. Soc. **122**, 10398 (2000)
181. A. Prodi, F. Bolletta, M. Montalti, N. Zaccheroni, Eur. J. Chem. **3**, 455 (1999)
182. V. Vivinelli, P. Ceroni, M. Maestri, V. Balzani, M. Gorka, F. Vögtle, J. Am. Chem. Soc. **124**, 6461 (2002)
183. B. Branchi, P. Ceroni, V. Balzani, G. Bergamini, F.G. Klaerner, F. Vögtle, Chem. Eur. J. **15**, 7876 (2009)
184. R. Malgas-Enus, S.F. Mapolie, Inorg. Chim. Acta **409**, 96 (2014)
185. R. Malgas, S.F. Mapolie, S.O. Ojwach, G.S. Smith, J. Darkwa, Catal. Commun. **9**, 1612 (2008)
186. P. Govender, H. Lemmerhirt, A.T. Hutton, B. Therrien, P.J. Bednarski, G.S. Smith, Organometallics **33**, 5535 (2014)
187. S.F. Mapolie, J.L. van Wyk, Inorg. Chim. Acta **394**, 649 (2013)
188. J. Wang, G. Yang, C.-Q. Li, W.-G. Shi, S.-H. Wang, Chem. Pap. **11**, 1532 (2014)
189. J. Wang, P. Zhang, S. Chen, C.Q. Li, Adv. Mater. Res. **160–162**, 529 (2010)
190. J. Wang, G. Yang, C. Li, P. Zhangi, Asian J. Chem. **27**, 407 (2015)
191. J. Martinovic, J.v. Wyk, S. Mapolie, N. Jahed, P. Baker, E. Iwuhoa, Electrochim. Acta **55**, 4296 (2010)
192. P. Govender, L.C. Sudding, C.M. Clavel, P.J. Dyson, B. Therrien, G.S. Smith, Dalton Trans. **42**, 1267 (2013)
193. P. Govender, F. Edafe, B.C.E. Makhubela, P.J. Dyson, B. Therrien, G.S. Smith, Inorg. Chim. Acta **409**, 112 (2014)
194. B. Donnio, Inorg. Chim. Acta **409**, 53 (2014)
195. B. Donnio, D. Guillon, Adv. Polym. Sci. **201**, 45 (2006)
196. A.G. Serrette, T.M. Swager, J. Am. Chem. Soc. **115**, 8879 (1993)
197. C.K. Lai, M.Y. Lu, F.J. Lin, Liq. Cryst. **23**, 313 (1997)
198. J. Barberá, M. Marcos, A. Omenat, J.-L. Serrano, J.I. Martinez, P.J. Alonso, Liq. Cryst. **27**, 255 (2000)
199. B. Donnio, J. Barberá, R. Giménez, D. Guillon, M. Marcos, J.L. Serrano, Macromolecules **35**, 370 (2002)
200. J.H. Cameron, A. Facher, G. Lattermann, S. Diele, Mol. Cryst. Liq. Cryst. **409**, 29 (2004)
201. N. Domracheva, A. Mirea, M. Schwoerer, L. Torre-Lorente, ChemPhysChem **6**, 110 (2005)
202. N. Domracheva, A. Mirea, M. Schwoerer, L. Torre-Lorente, ChemPhysChem **7**, 2567 (2006)
203. N.E. Domracheva, A. Mirea, M. Schwoerer, L. Torre-Lorente, G. Lattermann, Phys. Solid States **49**, 110 (2007)
204. N.E. Domracheva, A.V. Pyataev, V.E. Vorobeva, E.M. Zueva, J. Phys. Chem. B **117**, 7833 (2013)

205. M.S. Gruzdev, N.E. Domracheva, U.V. Chervonova, A.M. Kolker, A.S. Golubeva, J. Coord. Chem. **65**, 1812 (2012)
206. N.E. Domracheva, V.I. Morozov, M.S. Gruzdev, R.A. Manapov, A.V. Pyataev, G. Lattermann, Macromol. Chem. Phys. **211**, 791 (2010)
207. V.E. Vorobeva, N.E. Domracheva, A.V. Pyataev, M.S. Gruzdev, U.V. Chervonova, Low Temp. Phys. **41**, 15 (2015)
208. L. Shen, F. Li, Y. Sha, X. Hong, C. Huang, Tetrahedron Lett. **45**, 3961 (2004)
209. J.N. Mugo, S.F. Mapolie, J.L. van Wyk, Inorg. Chim. Acta **363**, 2643 (2010)
210. S.M. Cohen, S. Petoud, K.N. Raymond, Chem. Eur. J. **7**, 272 (2001)
211. B.-L. Li, Z.-T. Liu, G.-J. Deng, Q.-H. Fan, Eur. J. Org. Chem. 508 (2007)
212. P.J. Case, A.W. Harper, MRS Proceedings **771**(L4), 10 (2003)
213. A. Keller, M. Ianchuk, S. Ladeira, M. Taillefer, A.-M. Caminade, J.-P. Majoral, A. Ouali, Eur. J. Org. Chem. **2012**, 1056 (2012)
214. C. Müller, L.J. Ackerman, J.N.H. Reek, P.C.J. Kamer, P.W.N.M. van Leeuwen, J. Am. Chem. Soc. **126**, 14960 (2004)
215. A. Rether, M. Schuster, React. Funct. Polym. **57**, 13 (2003)
216. S.E. Gibson, J.T. Rendell, Chem. Commun. 922 (2008)
217. M.R. Rauckhorst, P.J. Wilson, S.A. Hatcher, C.M. Hadad, J.R. Parquette, Tetrahedron **59**, 3917 (2003)
218. R. Tiwari, S.H. Daware, S.B. Kale, RSC Adv. **5**, 42526 (2015)
219. F. Fernández-Trillo, J. Pacheco-Torres, J. Correa, P. Ballesteros, P. Lopez-Larrubia, S. Cerdán, R. Riguera, E. Fernandez-Megia, Biomacromol **12**, 2902 (2011)
220. A.J.L. Villaraza, A. Bumb, M.W. Brechbiel, Chem. Rev. **110**, 2921 (2010)
221. A.R. Menjoge, R.M. Kannan, D.A. Tomalia, Drug Discov. Today **15**, 171 (2010)
222. A. Louie, Chem. Rev. **110**, 3146 (2010)
223. C. Khemtong, C.W. Kessinger, J. Gao, Chem. Commun. 3497 (2009)
224. A. Bumb, M.W. Brechbiel, P. Choyke, Acta Radiol. **51**, 751 (2010)
225. J.L. Major, T.J. Meade, Acc. Chem. Res. **42**, 893 (2009)
226. S. Langereis, Q.G. de Lussanet, M.H.P. van Genderen, W.H. Beckes, E.W. Meijer, Macromolecules **37**, 3084 (2004)
227. S. Langereis, Q.G. de Lussanet, M.H.P. van Genderen, E.W. Meijer, R.G. Beets-Tan, A.W. Griffioen, J.M. van Engelshoven, W.H. Backes, NMR Biomed. **19**, 133 (2006)
228. K. Luo, G. Liu, X. Zhang, W. She, B. He, Y. Nie, L. Li, Y. Wu, Z. Zhang, Q. Gong, F. Gao, B. Song, H. Ai, Z. Gu, Macromol. Biosci. **9**, 1227 (2009)
229. S. Laus, A. Sour, R. Ruloff, É. Tóth, A.E. Merbach, Chem. Eur. J. **11**, 3064 (2005)
230. S. Garcıa-Gallego, M. Cangiotti, L. Fiorani, A. Fattori, M.A. Mũnoz-Ferńandez, R. Gomez, M.F. Ottaviani, F.J. De la Mata, Dalton Trans. **42**, 5874 (2013)
231. J. Lim, V.J. Venditto, E.E. Simanek, Bioorg. Med. Chem. **18**, 5749 (2010)
232. J. Roeser, B. Heinrich, C. Bourgogne, M. Rawiso, S. Michel, V. Hubscher-Bruder, F. Arnaud-Neu, S. Méry, Macromolecules **46**, 7075 (2013)
233. A. Ossenbach, H. Rüegger, A. Zhang, K. Fischer, A.D. Schlüter, M. Schmidt, Macromolecules **42**, 8781 (2009)
234. F. Le Derf, E. Levillain, G. Trippé, A. Gorgues, M. Sallé, R.-M. Sebastian, A.-M. Caminade, J.P. Majoral, Angew. Chem. Int. Ed. **40**, 224 (2001)
235. D. Alivertis, G. Paraskevopoulos, V. Theodorou, K. Skobridis, Tetrahedron Lett. **50**, 6019 (2009)
236. B. Sethi, S. Chandra, S. Kumar, R. Singh, L.P. Singh, J. Electroanal. Chem. **651**, 185 (2011)
237. Y. Pan, M. Lu, Z. Peng, J.S. Melinger, Org. Biomol. Chem. **1**, 4465 (2003)
238. X. Wang, J. Hu, T. Liu, G. Zhang, S. Liu, J. Mater. Chem. **22**, 8622 (2012)
239. V. Balzani, G. Bergamini, P. Ceroni, F. Vogtle, Coord. Chem. Rev. **251**, 525 (2007)
240. P. Antoni, M. Malkoch, G. Vamvounis, D. Nyström, A. Nyström, M. Lindgren, A. Hult, J. Mater. Chem. **18**, 2545 (2008)
241. B. Branchi, P. Ceroni, G. Bergamini, V. Balzani, M. Maestri, J. van Heyst, S.K. Lee, F. Luppertz, F. Vögtle, Chem. Eur. J. **12**, 8926 (2006)

242. G. Bergamini, A. Sottilotta, M. Maestri, P. Ceroni, F. Vögtle, Chem. Asian J. **5**, 1884 (2010)
243. L.M. Lima, R. Delgado, M.G. Drew, P. Brandão, V. Félix, Dalton Trans. 6593 (2008)
244. Z.S. Pillai, P. Ceroni, M. Kubeil, J.M. Heldt, H. Stephan, G. Bergamini, Chem. Asian J. **8**, 771 (2013)
245. J.V. Ros-Lis, R. Martínez-Máñez, F. Sancenón, J. Soto, M. Spieles, K. Rurack, Chem. Eur. J. **14**, 10101 (2008)
246. J. Havlícková, H. Medová, T. Vitha, J. Kotek, I. Císarová, P. Hermann, Dalton Trans. 5378 (2008)
247. B. Branchi, G. Bergamini, L. Fiandro, P. Ceroni, A. Alvino, G. Doddi, F. Vögtle, F.G. Klärner, Dalton Trans. **40**, 1356 (2011)
248. B. Branchi, P. Ceroni, V. Balzani, F.G. Klärner, F. Vögtle, Chem. Eur. J. **16**, 6048 (2010)
249. C. Saudan, V. Balzani, M. Gorka, S.K. Lee, M. Maestri, V. Vicinelli, F. Vögtle, J. Am. Chem. Soc. **125**, 4424 (2003)
250. C. Saudan, V. Balzani, M. Gorka, S.K. Lee, J. van Heyst, M. Maestri, P. Ceroni, V. Vicinelli, F. Vögtle, Chem. Eur. J. **10**, 899 (2004)
251. C. Saudan, P. Ceroni, V. Vicinelli, M. Maestri, V. Balzani, M. Gorka, S.K. Lee, J. van Heyst, F. Vögtle, Dalton Trans. 1597 (2004)
252. G. Bergamini, P. Ceroni, V. Balzani, L. Cornelissen, J. van Heyst, S.-K. Lee, F. Vögtle, J. Mater. Chem. **15**, 2959 (2005)
253. G. Bergamini, C. Saudan, P. Ceroni, M. Maestri, V. Balzani, M. Gorka, S.K. Lee, J. van Heyst, F. Vögtle, J. Am. Chem. Soc. **126**, 16466 (2004)
254. C. Saudan, V. Balzani, P. Ceroni, M. Gorka, M. Maestri, V. Vicinelli, F. Vogtle, Tetrahedron **59**, 3845 (2003)
255. R. Malgas-Enus, S.F. Mapolie, Polyhedron **47**, 87 (2012)
256. E. Marchi, M. Baroncini, G. Bergamini, J. Van Heyst, F. Vögtle, P. Ceroni, J. Am. Chem. Soc. **134**, 15277 (2012)
257. C. Larpent, C. Genies, A.P.D. Delgado, A.M. Caminade, J.P. Majoral, J.F. Sassi, F. Leising, Chem. Commun. 1816 (2004)
258. A. Martin, F. Manea, R. Fiammengo, L.J. Prins, L. Pasquato, P. Scrimin, J. Am. Chem. Soc. **129**, 6982 (2007)
259. G. Zaupa, L.J. Prins, P. Scrimin, Bioorg. Med. Chem. Lett. **19**, 3816 (2009)
260. G. Zaupa, P. Scrimin, L.J. Prins, J. Am. Chem. Soc. **130**, 5699 (2008)
261. C.K. Jang, J.Y. Jaung, Mater. Lett. **62**, 3209 (2008)
262. W. Maes, W. Dehaen, Eur. J. Org. Chem. 4719 (2009)
263. M.A. Oar, W.R. Dichtel, J.M. Serin, J.M.J. Fréchet, Chem. Mater. **18**, 3682 (2006)
264. P. Vinš, A. de Cózar, I. Rivilla, K. Nováková, R. Zangi, J. Cvačka, I. Arrastia, A. Arrieta, P. Dražar, J.I. Miranda, F.P. Cossío, Tetrahedron **72**, 1120 (2016)
265. R.E.H. Ramirez, I.V. Lijanova, N.V. Likhanova, O.O. Xometl, J. Incl. Phenom. Macrocycl. Chem. **84**, 49 (2016)
266. M. Shema-Mizrachi, G.M. Pavan, E. Levin, A. Danani, N.G. Lemcoff, J. Am. Chem. Soc. **133**, 14359 (2011)
267. N. Semenishyn, A. Mahammed, Z. Gross, Eur. J. Org. Chem. **2015**, 5079 (2015)
268. D.K.P. Ng, C. R. Chimie **6**, 903 (2003)
269. M. Kimura, Y. Sugihara, T. Muto, K. Hanabusa, H. Shirai, N. Kobayashi, Chem. Eur. J. **5**, 3495 (1999)
270. J. Leclaire, R. Dagiral, A. Pla-Quintana, A.M. Caminade, J.P. Majoral, Eur. J. Inorg. Chem. 2890 (2007)
271. Z. Iqbal, N. Masilela, T. Nyokong, A. Lyubimtsev, M. Hanack, T. Ziegler, Photochem. Photobiol. Sci. **11**, 679 (2012)
272. T.J. Wadas, E.H. Wong, G.R. Weisman, C.J. Anderson, Chem. Rev. **110**, 2858 (2010)
273. O. Rolland, C.-O. Turrin, A.-M. Caminade, J.-P. Majoral, New J. Chem. **33**, 1809 (2009)
274. V.J. Venditto, C. Aida, S. Regino, M.W. Brechbiel, Mol. Pharm. **2**, 302 (2005)
275. G.P. Yan, C.W. Ai, L. Li, R.F. Zong, F. Liu, Chin. Sci. Bull. **55**, 3085 (2010)
276. M. Longmire, P.L. Choyke, H. Kobayashi, Curr. Top. Med. Chem. **8**, 1180 (2008)

277. S. Moreno, P. Ortega, F.J. de la Mata, M.F. Ottaviani, M. Cangiotti, A. Fattori, M.Á. Muñoz-Fernández, R. Gómez, Inorg. Chem. **54**, 8943 (2015)
278. C. Lee, K. Ji, E.E. Simanek, Molecules **21**, 335 (2016)
279. I. Dijkgraaf, A.Y. Rijnders, A. Soede, A.C. Dechesne, G.W. van Esse, A.J. Brouwer, F.H.M. Corstens, O.C. Boerman, D.T.S. Rijkers, R.M.J. Liskamp, Org. Biomol. Chem. **5**, 935 (2007)
280. L.M. Sena, S.J. Fishman, K.J. Jenkins, H. Xu, M.W. Brechbiel, C.A. Regino, N. Kosaka, M. Bernardo, P.L. Choyke, H. Kobayashi, Nanomedicine **5**, 1183 (2010)
281. C.C. Cyran, Y.J. Fu, H.J. Raatschen, V. Rogut, B. Chaopathomkul, D.M. Shames, J. Magn. Reson. Imaging **27**, 581 (2008)
282. J. Rudovský, P. Hermann, M. Botta, S. Aime, I. Lukeš, Chem. Commun. 2390 (2005)
283. J.A. Pikkemaat, R.T. Wegh, R. Lamerichs, R.A. van de Molengraaf, S. Langereis, D. Burdinski, A.Y.F. Raymond, H.M. Janssen, D.F.M. de Waal, N.P. Willard, E.W. Meijer, H. Grüll, Contrast Media Mol. Imaging **2**, 229 (2007)
284. J.M. Ren, T.G. McKenzie, Q. Fu, E.H.H. Wong, J. Xu, Z. An, S. Shanmugam, T.P. Davis, C. Boyer, G.G. Qiao, Chem. Rev. **116**, 6743 (2016)
285. C.L. Fraser, G.L. Fiore, Adapting polymeric metal complexes for biomedical applications, in *Polymers for Biomedical Applications*, vol. 977, Ch. 7 (2008), p. 95 (ACS Symp. Ser.)
286. B. Zhang, L.-H. Zhang, X. Huagong, Modern. Chem. Ind. **34**, 58 (2014)
287. W. Wu, W. Wang, J. Li, Prog. Polym. Sci. **46**, 55 (2015)
288. A. Winter, U.S. Schubert, Chem. Soc. Rev. **45**, 5311 (2016)
289. L. He, W. Bu, Synthesis, Design, Characterization, and application of metallo-supramolecular polymers, in *Non-covalent Interactions in the Synthesis and Design of New Compounds*, ed. by A.M. Maharramov, K.T. Mahmudov, M.N. Kopylovich, A.J.L. Pombeiro (Wiley, Weinheim, 2016)
290. V. Marin, E. Holder, R. Hoogenboom, U.S. Schubert, Chem. Soc. Rev. **36**, 618 (2007)
291. M. Kamigaito, Metal-containing star and hyperbranched polymers, in *Redox Systems Under Nano-Space Control*, ed. by T. Hirao (Springer, Berlin, Heidelberg, NY, 2006)
292. C.-A. Fustin, P. Guillet, U.S. Schubert, J.-F. Gohy, Adv. Mater. **19**, 1665 (2007)
293. X. Wu, C.L. Fraser, Macromolecules **33**, 4053 (2000)
294. R.M. Johnson, A. Pfister, C.L. Fraser, in *Metal-Containing and Metallosupramolecular Polymers and Materials*, vol. 928, Ch. 2 (2006), p. 17 (ACS Symp. Ser.)
295. Y. Chujo, A. Naka, M. Kramer, K. Sada, T. Saegusa, J. Macromol. Sci. Pure Appl. Chem. A **32**, 1213 (1995)
296. G.-I. Konishi, Y. Chujo, Macromol. Res. **16**, 70 (2008)
297. A. Pfister, C.L. Fraser, Biomacromol **7**, 459 (2006)
298. G.L. Fiore, J.L. Klinkenberg, A. Pfister, C.L. Fraser, Biomacromol **10**, 128 (2009)
299. G. Konishi, Y. Chujo, Polym. Bull. **9**, 43 (1999)
300. P.S. Corbin, M.P. Webb, J.E. McAlvin, C.L. Fraser, Biomacromol **2**, 223 (2001)
301. C.L. Fraser, A.P. Smith, X. Wu, J. Am. Chem. Soc. **122**, 9026 (2000)
302. C.L. Fraser, A.P. Smith, J. Polym. Sci. Part A Polym. Chem. **38**, 4704 (2000)
303. G. Zhou, I.I. Harruna, C.W. Ingram, Polymer **46**, 10672 (2005)
304. R.M. Johnson, C.L. Fraser, Biomacromol **5**, 580 (2004)
305. G. Zhou, J. He, I.I. Harruna, J. Polym. Sci. Part A Polym. Chem. **45**, 4225 (2007)
306. G. Zhou, J. He, I.I. Harruna, J. Polym. Sci. Part A Polym. Chem. **45**, 4204 (2007)
307. G.L. Fiore, J.L. Klinkenberg, C.L. Fraser, Macromolecules **41**, 9397 (2008)
308. R.M. Johnson, C.L. Fraser, Macromolecules **37**, 2718 (2004)
309. A.P. Smith, C.L. Fraser, J. Polym. Sci. Part A Polym. Chem. **40**, 4250 (2002)
310. A.P. Smith, C.L. Fraser, Macromolecules **35**, 594 (2002)
311. A.P. Smith, C.L. Fraser, Macromolecules **36**, 5520 (2003)
312. G.L. Fiore, C.L. Fraser, Macromolecules **41**, 7892 (2008)
313. R. Hoogenboom, D. Wouters, U.S. Schubert, Macromolecules **36**, 4743 (2003)
314. R. Hoogenboom, J. Huskens, U.S. Schubert, ACS Symp. Ser. **928**, 62 (2005)
315. R. Hoogenboom, B.C. Moore, U.S. Schubert, Chem. Commun. 4010 (2006)

316. R. Hoogenboom, B.C. Moore, U.S. Schubert, Macromol. Rapid Commun. **31**, 840 (2010)
317. S. Tang, A. Habicht, S. Li, S. Seiffert, B.D. Olsen, Macromolecules **49**, 5599 (2016)
318. M.A.R. Meier, U.S. Schubert, Chem. Commun. 4610 (2005)
319. K. Naka, G. Konishi, K. Kotera, Y. Chujo, Polym. Bull. **41**, 263 (1998)
320. J.L. Bender, Q.-D. Shen, C.L. Fraser, Tetrahedron **60**, 7277 (2004)
321. J.L. Bender, P.S. Corbin, C.L. Fraser, D.H. Metcalf, F.S. Richardson, E.L. Thomas, A.M. Urbas, J. Am. Chem. Soc. **124**, 8526 (2002)
322. D.C. Thévenaz, C.A. Monnier, S. Balog, G.L. Fiore, Biomacromol **15**, 3994 (2014)
323. K.-I. Fukukawa, R. Rossin, A. Hagooly, E.D. Pressly, J.N. Hunt, B.W. Messmore, K.L. Wooley, M.J. Welch, C.J. Hawker, Biomacromol **9**, 1329 (2008)
324. Y. Li, M. Beija, S. Laurent, L. vander Elst, R.N. Muller, H.T.T. Duong, A.B. Lowe, T.P. Davis, C. Boyer, Macromolecules **45**, 4196 (2012)
325. Y. Li, S. Laurent, L. Esser, L.V. Elst, R.N. Muller, A.B. Lowe, C. Boyer, T.P. Davis, Polym. Chem. **5**, 2592 (2014)
326. T. Zhang, C. Zhang, J. Xing, J. Xu, C. Li, P.C. Wang, X.-J. Liang, Multifunctional dendrimers for drug nanocarriers, in *Novel Approaches for Drug Delivery*, ed. by R.K. Keservani, A.K. Sharma, R.K. Kesharwani (IGI Global, Hershey, 2017)
327. L. Zhang, R. Liu, H. Peng, P. Li, Z. Xu, A.K. Whittaker, Nanoscale **8**, 10491 (2016)
328. C.T. Adkins, J.N. Dobish, C.S. Brown, B. Mayrsohn, S.K. Hamilton, F. Udoji, K. Radford, T.E. Yankeelov, J.C. Gore, E. Harth, Polym. Chem. **3**, 390 (2012)
329. B. Mizrahi, S.A. Shankarappa, J.M. Hickey, J.C. Dohlman, B.P. Timko, K.A. Whitehead, J.-J. Lee, R. Langer, D.G. Anderson, D.S. Kohane, Adv. Funct. Mater. **23**, 1527 (2013)
330. L. Viau, M. Even, O. Maury, D.M. Haddleton, H. Le Bozec, Macromol. Rapid Commun. **24**, 630 (2003)
331. R. Hoogenboom, U.S. Schubert, Chem. Soc. Rev. **35**, 622 (2006)
332. L. Viau, M. Even, O. Maury, D.M. Haddleton, H. Le Bozec, C. R. Chimie **8**, 1298 (2005)
333. R.M. Johnson, P.S. Corbin, C. Ng, C.L. Fraser, Macromolecules **33**, 7404 (2000)
334. A.A. Farah, W.J. Pietro, J. Polym. Sci. Part A Polym. Chem. **43**, 6057 (2005)
335. X. Wu, J.E. Collins, J.E. McAlvin, R.W. Cutts, C.L. Fraser, Macromolecules **34**, 2812 (2001)
336. J.E. Collins, C.L. Fraser, Macromolecules **31**, 6715 (1998)
337. S.J. Payne, G.L. Fiore, C.L. Fraser, J.N. Demas, Anal. Chem. **82**, 917 (2010)
338. Y. Deng, S.-J. Liu, B.-M. Zhao, P. Wang, Q.-L. Fan, W. Huang, L.-H. Wang, J. Lumin. **131**, 2166 (2011)
339. A.A. Farah, W.J. Pietro, Can. J. Chem. **82**, 595 (2004)
340. J.J.S. Lamba, C.L. Fraser, J. Am. Chem. Soc. **119**, 1801 (1997)
341. J.E. McAlvin, C.L. Fraser, Macromolecules **32**, 6925 (1999)
342. J.E. McAlvin, S.B. Scott, C.L. Fraser, Macromolecules **33**, 6953 (2000)
343. G. Hochwimmer, O. Nuyken, U.S. Schubert, Macromol. Rapid Commun. **19**, 309 (1998)
344. U.S. Schubert, O. Nuyken, G. Hochwimmer, Des. Monom. Polym. **3**, 245 (2000)
345. J.E. McAlvin, C.L. Fraser, Macromolecules **32**, 1341 (1999)
346. C. Park, J.E. McAlvin, C.L. Fraser, E.L. Thomas, Chem. Mater. **14**, 1225 (2002)
347. M. Chen, K.P. Ghiggino, S.H. Thang, G.J. Wilson, Angew. Chem. Int. Ed. **44**, 4368 (2005)
348. M. Chen, K.P. Ghiggino, A. Launikonis, A.W.H. Mau, E. Rizzardo, W.H.F. Sasse, S.H. Thang, G.J. Wilson, J. Mater. Chem. **13**, 2696 (2003)
349. A. Wild, A. Winter, F. Schlütter, U.S. Schubert, Chem. Soc. Rev. **40**, 1459 (2011)
350. U.S. Schubert, C. Eschbaumer, O. Nuyken, G. Hochwimmer, J. Incl. Phenom. **35**, 23 (1999)
351. U.S. Schubert, G. Hochwimmer, M. Heller, A.C.S. Symp, Ser. **812**, 163 (2002)
352. M. Heller, U.S. Schubert, Macromol. Symp. **177**, 87 (2002)
353. J.-F. Gohy, M. Chiper, P. Guillet, C.-A. Fustin, S. Hoeppener, A. Winter, R. Hoogenboom, U.S. Schubert, Soft Matter **5**, 2954 (2009)
354. J.L. Gorczynski, J. Chen, C.L. Fraser, J. Am. Chem. Soc. **127**, 14956 (2005)
355. J. Chen, J.L. Gorczynski, G. Zhang, C.L. Fraser, Macromolecules **43**, 4909 (2010)
356. Q.P. Liu, Y.C. Chen, Y. Wu, J. Zhu, J.G. Deng, Synlett 1503 (2006)

357. W. Zhao, C. Li, B. Liu, X. Wang, P. Li, Y. Wang, C. Wu, C. Yao, T. Tang, X. Liu, D. Cui, Macromolecules **47**, 5586 (2014)
358. Y. Tao, Q. Xu, N. Li, J. Lu, L. Wang, X. Xia, Polymer **52**, 4261 (2011)
359. N. Qiu, Y. Li, S. Han, G. Cui, T. Satoh, T. Kakuchi, Q. Duan, J. Photochem. Photobiol. A Chem. **283**, 38 (2014)
360. T. Ren, A. Wang, W. Yuan, L. Li, Y. Feng, J. Polym. Sci. Part A Polym. Chem. **49**, 2303 (2011)
361. W. Yuan, H. Zou, W. Guo, A. Wang, J. Ren, J. Mater. Chem. **22**, 24783 (2012)
362. K.-Y. Baek, S.-H. Lee, S.S. Hwang, Macromol. Res. **19**, 461 (2011)
363. T. Rudolph, S. Crotty, U.S. Schubert, F.H. Schacher, e-Polymers **15**, 227 (2015)
364. L.R.H. High, S.J. Holder, H.V. Penfold, Macromolecules **40**, 7157 (2007)
365. W.R. Dichtel, K.Y. Baek, J.M.J. Fréchet, I.B. Rietveld, S.A. Vinogradov, J. Polym. Sci. Part A Polym. Chem. **44**, 4939 (2006)
366. L. Wu, R. McHale, G. Feng, X. Wang, Int. J. Polym. Sci. **2011**, Article ID 109693, 11 pp. (2011)
367. A. Bilgin, C. Yagcı, Eur. Polym. J. **61**, 240 (2014)
368. Z. Gao, J. Liang, X. Tao, Y. Cui, T. Satoh, T. Kakuchi, Q. Duan, Macromol. Res. **20**, 508 (2012)
369. T.L. Mindt, H. Struthers, L. Brans, T. Anguelov, C. Schweinsberg, V. Maes, D. Tourwé, R. Schibli, J. Am. Chem. Soc. **128**, 15096 (2006)
370. T.L. Mindt, C. Müller, M. Melis, M. de Jong, R. Schibli, Bioconjugate Chem. **19**, 1689 (2008)
371. H. Struthers, B. Spingler, T.L. Mindt, R. Schibli, Chem. Eur. J. **14**, 6173 (2008)
372. N. Xiao, Y. Chen, X. Shen, C. Zhang, S. Yano, M. Gottschaldt, U.S. Schubert, T. Kakuchi, T, Satoh. Polym. J. **45**, 216 (2013)
373. C. Zhang, X. Shen, R. Sakai, M. Gottschald, U. Schubert, S. Hirohara, M. Tanihara, S. Yano, M. Obata, N. Xiao, T. Satoh, T. Kakuchi, J. Polym. Sci. A **49**, 746 (2011)
374. Y. Chen, N. Xiao, T. Satoh, T. Kakuchi, Polym. Chem. **5**, 4993 (2014)
375. Y. Chen, N. Xiao, M. Fukuoka, K. Yoshida, Q. Duan, T. Satoh, T. Kakuchi, Polym. Chem. **6**, 3608 (2015)
376. L. Munuera, R.K. O'Reilly, Dalton Trans. **39**, 388 (2010)
377. W. Wu, R. Tang, Q. Li, Z. Li, Chem. Soc. Rev. **44**, 3997 (2015)
378. F. Sun, X. Luo, L. Kang, X. Peng, C. Lu, Polym. Chem. **6**, 1214 (2015)
379. M. HaiiBler, H. Dong, B.Z. Tang, Hyperbranched polymer containing transition metals: synthetic pathways and potential applications, in *Inorganic and Organometallic Macromolecules*: *Design and Applications*, ed. by A.S. Abd-El-Aziz, C.E. Carraher, C.U. Pittman, M. Zeldin (Springer, NY, 2008)
380. C. Hajji, R. Haag, Top. Organomet. Chem. **20**, 149 (2006)
381. Y. Zheng, S. Li, Z. Weng, C. Gao, Chem. Soc. Rev. **44**, 4091 (2015)
382. A. Lederer, W. Burchard, *Hyperbranched Polymers: Macromolecules in between Deterministic Linear Chains and Dendrimer Structures* (RSC Polymer Chemistry Series, Cambridge, 2015)
383. I.N. Kurniasih, J. Keilitz, R. Haag, Chem. Soc. Rev. **44**, 4145 (2015)
384. R. Salazar, L. Fomina, S. Fomine, Polym. Bull. **47**, 151 (2001)
385. K.R. Kumar, J.N. Kizhakkedathu, D.E. Brooks, Macromol. Chem. Phys. **205**, 567 (2004)
386. S. Nowag, C. Frangville, G. Multhaup, J.D. Marty, C. Mingotaud, R. Haag, J. Mater. Chem. B **2**, 3915 (2014)
387. S. Fehse, S. Nowag, M. Quadir, K.S. Kim, R. Haag, G. Multhaup, Biomacromol **15**, 1910 (2014)
388. R. Albrecht, S. Fehse, K. Pant, S. Nowag, H. Stephan, R. Haag, C.C. Tzschucke, Macromol. Biosci. **16**, 412 (2016)
389. S.S. Mahapatra, U. Das, N. Karak, J. Lumin. **128**, 1917 (2008)
390. S.S. Mahapatra, N. Karak, Polym. J. **41**, 20 (2009)

391. M. Krämer, N. Pérignon, R. Haag, J.-D. Marty, R. Thomann, N. Lauth-de Viguerie, C. Mingotaud, Macromolecules **38**, 8308 (2005)
392. H. Yoo, S.-Y. Kwak, J. Membr. Sci. **448**, 125 (2013)
393. K.N. Han, B.Y. Yu, S.Y. Kwak, J. Membrane Sci. **396**, 83 (2012)
394. J. Feng, Y. Li, M. Yang, Eur. Polym. J. **44**, 3314 (2008)
395. J. Feng, Y. Li, M. Yang, J. Polym. Sci. A **47**, 222 (2009)
396. N.W. Ding, W.H. Lin, W.L. Sun, Z.Q. Shen, Sci. China Chem. **54**, 320 (2011)
397. N. Ding, W. Sun, Y. Lin, Z. Shen, Chin. J. Polym. Sci. **30**, 759 (2012)
398. Y. Lei, H. Li, W. Gao, M. Liu, J. Chen, J. Ding, X. Huang, H. Wu, J. Mater. Chem. C **2**, 7402 (2014)
399. R.L. Xu, H.W. Liu, W.F. Shi, J. Polym. Sci. Part B Polym. Phys. **44**, 826 (2006)
400. C. Gao, J. Hou, D.Y. Yan, Z.J. Wang, React. Funct. Polym. **58**, 65 (2004)
401. C. Gao, D.Y. Yan, Chin. Sci. Bull. **45**, 1760 (2000)
402. J. Wu, W. Liu, H. Han, R. Sun, M. Xie, X. Liao, Polym. Chem. **6**, 4801 (2015)
403. Z. Dong, Z. Ye, Appl. Catal. A General **489**, 61 (2015)
404. Y. Liu, L. Xu, J. Liu, X. Liu, C. Chen, G. Li, Y. Meng, Chem. Eng. J. **285**, 698 (2016)
405. J.K. Kassube, H. Wadepohl, L.H. Gade, Adv. Synth. Catal. **351**, 607 (2009)
406. G. van Koten, D. Milstein (eds.), *Organometallic Pincer Complexes* (Springer, Heidelberg, NY, Dordrecht, London, 2012)
407. G. van Koten, R.A. Gossage (eds.), *The Privileged Pincer-Metal Platform: Coordination Chemistry & Applications* (Springer, Heidelberg, NY, Dordrecht, London, 2016)
408. S.-E. Stiriba, M.Q. Slagt, H. Kautz, R.J.M.K. Gebbink, R. Thomann, H. Frey, G. van Koten, Chem. Eur. J. **10**, 1267 (2004)
409. M.Q. Slagt, S.-E. Stiriba, H. Kautz, R.J.M.K. Gebbink, H. Frey, G. Van Koten, Organometallics **23**, 1525 (2004)
410. C. Schlenk, A.W. Kleij, H. Frey, G. van Koten, Angew. Chem. Int. Ed. **39**, 3445 (2000)
411. W. Yang, H.Y. Zhen, C.Y. Jiang, L.J. Su, J.X. Jiang, H.H. Shi, Y. Cao, Synth. Met. **153**, 189 (2005)
412. R. Guan, Y. Xu, L. Ying, W. Yang, H. Wu, Q. Chen, Y. Cao, J. Mater. Chem. **19**, 531 (2009)
413. J. Liu, L. Yu, C. Zhong, R. He, W. Yang, H. Wu, Y. Cao, RSC Adv. **2**, 689 (2012)
414. T. Guo, R. Guan, J. Zou, J. Liu, L. Ying, W. Yang, H. Wu, Y. Cao, Polym. Chem. **2**, 2193 (2011)
415. T. Guo, L. Yu, B. Zhao, Y. Li, Y. Tao, W. Yang, Q. Hou, H. Wu, Y. Cao, Macromol. Chem. Phys. **213**, 820 (2012)
416. T. Guo, L. Yu, Y. Yang, Y. Li, Y. Tao, Q. Hou, L. Ying, W. Yang, H. Wu, Y. Cao, J. Lumin. **167**, 179 (2015)
417. J. Sun, J. Yang, C. Zhang, H. Wang, J. Li, S. Su, H. Xu, T. Zhang, Y. Wu, W.-Y. Wong, B. Xu, New J. Chem. **39**, 5180 (2015)
418. J. Sun, H. Wang, T. Yang, X. Zhang, J. Li, T. Zhang, Y. Wu, W. Chen, W.-Y. Wong, Dyes Pigm. **125**, 339 (2016)
419. C.W. Tse, K.W. Cheng, W.K. Chan, J. Inorg. Organomet. Polym. **18**, 59 (2008)
420. C. Hajji, S. Roller, M. Beigi, A. Liese, R. Haag, Adv. Synth. Catal. **348**, 1760 (2006)
421. M. Beigi, S. Roller, R. Haag, A. Liese, Eur. J. Org. Chem. 2135 (2008)
422. M. Beigi, R. Haag, A. Liese, Adv. Synth. Catal. **350**, 919 (2008)
423. J. Keilitz, R. Haag, Eur. J. Org. Chem. 3272 (2009)
424. J. Wang, G. Yang, C.Q. Li, W.G. Shi, Chem. J. Chin. Univ. **35**, 1536 (2014)
425. J. Wang, N. Zhang, C.Q. Li, W.G. Shi, Z.Y. Lin, J. Organomet. Chem. **822**, 104 (2016)
426. V.S. Thengarai, J. Keilitz, R. Haag, Inorg. Chim. Acta **409**, 179 (2014)
427. M.P. Kutyreva, A.R. Gataulina, G.A. Kutyrev, N.A. Ulakhovich, T. Newman, E.M. Khasanova, O.V. Bondar, S.V. Yurtaeva, S.A. Ziganshina, E.V. Khaldeeva, Inorg. Chim. Acta **450**, 101 (2016)
428. X. Fang, R. Chen, L. Xiao, Q. Chen, Polym. Int. **61**, 136 (2011)
429. B. Bao, L. Yuwen, X. Zhan, L. Wang, J. Polym. Sci. Part A Polym. Chem. **48**, 3431 (2010)

430. A. Goswami, A.K. Singh, React. Funct. Polym. **61**, 255 (2004)
431. J.N. Asaad, N.E. Ikladious, F. Awad, T. Müller, Canad. J. Chem. Eng. **91**, 257 (2013)
432. N.E. Ikladious, S.H. Mansour, N. Rozik, K. Dirnberger, C.D. Eisenbach, J. Polym. Sci. Part A Polym. Chem. **46**, 5568 (2008)
433. N.E. Ikladious, J.N. Asaad, N.N. Rozik, Des. Monom. Polym. **12**, 469 (2009)
434. C. Li, H. Chen, B. Liu, B. Wang, R. Luo, N. Shan, J. Appl. Polym. Sci. **131**, 40117 (2014)
435. Q. Zhu, F. Qiu, B. Zhu, X. Zhu, RSC Adv. **3**, 2071 (2013)
436. M. Elsabahy, G.S. Heo, S.-M. Lim, G. Sun, K.L. Wooley, Chem. Rev. **115**, 10967 (2015)
437. D. Ding, G. Wang, J. Liu, K. Li, K.Y. Pu, Y. Hu, J.C.Y. Ng, B.Z. Tang, B. Liu, Small **8**, 3523 (2012)
438. K. Kirkorian, A. Ellis, L.J. Twyman, Chem. Soc. Rev. **41**, 6138 (2012)
439. X. Zheng, I.R. Oviedo, L.J. Twyman, Macromolecules **41**, 7776 (2008)
440. X. Jiang, Y. Du, C. Liu, P. Huo, Z. Geng, S. Zhang, G. Wang, Chin. J. Polym. Sci. **32**, 73 (2014)
441. A. Ellis, L.J. Twyman, Macromolecules **46**, 7055 (2013)
442. L.J. Twyman, A. Ellis, P.J. Gittins, Macromolecules **44**, 6365 (2011)
443. L.J. Twyman, Y. Ge, Chem. Comm. **15**, 1658 (2006)
444. L.J. Twyman, A. Ellis, P.J. Gittins, Chem. Commun. **48**, 154 (2012)
445. M. Guo, X. Yan, T. Goodsoon III, Adv. Mater. **20**, 4167 (2008)
446. Y. Kwon, T. Hayakawa, M. Kakimoto, Chem. Lett. **35**, 1306 (2006)
447. S. Choi, S.-H. Hong, S.H. Cho, S.-D. Park, S.-M. Park, O. Kim, M. Ree, Adv. Mater. **20**, 1766 (2008)
448. Y. Li, M. Yan, M. Jiang, R. Dhakal, P.S. Thapaliya, X. Yan, J. Photon, Energy **1**, 011115 (2011)
449. J. Wang, J. Mei, A. Qin, J. Sun, B. Zhong, Sci. China Chem. **53**, 2409 (2010)
450. J.M. Yu, Y. Chen, Macromolecules **42**, 8052 (2009)
451. F.L. Bai, Q.G. He, H.M. Huang, H.Z. Lin, J.L. Yang, Synthetic Met. **137**, 971 (2003)